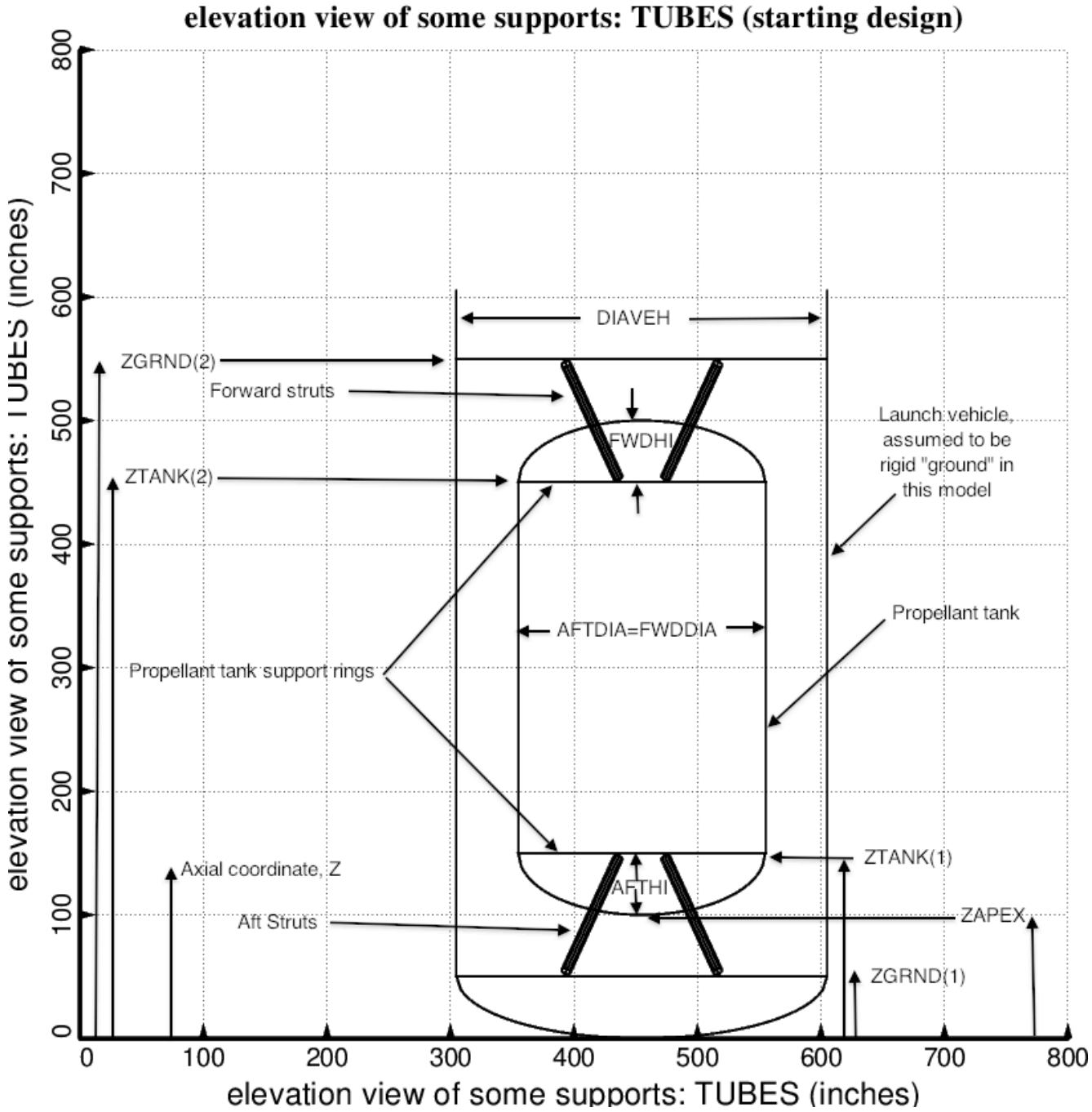

Fig. 1a **Starting design of the long propellant tank with two sets of struts, aft and forward**, with 4 pairs of struts in each of these two sets. Compare with the optimized configuration shown in Fig. 4. (NOTE: In this elevation view of the starting design only one of the four pairs of struts is displayed at each of the aft and forward axial locations. See Fig. 2 for the plan view of all four pairs of struts at the aft axial location and Fig. 3 for those at the forward axial location.) The GENOPT-user-created names of several of the decision variable candidates are given. These decision variable candidates are defined in Tables 1 and 2. The end domes of the propellant tank are 2:1 ellipsoidal shells in the particular cases described here, but may have any ratios of major to minor axes.

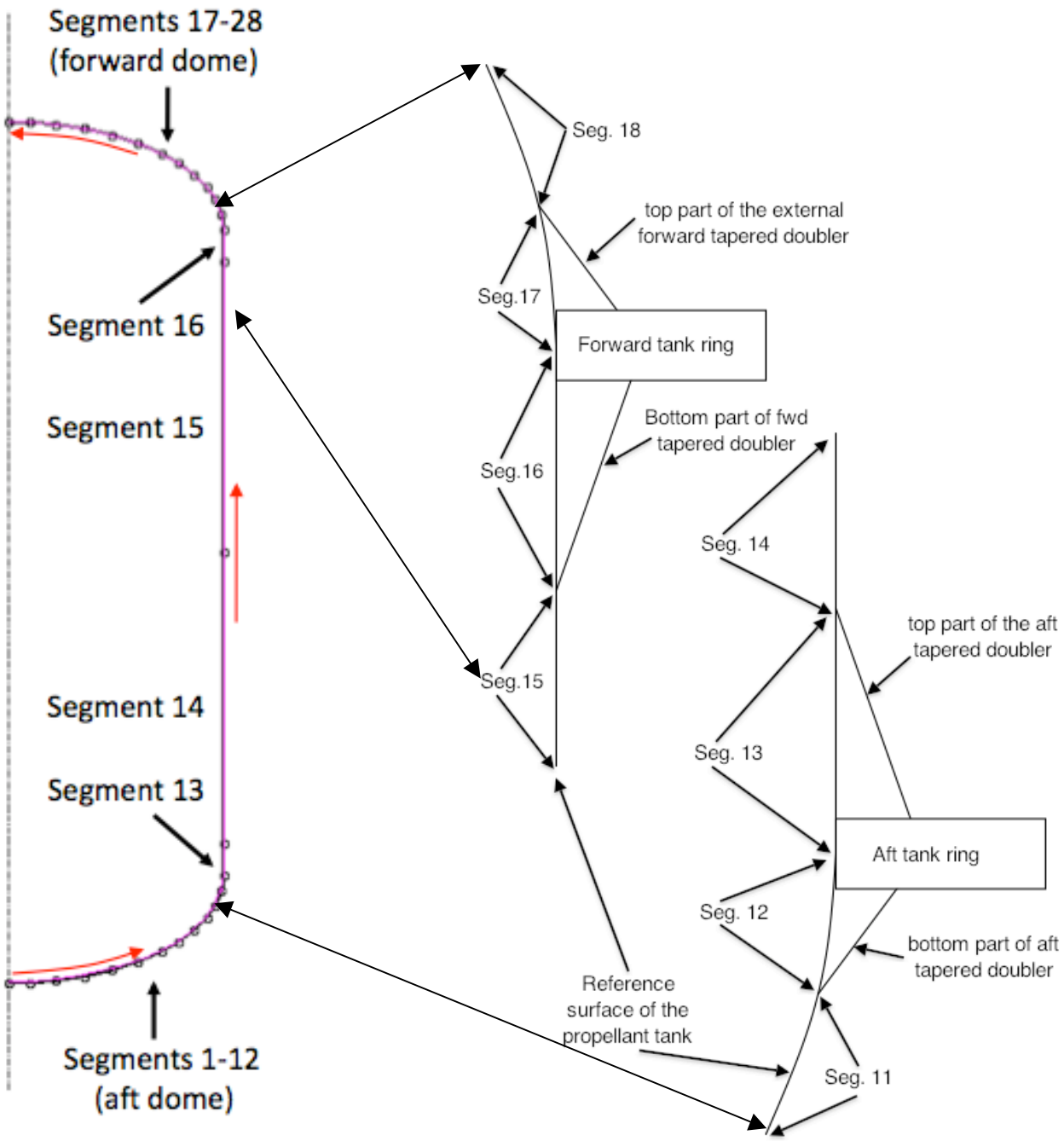

Fig. 1b **BIGBOSOR4 model of the propellant tank**. This tank model contains 28 shell segments. The points shown in the leftmost image lie on the shell reference surface. These points indicate **only the end points of each shell segment** in the model. Each shell segment contains many nodal points, as follows: 13 nodal points in each of Segments 1 – 13 and 16 – 28, and 53 nodal points in each of Segments 14 and 15 (the two long cylindrical segments of the propellant tank). Red arrows indicate the direction of increasing arc length along the meridian of the tank. Images on the right-hand side: details of the forward and aft reinforcements where the struts are attached to the centroids of the forward and aft external propellant tank support rings.

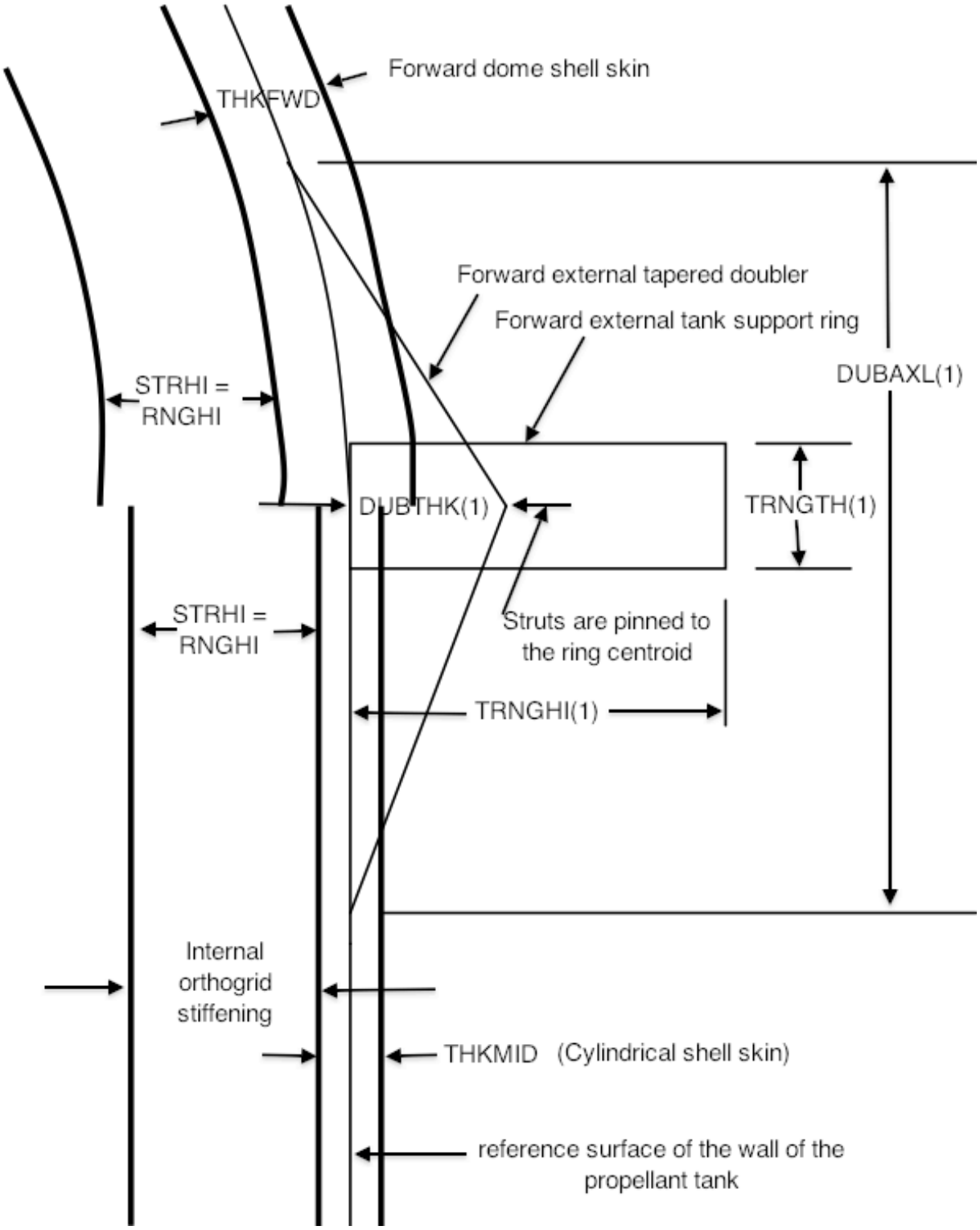

Fig. 1c Configuration of the forward part of the propellant tank in the neighborhood of the forward cylinder/dome junction. The names of several of the decision variable candidates are given. (See Tables 1, 2.)

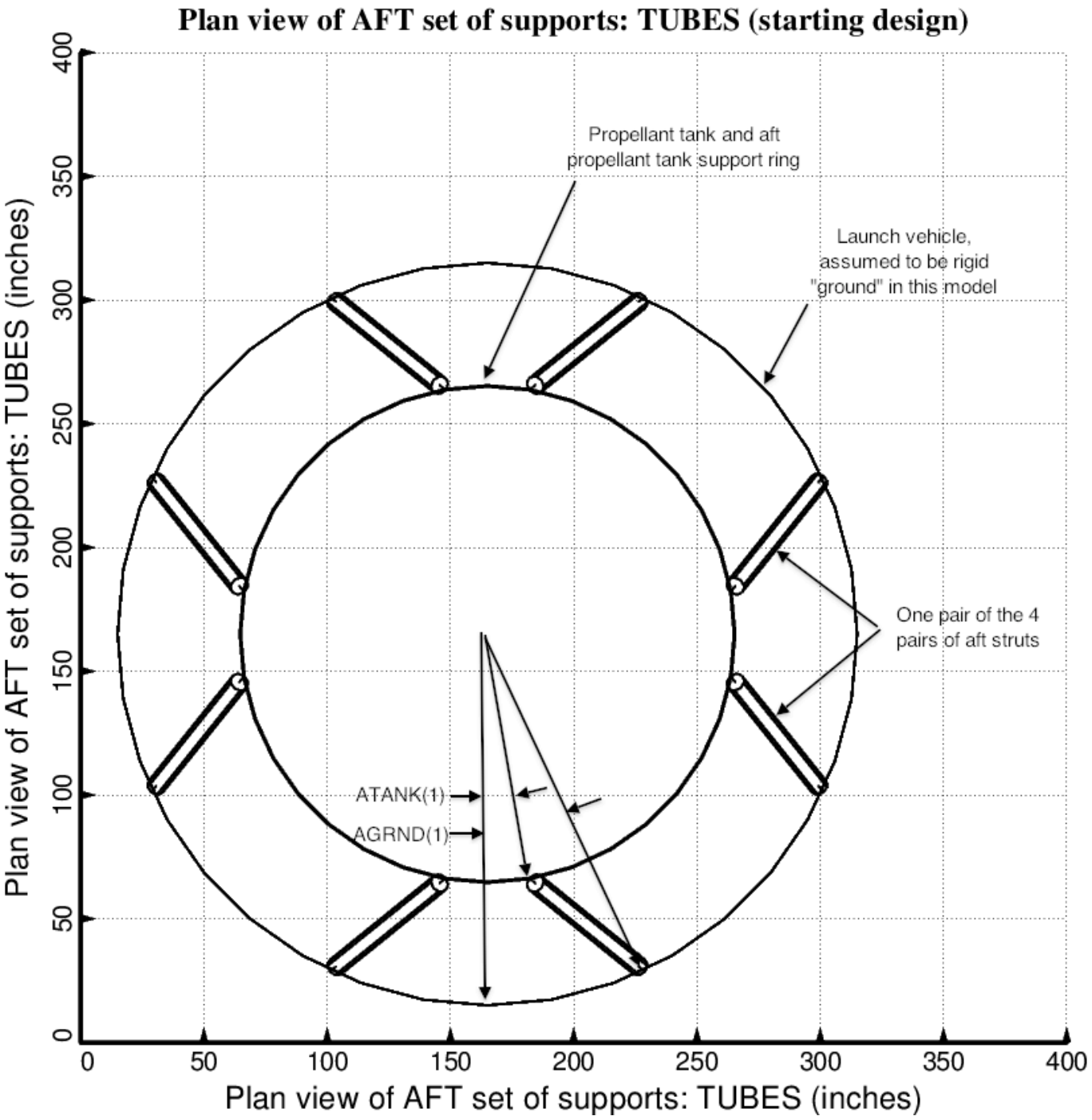

Fig. 2 **Starting design of the long propellant tank with two sets of struts, aft and forward**, with 4 pairs of struts in each of these two sets. Shown here is a plan view of the starting design of the **aft** set of struts. Compare with the optimized configuration shown in Fig. 5. See Tables 1 and 2 for the definitions of ATANK and AGRND.

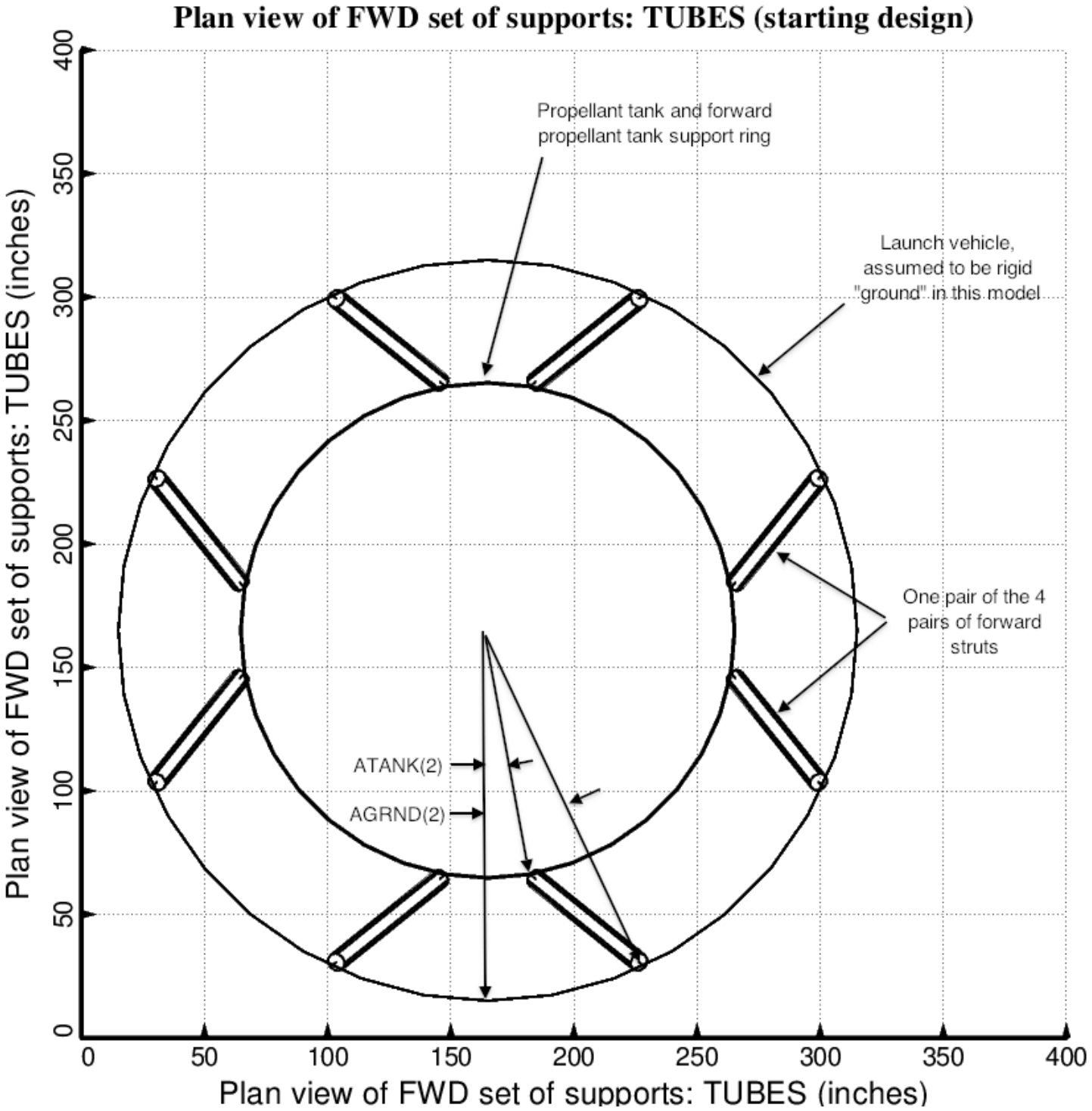

Fig. 3 **Starting design of the long propellant tank with two sets of struts, aft and forward**, with 4 pairs of struts in each of these two sets. Shown here is the plan view of the starting design of the **forward** set of struts. Compare with the optimized configuration shown in Fig. 6. See Tables 1 and 2 for the definitions of ATANK and AGRND.

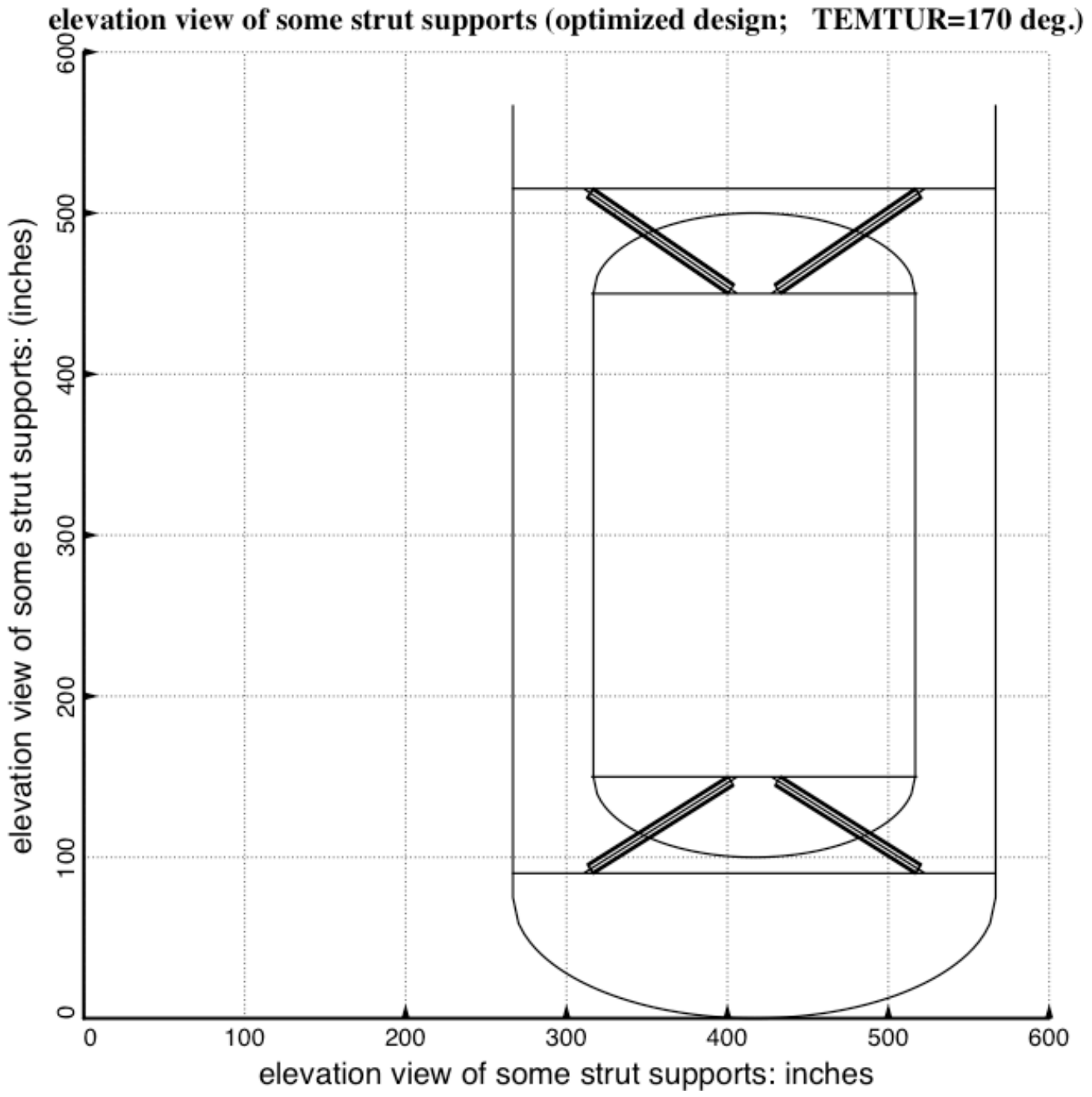

Fig. 4 **Optimized design of the long propellant tank with two sets of struts, aft and forward**, with 4 pairs of struts in each of these two sets. Compare with the starting configuration shown in Fig. 1a. (NOTE: In this elevation view only one of the four pairs of struts is displayed at each axial location, aft and forward). This optimum design was found with use of the "temporary" (varying density) versions of bosdec (bosdec.density.var) and addbosor4 (addbosor4.density.var). "Temporary" means that the density including the mass of the propellant "lumped" into the propellant tank shell wall varies along a shell segment meridian.

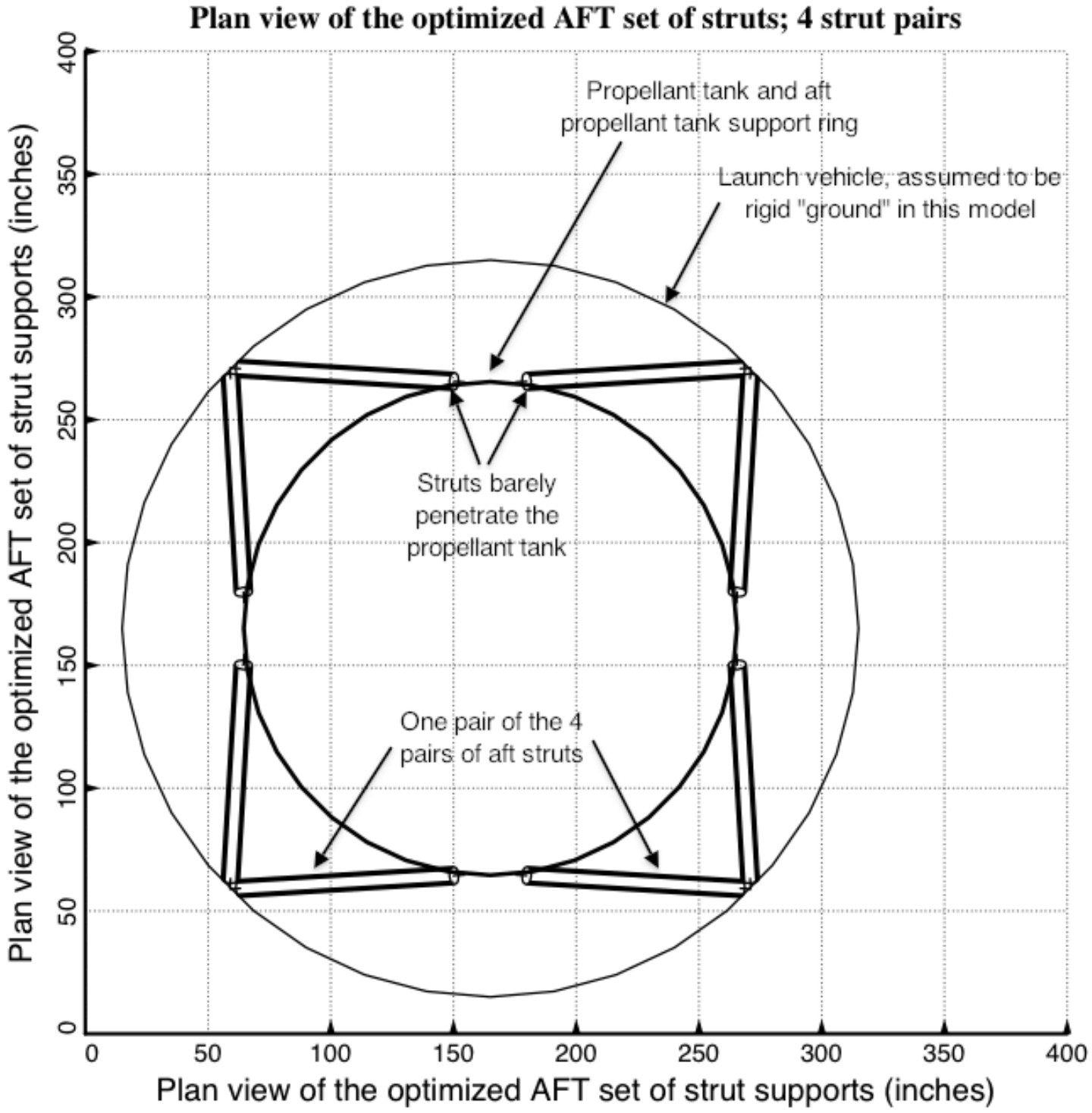

Fig. 5 **Optimized design of the long propellant tank with two sets of struts, aft and forward**, with 4 pairs of struts in each of these two sets. Shown here is a plan view of the optimized **aft** set of 4 pairs of struts. Compare with the starting configuration shown in Fig. 2. This optimum design was found with use of the "temporary" (varying density) versions of bosdec (bosdec.density.var) and addbosor4 (addbosor4.density.var).

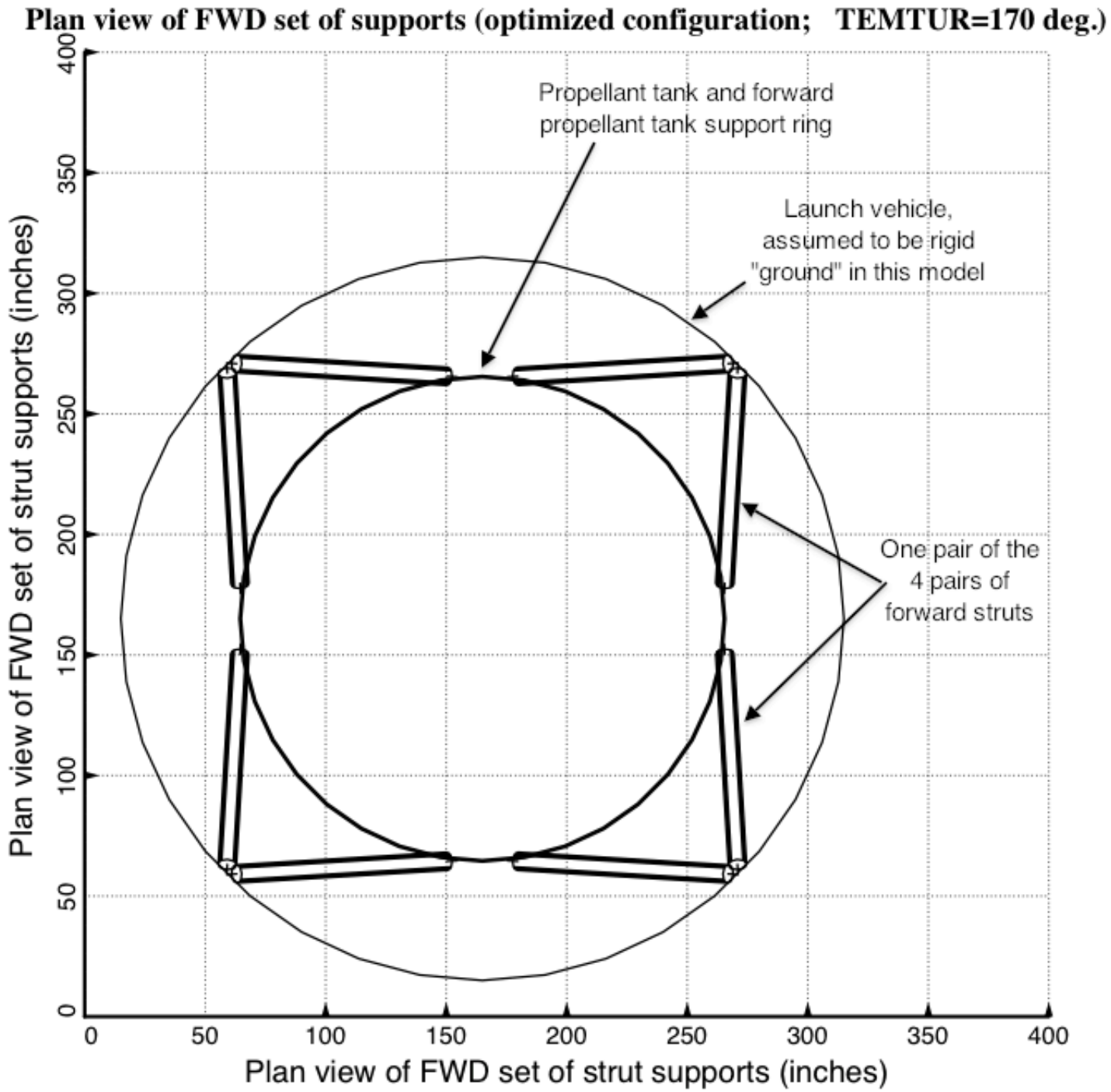

Fig. 6 **Optimized design of the long propellant tank with two sets of struts, aft and forward**, with 4 pairs of struts in each of these two sets. Shown here is the plan view of the optimized **forward** set of struts. Compare with the starting configuration shown in Fig. 3. This optimum design was found with use of the "temporary" (varying density) versions of bosdec (bosdec.density.var) and addbosor4 (addbosor4.density.var).

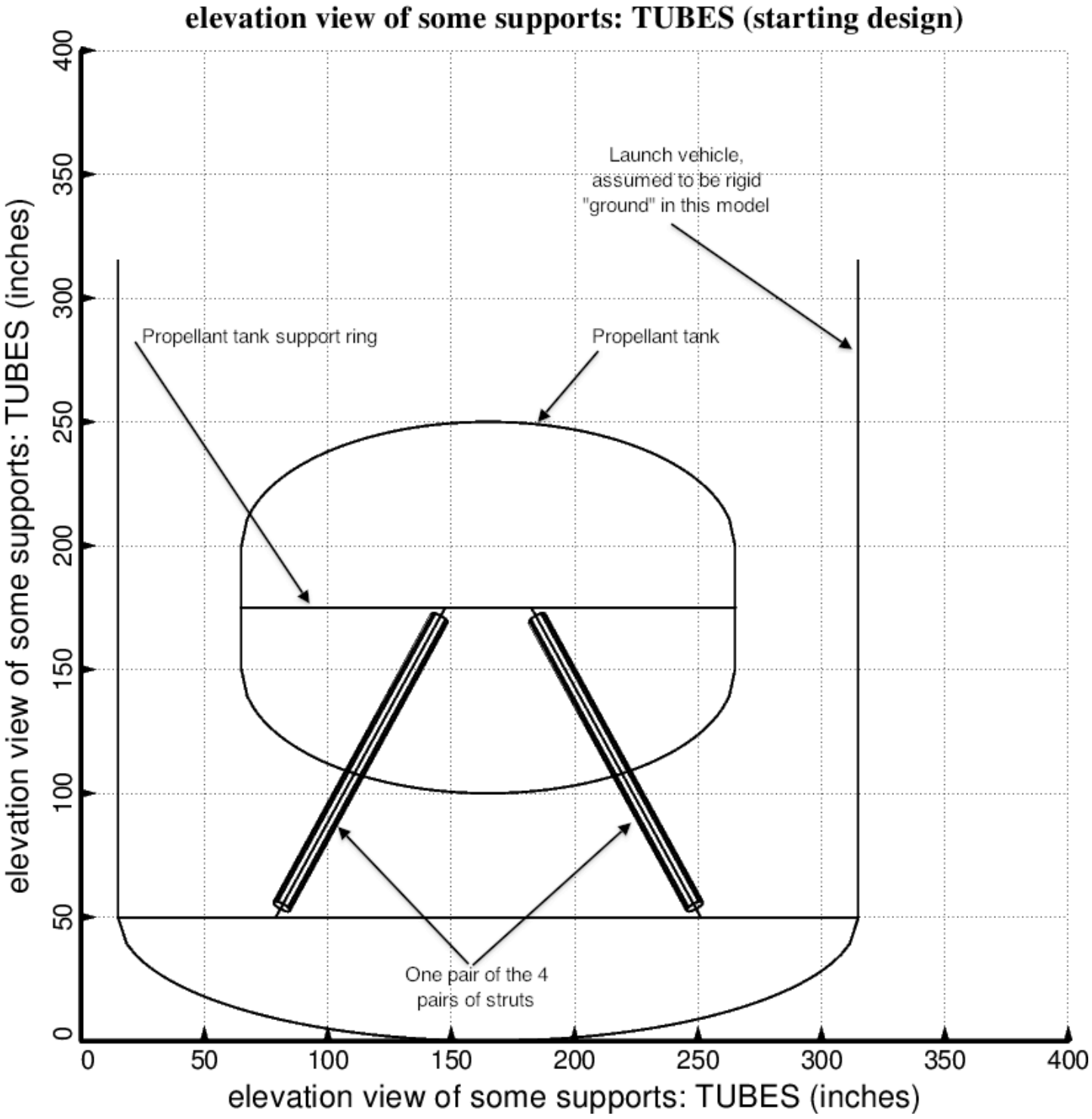

Fig. 7 **Starting design of the short propellant tank with one set of struts**, called "aft", with 4 pairs of struts in this one set. Compare with the optimized configuration shown in Fig. 9. (NOTE: In this elevation view only one of the four pairs of struts is displayed)

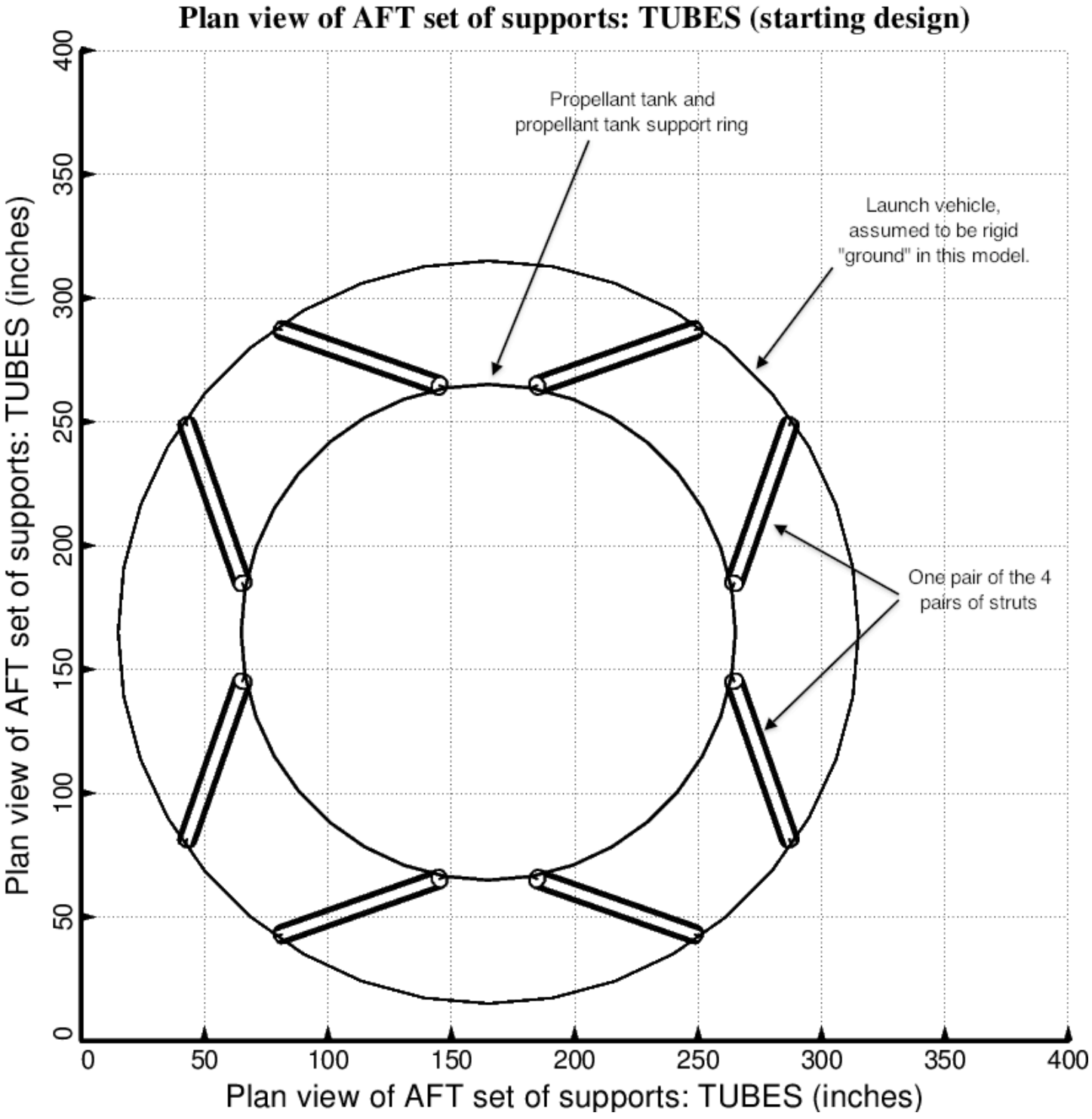

Fig. 8 **Starting design of the short propellant tank with one set of struts**, called "aft", with 4 pairs of struts in this one set. Compare with the optimized configuration shown in Fig. 10.

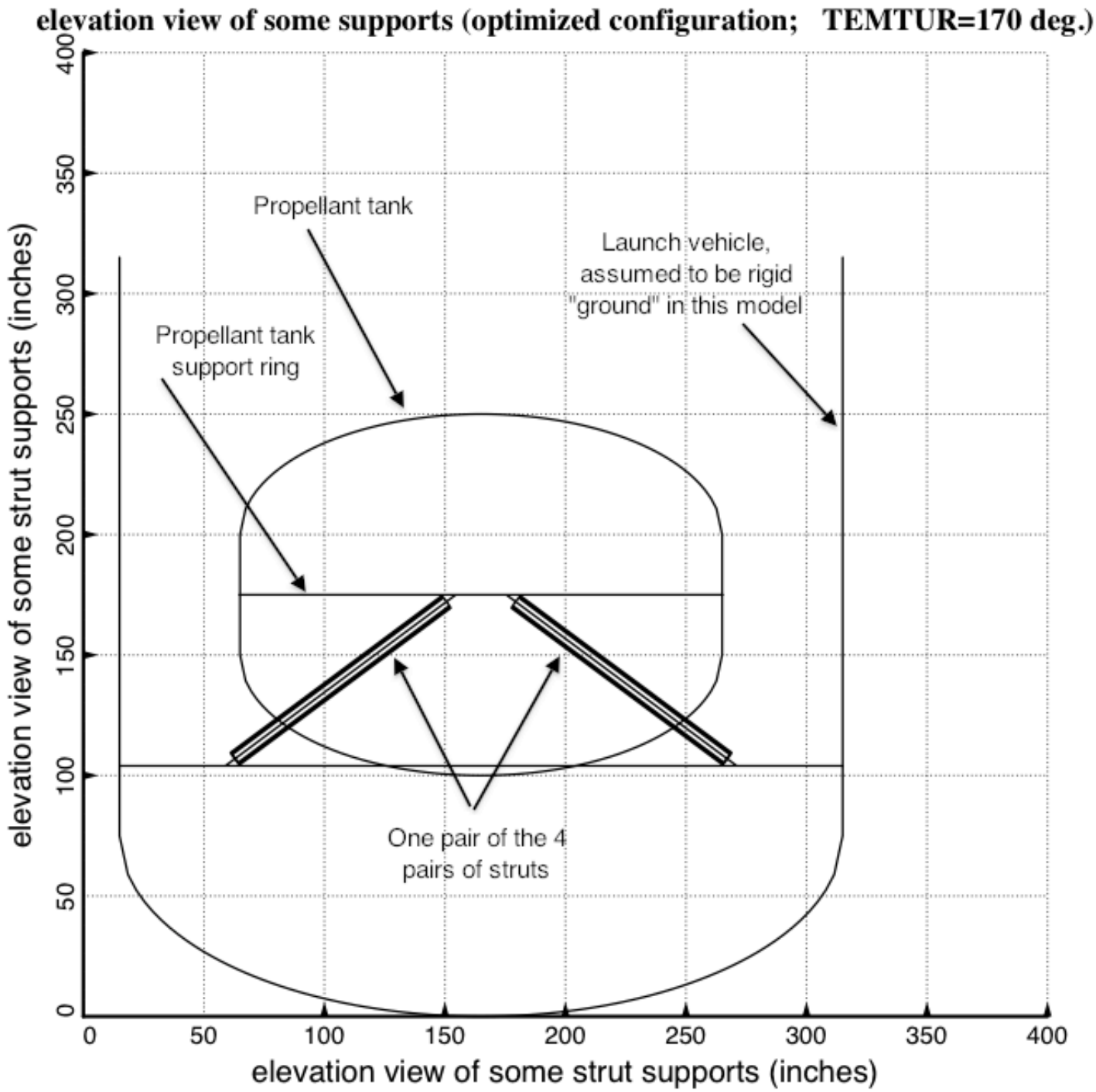

Fig. 9 **Optimized design of the short propellant tank with one set of struts**, called "aft", with 4 pairs of struts in this one set. Compare with the starting configuration shown in Fig. 7. (NOTE: In this elevation view only one of the four pairs of struts is displayed). This optimum design was found with use of the "temporary" (varying density) versions of bosdec (bosdec.density.var) and addbosor4 (addbosor4.density.var).

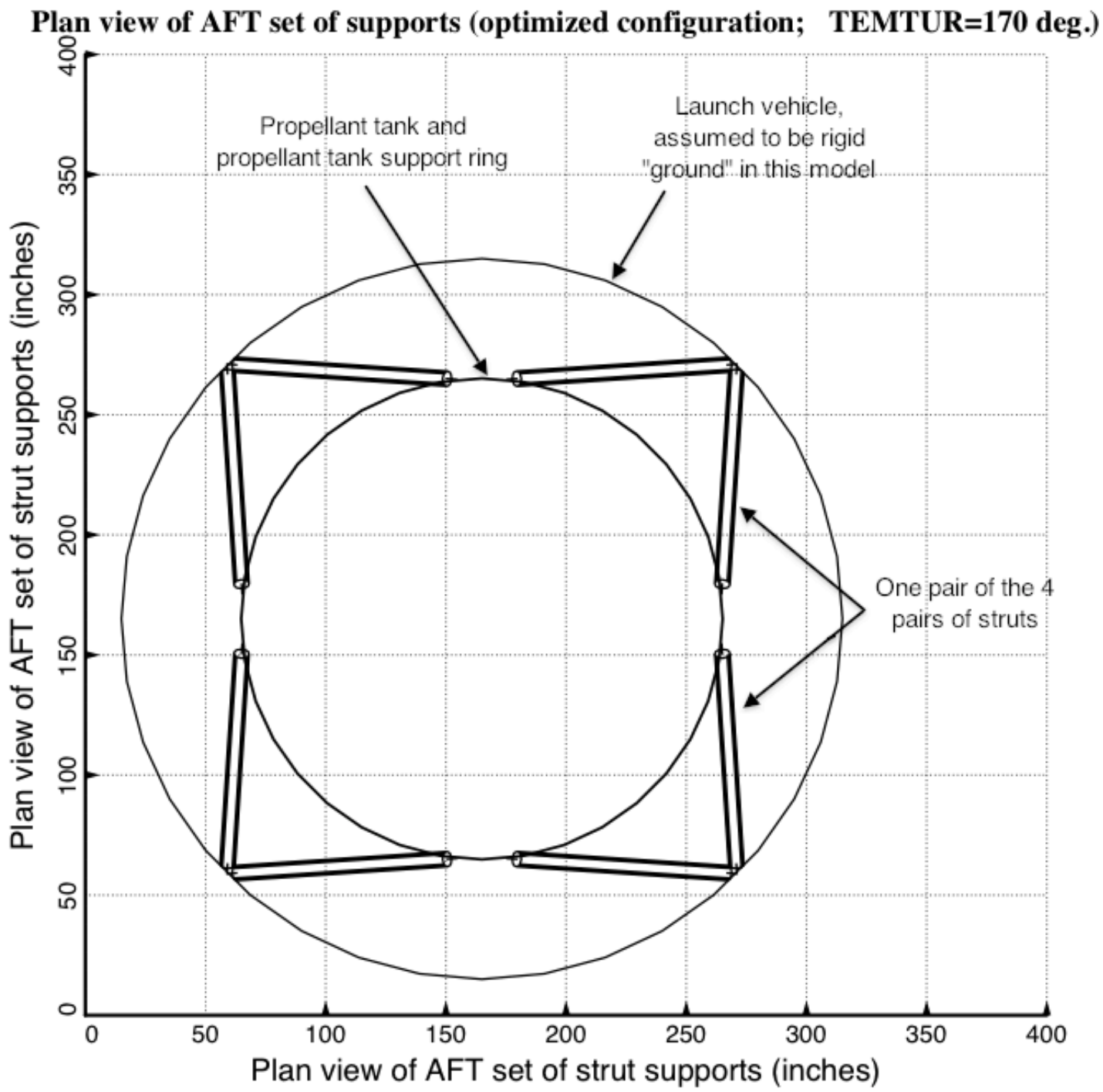

Fig. 10 **Optimized design of the short propellant tank with one set of struts**, called "aft", with 4 pairs of struts in this one set. Compare with the starting configuration shown in Fig. 8. This optimum design was found with use of the "temporary" (varying density) versions of bosdec (bosdec.density.var) and addbosor4 (addbosor4.density.var).

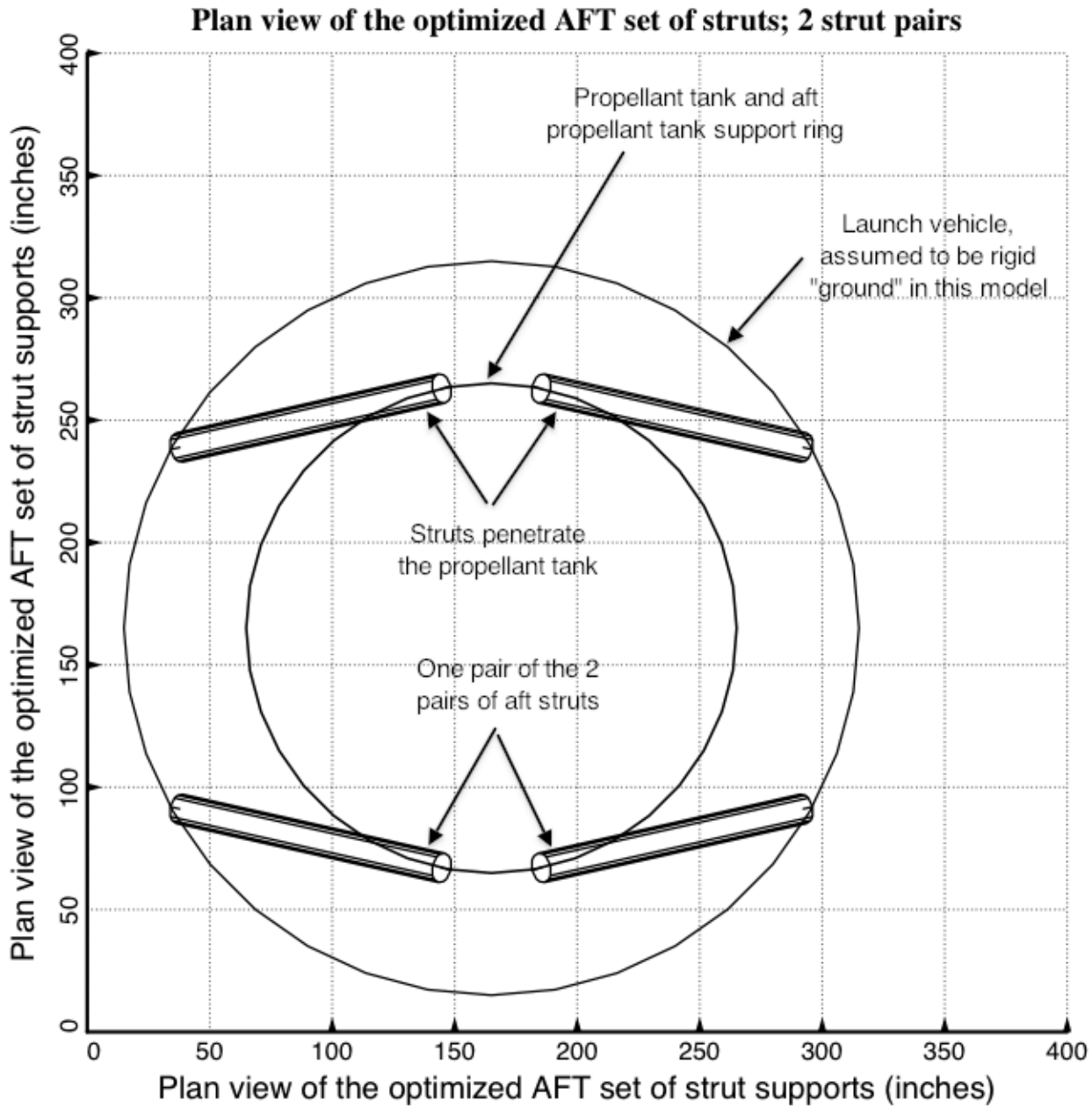

Fig. 11 **Optimized design of the long propellant tank with two sets of struts, aft and forward, with 2 pairs of struts in each of these two sets**. This is the aft set of 2 strut pairs. Notice that the struts penetrate the propellant tank. In the work reported here no constraint was introduced to avoid clearance problems of this type. Also, notice that the configuration appears to be "softer" with regard to lateral or pitching motions in the vertical direction in the plane of the paper than with regard to motions in the horizontal direction in the plane of the paper. **The GENOPT/TANK software, in particular the addition of spring supports to the BIGBOSOR4 capability [14], is valid only if the "ring" of springs at each axial location forms a support stiffness that is essentially isotropic in the plane of the "ring". Therefore, it is not valid to optimize a tank/strut system with less than three pairs of struts at each axial location in the propellant tank.**

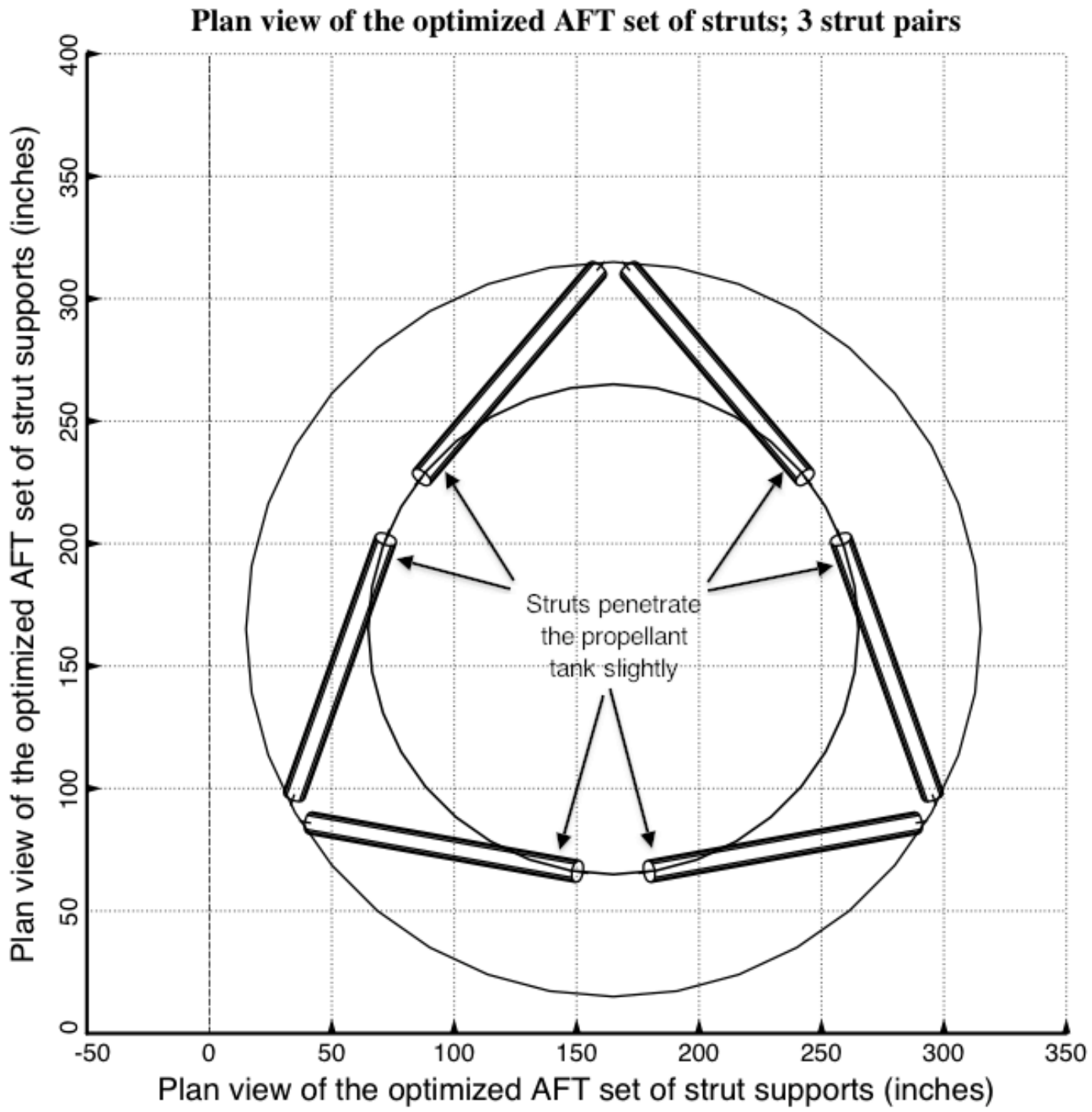

Fig. 12 **Optimized design of the long propellant tank with two sets of struts, aft and forward, with 3 pairs of struts in each of these two sets.** Notice that there is a small clearance problem at the end of the struts attached to the propellant tank. In the work reported here no constraint was introduced to avoid clearance problems of this type.

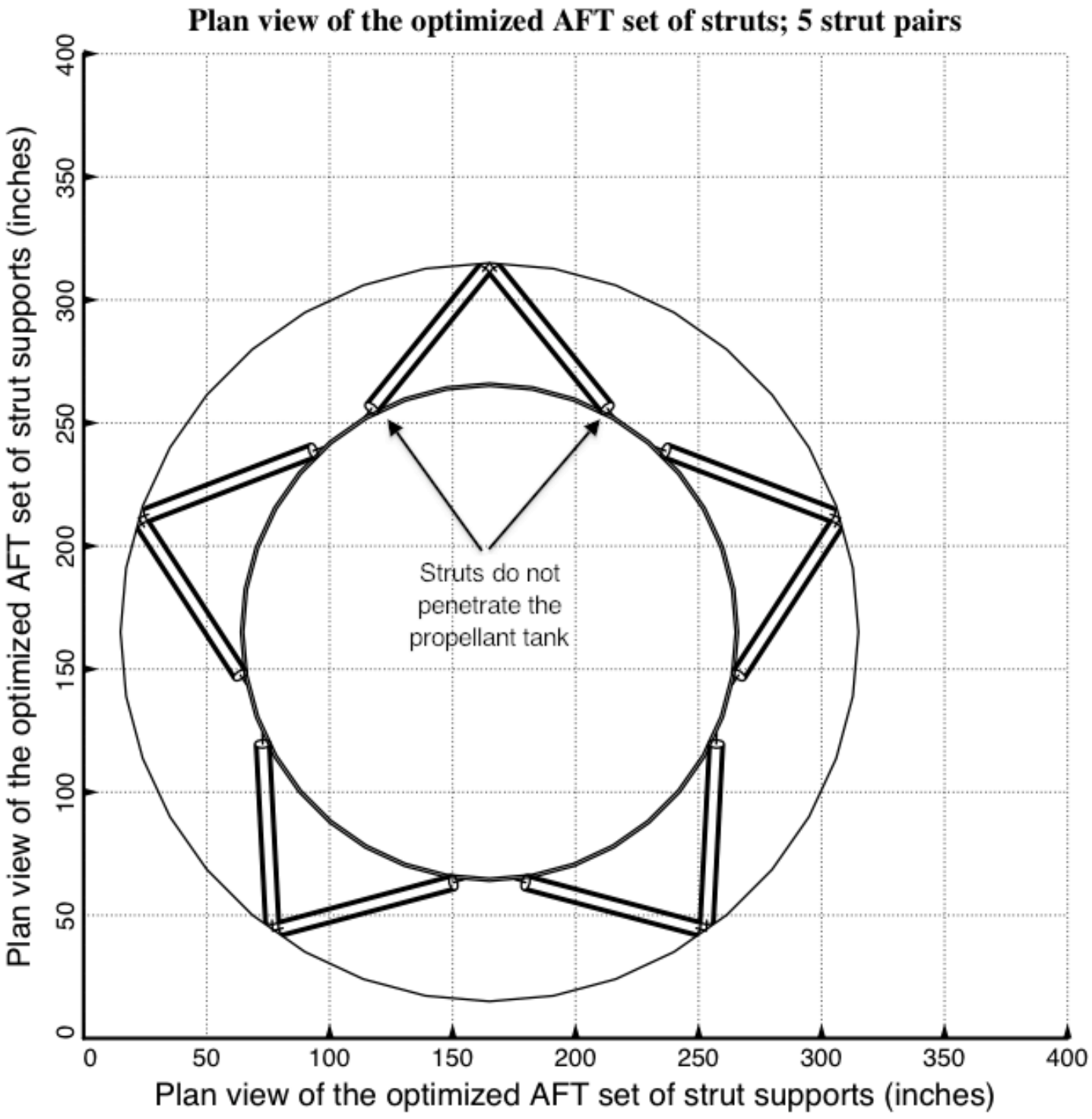

Fig. 13 **Optimized design of the long propellant tank with two sets of struts, aft and forward, with 5 pairs of struts in each of these two sets.** Notice that there is almost no clearance problem at the end of the struts attached to the propellant tank.

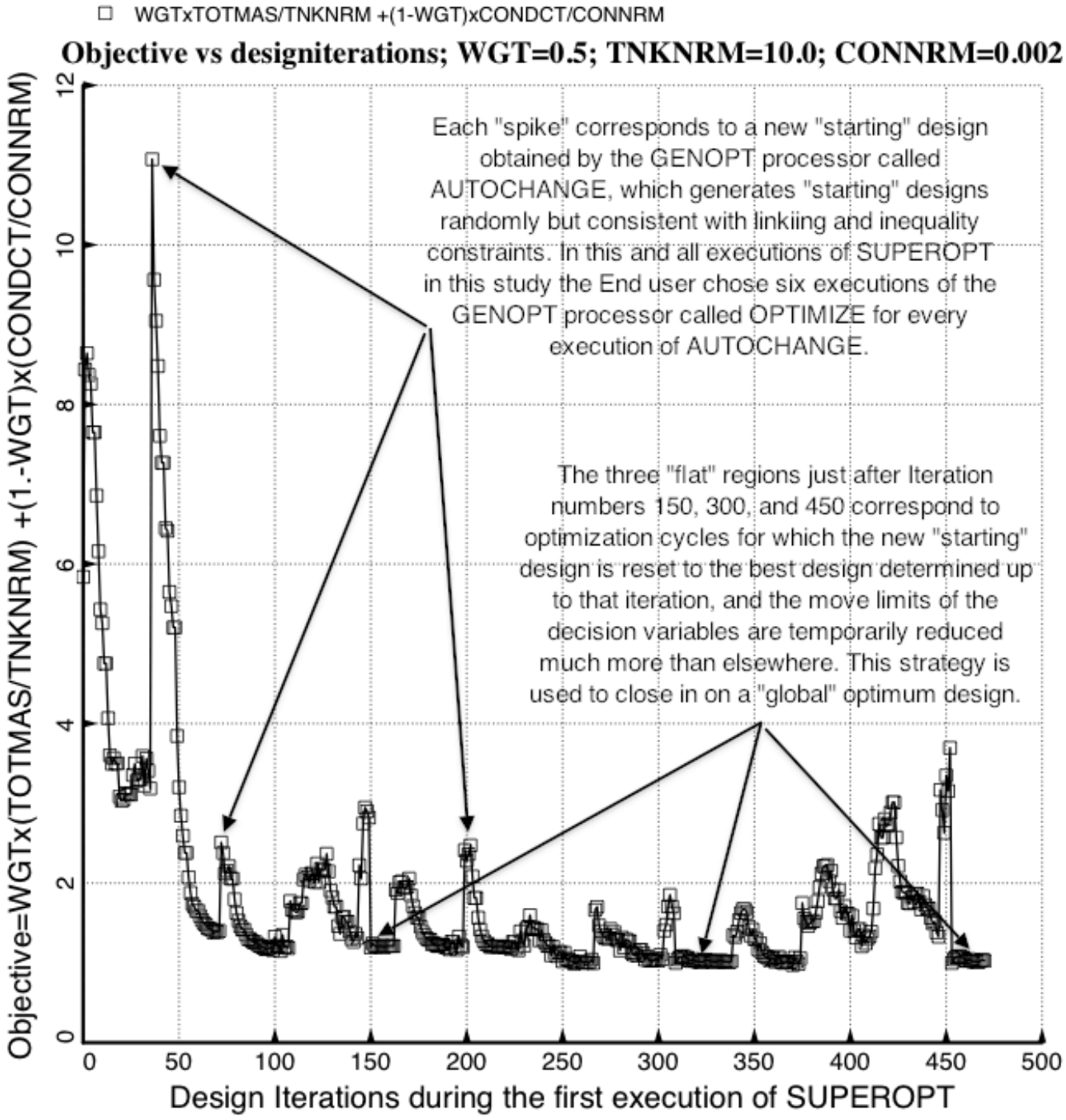

Fig. 14 **Results from the specific case called "test"**: Optimization of the long propellant tank with two sets of struts (aft and forward), 4 pairs of struts in each set. This plot is created with use of the files generated after completion of the first execution of the GENOPT processor called "SUPEROPT" during the very long execution of the GENOPT processor called "SUPERDUPEROPT" (96 hours for 4 automatic successive executions of SUPEROPT). WGT, TNKNRM and CONNRM are specified by the End user in "BEGIN".

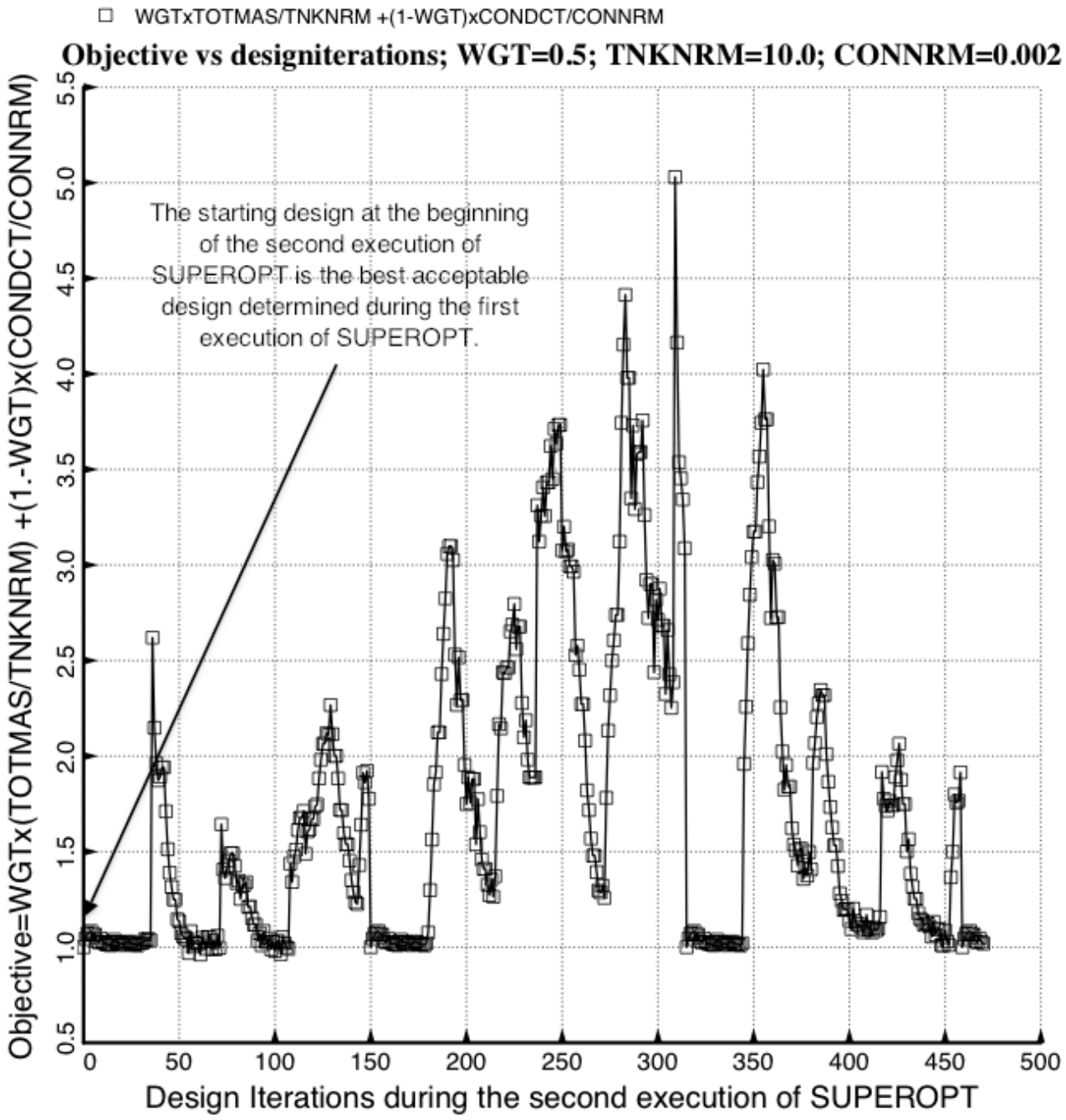

Fig. 15 **Results from the specific case called "test"**: Optimization of the long propellant tank with two sets of struts (aft and forward), 4 pairs of struts in each set. This plot is created with use of the files generated after completion of the second execution of the GENOPT processor called "SUPEROPT" during the very long execution of the GENOPT processor called "SUPERDUPEROPT" (96 hours for 4 automatic successive executions of SUPEROPT). Results from the third and fourth executions of SUPEROPT exist in [20] but are not shown in this paper.

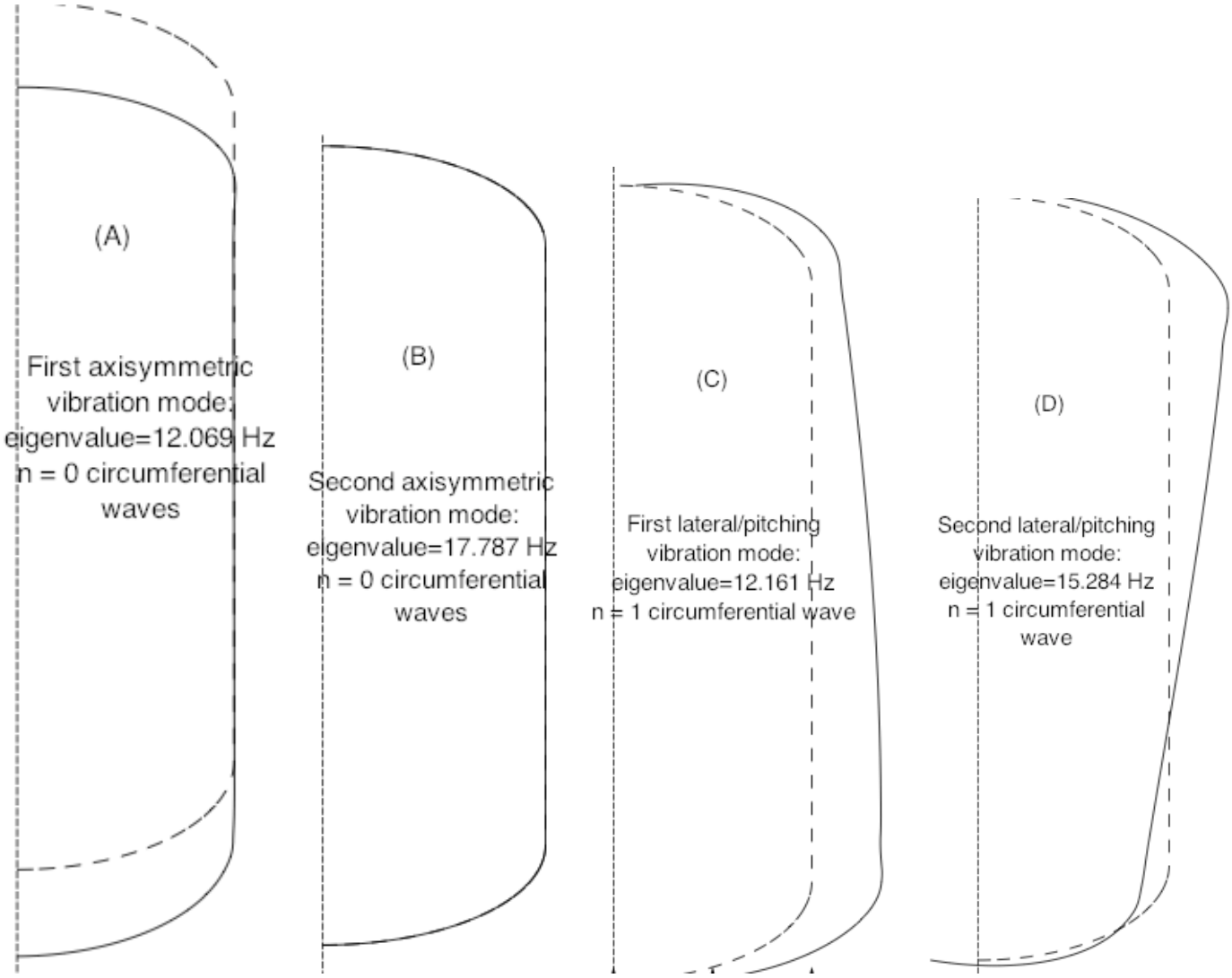

Fig. 16a **Four Vibration modes from GENOPT/TANK/BIGBOSOR4 for the optimized propellant tank with aft and forward sets of struts, 4 pairs of struts at each axial location. These are vibration modes in which the propellant tank moves approximately as a rigid body and there exists significant extension and compression of the supporting struts.** The struts are not shown because BIGBOSOR4 cannot plot springs. Compare (A) with the prediction from STAGS shown in Fig. 25c, (B) with the predictions from STAGS shown in Figs. 25e and 25h, (C) with the predictions from STAGS shown in Figs. 25a and 25d, and (D) with predictions from STAGS shown in Fig. 25g.

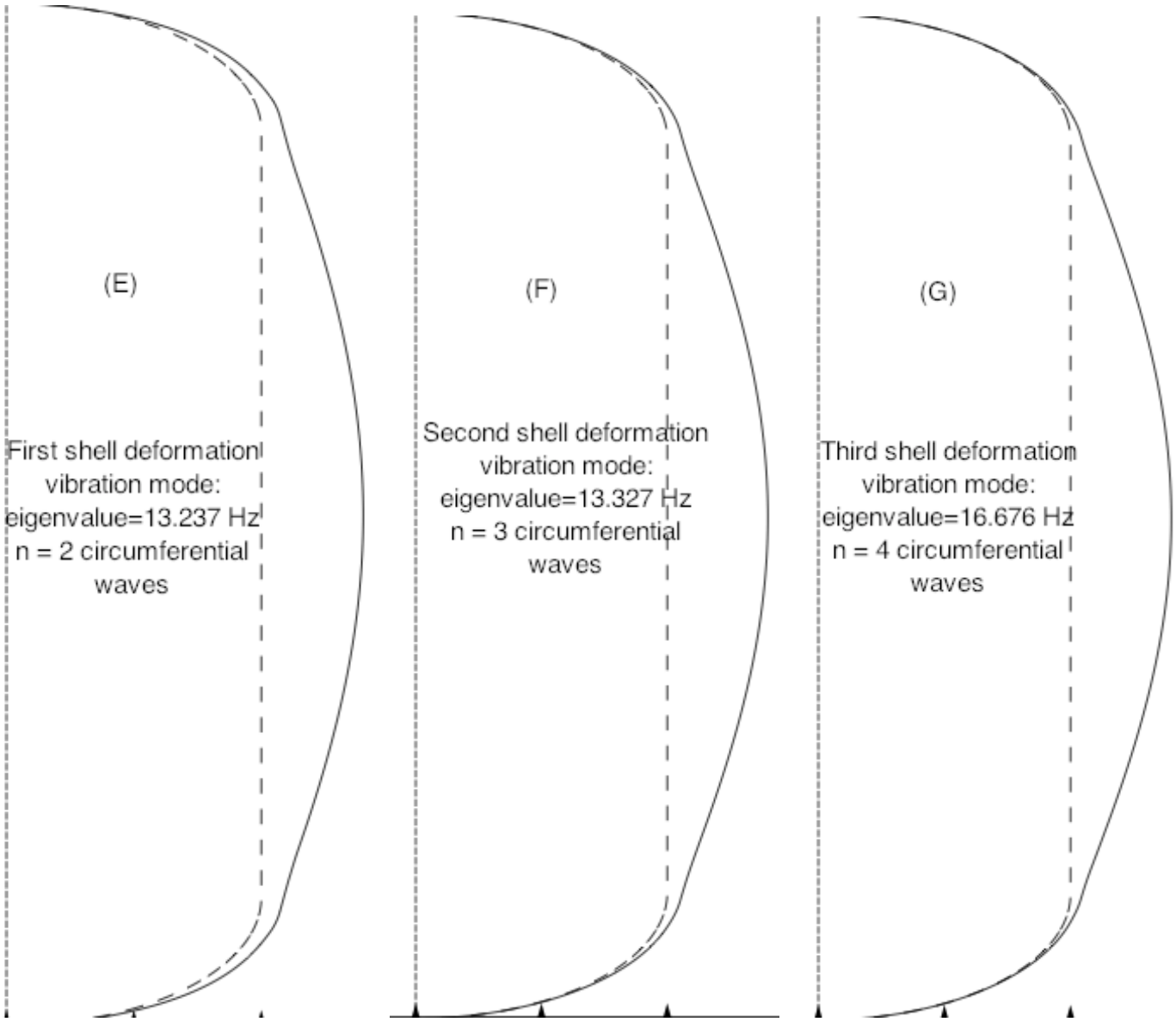

Fig. 16b **Three Vibration modes from GENOPT/TANK/BIGBOSOR4 for the optimized propellant tank with aft and forward sets of struts, 4 pairs of struts at each axial location. These are vibration modes in which the cylindrical part of the propellant tank deforms primarily as a thin shell, and there exists little extension and compression of the supporting struts.** The struts are not shown because BIGBOSOR4 cannot plot springs. Compare (E) with the prediction from STAGS shown in Fig. 25b, (F) with the predictions from STAGS shown in Figs. 25a and 25d, and (G) with the predictions from STAGS shown in Fig. 25f.

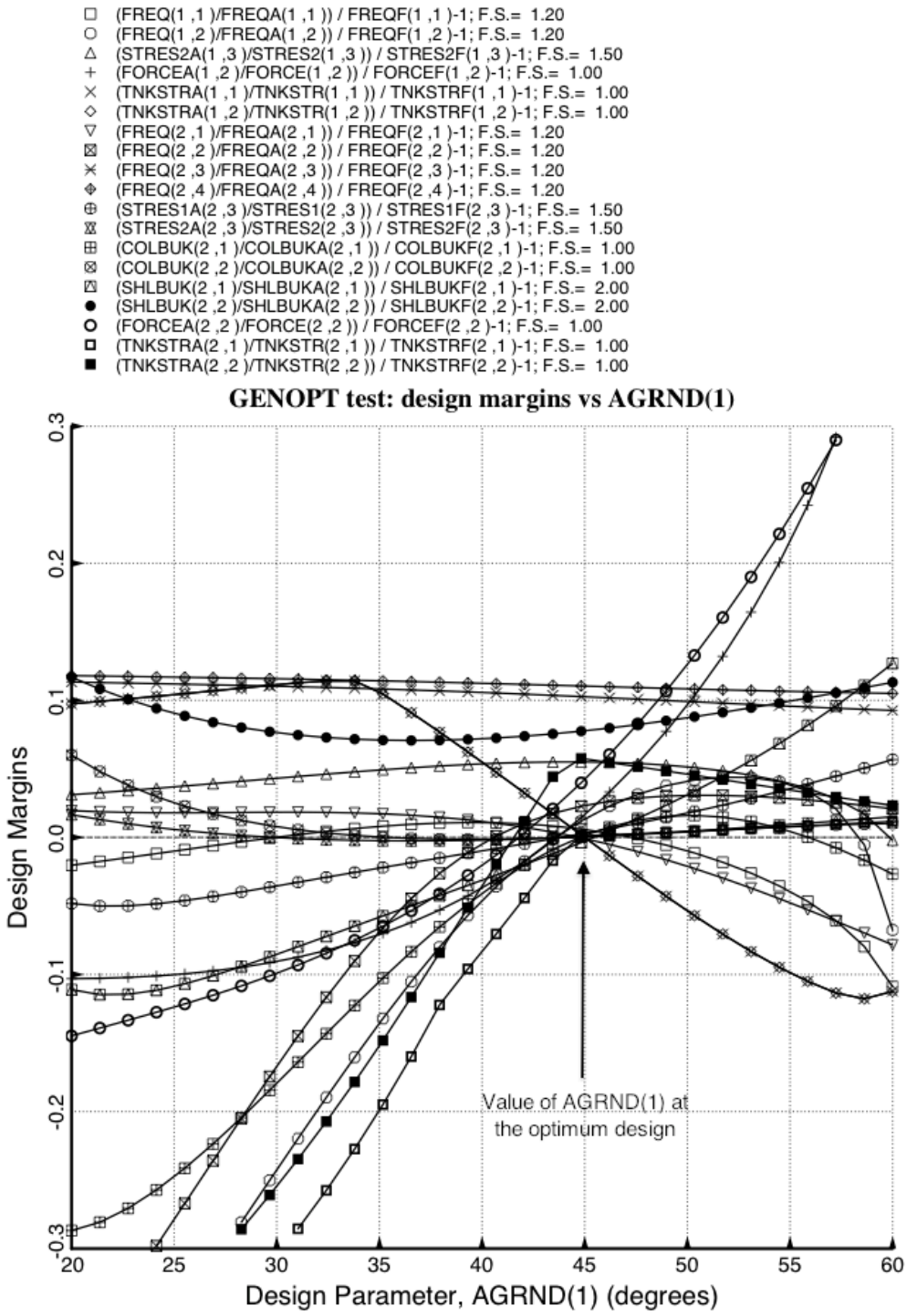

Fig. 17 Results from the specific case called "test": Optimized long propellant tank with two sets of struts (aft and forward), 4 pairs of struts in each set. Shown here are **"design sensitivity"** plots from an analysis in which all decision variables are held constant except for AGRND(1) = circumferential angle to the pinned "ground" end of the forward slanting strut in the first strut pair in the aft set of struts (Fig. 2). Typical behavior at the optimum design is exhibited: several margins are critical or near-critical at the optimum value of AGRND(1).

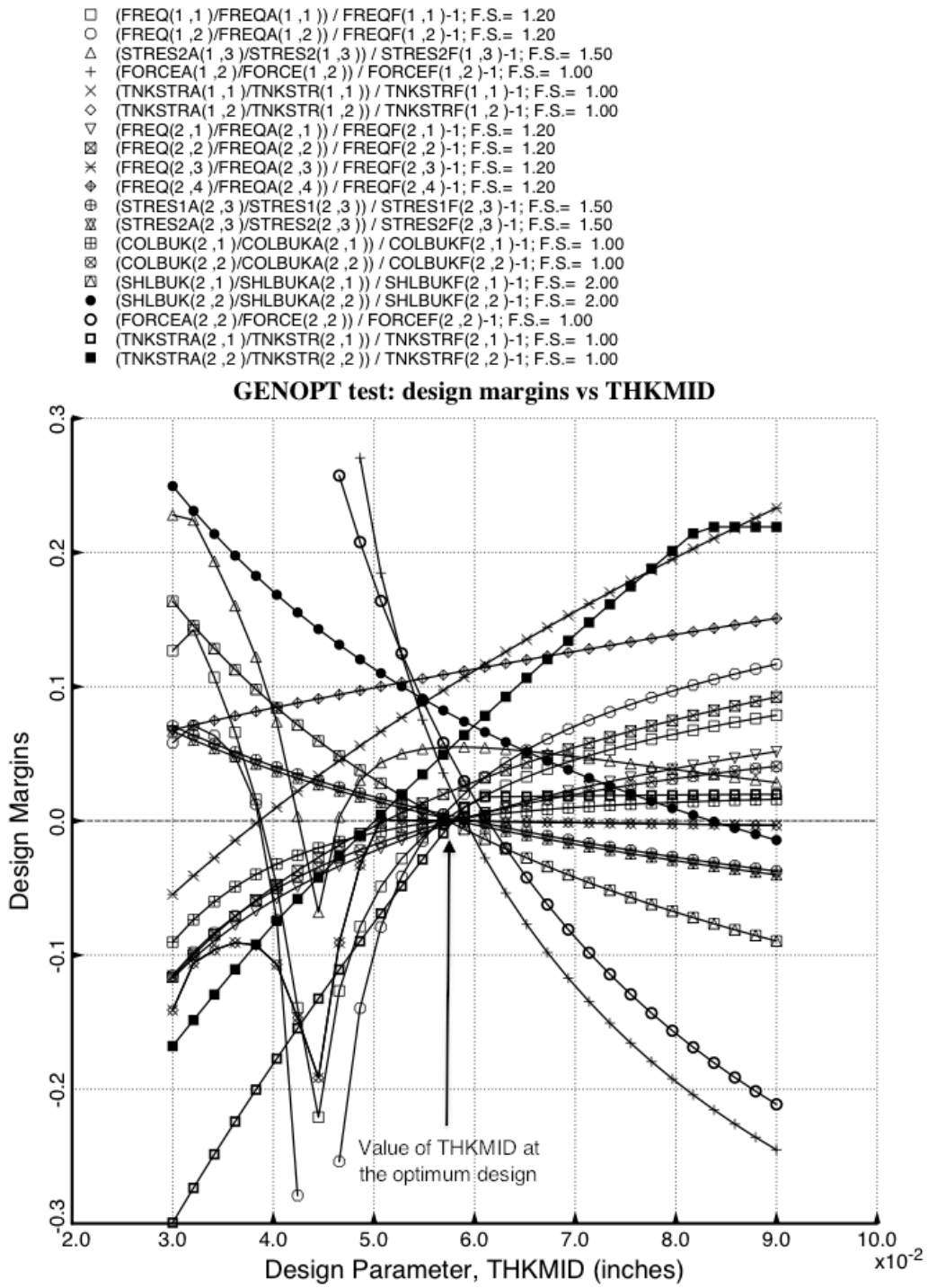

Fig. 18 Results from the specific case called "test": Optimized long propellant tank with two sets of struts (aft and forward), 4 pairs of struts in each set. Shown here are **"design sensitivity"** plots from an analysis in which all decision variables are held constant except for THKMID = thickness of the skin of the cylindrical part of the propellant tank (Fig. 1c). Typical behavior at the optimum design is exhibited: several margins are critical or near-critical at the optimum value of THKMID.

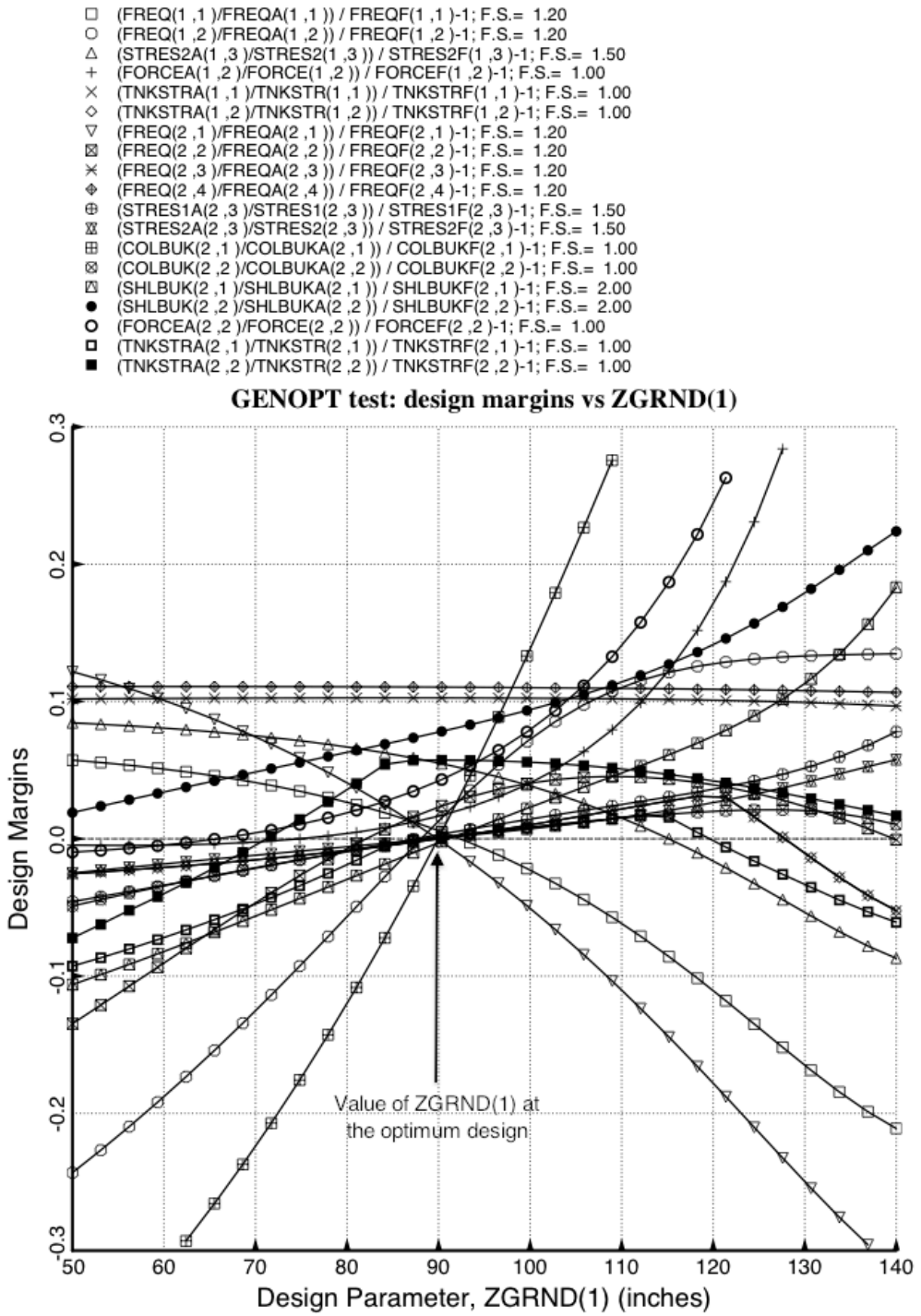

Fig. 19 Results from the specific case called "test": Optimized long propellant tank with two sets of struts (aft and forward), 4 pairs of struts in each set. Shown here are **"design sensitivity"** plots from an analysis in which all decision variables are held constant except for ZGRND(1) = the global axial coordinate of the "ground" ends of the aft set of struts (Fig.1a). Typical behavior at the optimum design is exhibited: several margins are critical or near-critical at the optimum value of ZGRND(1).

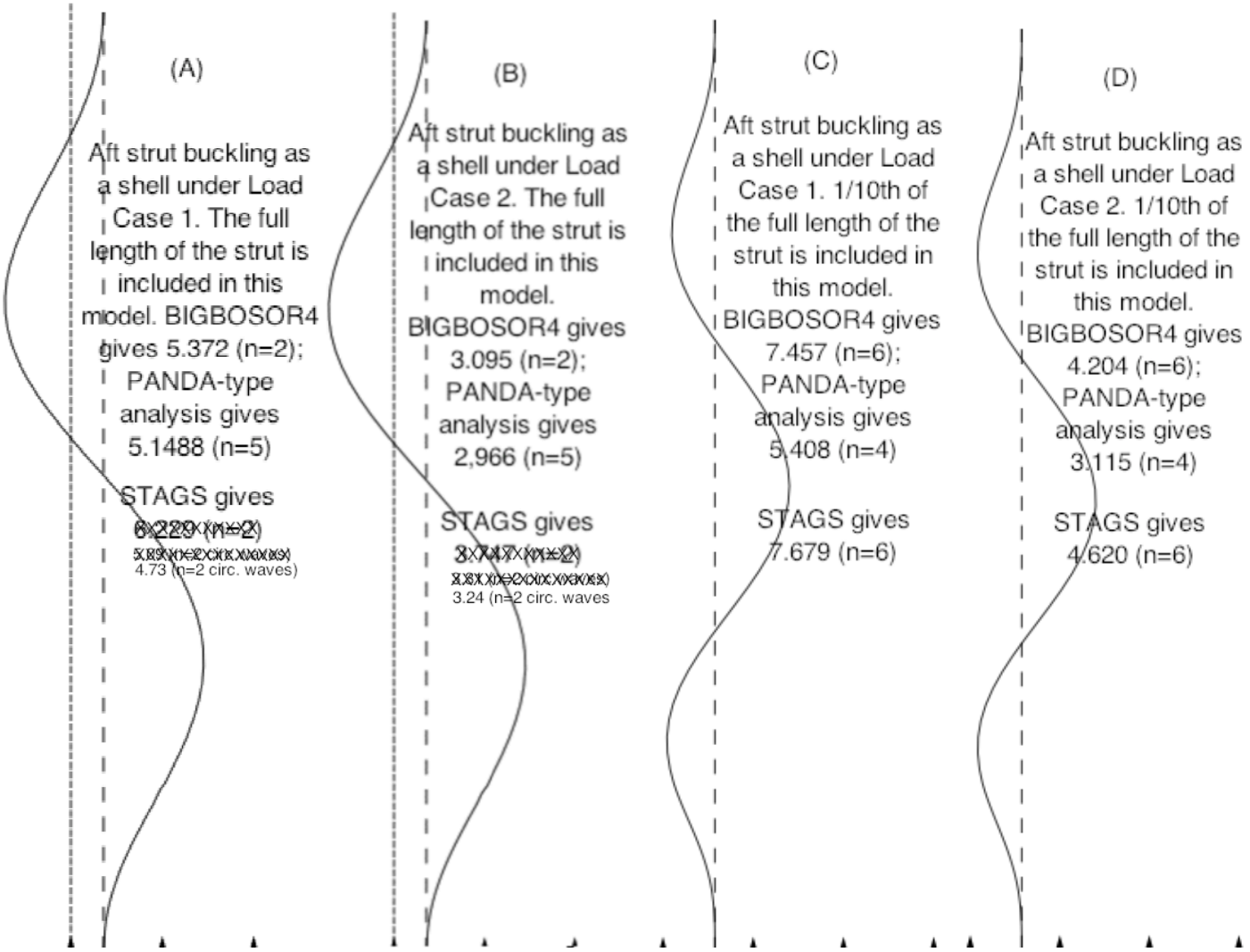

Fig 20 **Aft strut buckling mode shapes for the strut buckling as a thin shell rather than as a column**. For computation of the design margin corresponding to buckling of the strut as a thin shell, GENOPT selects the lower of the load factors from the BIGBOSOR4 model and the PANDA-type model [15]. The strut shell buckling mode shapes displayed here are predicted by BIGBOSOR4 for the optimized long propellant tank with two sets of struts, aft and forward, 4 pairs of struts in each set. Buckling load factors from BIGBOSOR4 [2,3], from a PANDA-type of analysis [15] and from STAGS [16 – 19] are listed. The differences in the BIGBOSOR4 and STAGS predictions for the buckling load factors in (A) and (B) are primarily due to the different predictions from GENOPT/TANK and STAGS of maximum compressive load in an aft strut in Load Case 1 (axial acceleration): -22693 lbs according to GENOPT/TANK and -24841 lbs according to STAGS, and in Load Case 2 (lateral acceleration): -39393 lbs according to GENOPT/TANK and -36298 lbs according to STAGS. [See Table 7(b).]. The shell buckling modes shown in Parts (A) and (B) are from strut models that contain the entire length of the strut minus the lengths of the end fittings. The shell buckling modes shown in Parts (C) and (D) are from strut models that contain only 1/10th of that length. Notice that the buckling load factors predicted from the PANDA-type model are much less sensitive to the length of strut included in the strut shell buckling model than are the load factors predicted by BIGBOSOR4 and STAGS.

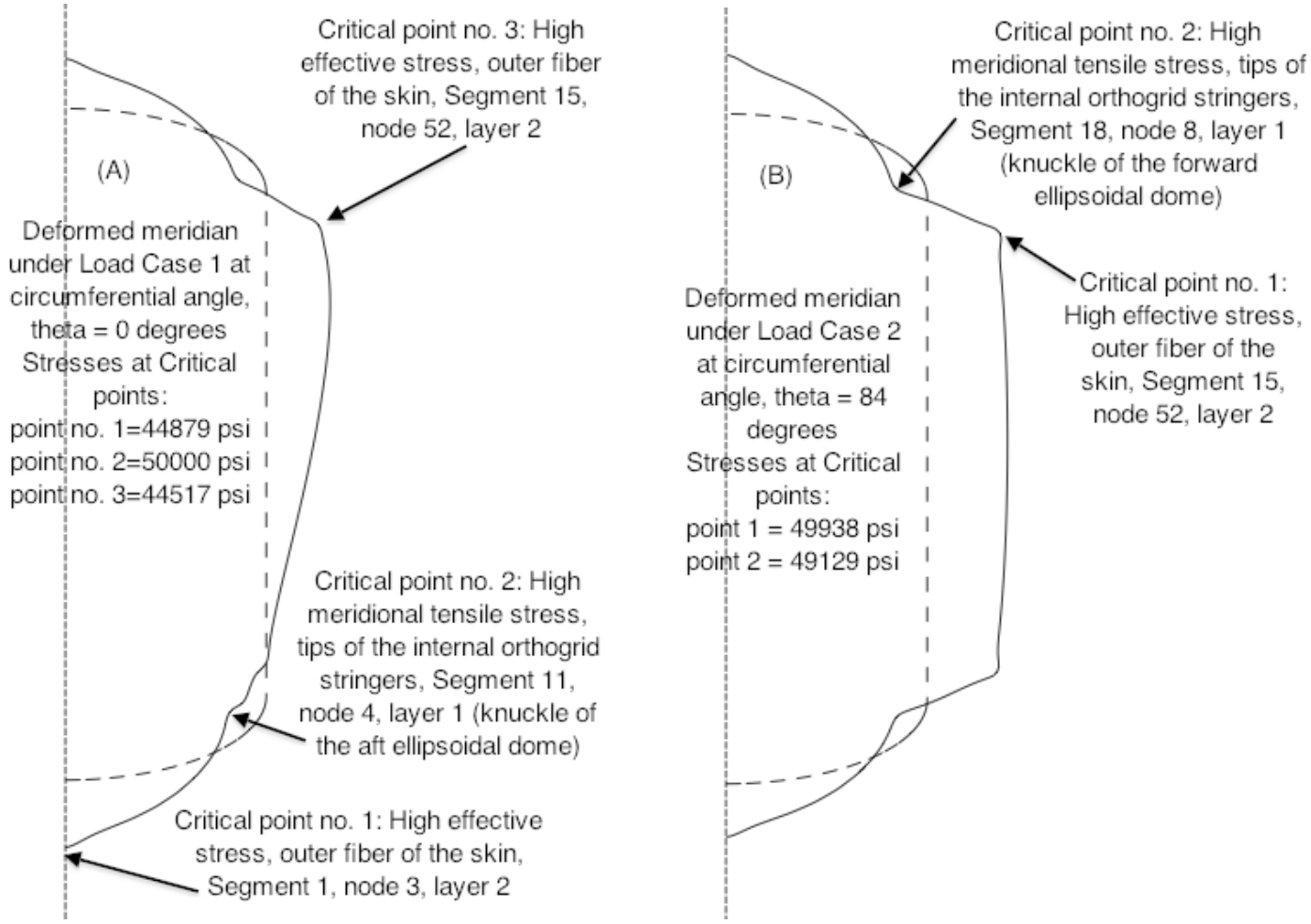

Fig. 21a **Deformed meridians, critical and near-critical stresses and their locations under (A) Load Case 1 (10g axial acceleration plus 25 psi internal pressure + 200-degree tank cool-down) and (B) Load Case 2 (10g lateral acceleration plus 25 psi internal pressure + 200-degree tank cool-down) as predicted from the GENOPT/TANK model of the specific case called "test"**. (See Figs. 4 – 6.) The struts are not shown because in the linear non-axisymmetric stress analysis the struts are replaced in the GENOPT/BIGBOSOR4 model by the concentrated loads that they apply to the propellant tank. Compare the maximum stresses shown here with the STAGS predictions of the maximum stresses plotted in Figs. 26a-26f for Load Case 1 and in Figs. 27a and 27b for Load Case 2. The deformations of the lower and upper domes are entirely caused by the 25 psi uniform internal ullage pressure plus the linearly varying normal propellant pressure heads generated from the 10g axial and lateral acceleration components. The somewhat odd appearances of these axisymmetric deformations in the immediate neighborhoods of the apexes of the domes (very local outward bulges) are caused by the following: 1. The innermost layer of the dome, which represents the internal orthogrid with smeared stiffeners, is orthotropic rather than isotropic because the thickness and spacing of the optimized orthogrid stringers (STRTHK=0.1370 and STRSPC=3.426 inches, respectively) are different from those of the orthogrid rings (RNGTHK=0.3431 and RNGSPC=4.042 inches, respectively). 2. The pole conditions imposed by BIGBOSOR4 at the apexes of domes are strictly valid only for isotropic material. The STAGS model displayed in Figs. 26a and 26c show a similar local outward bulge.

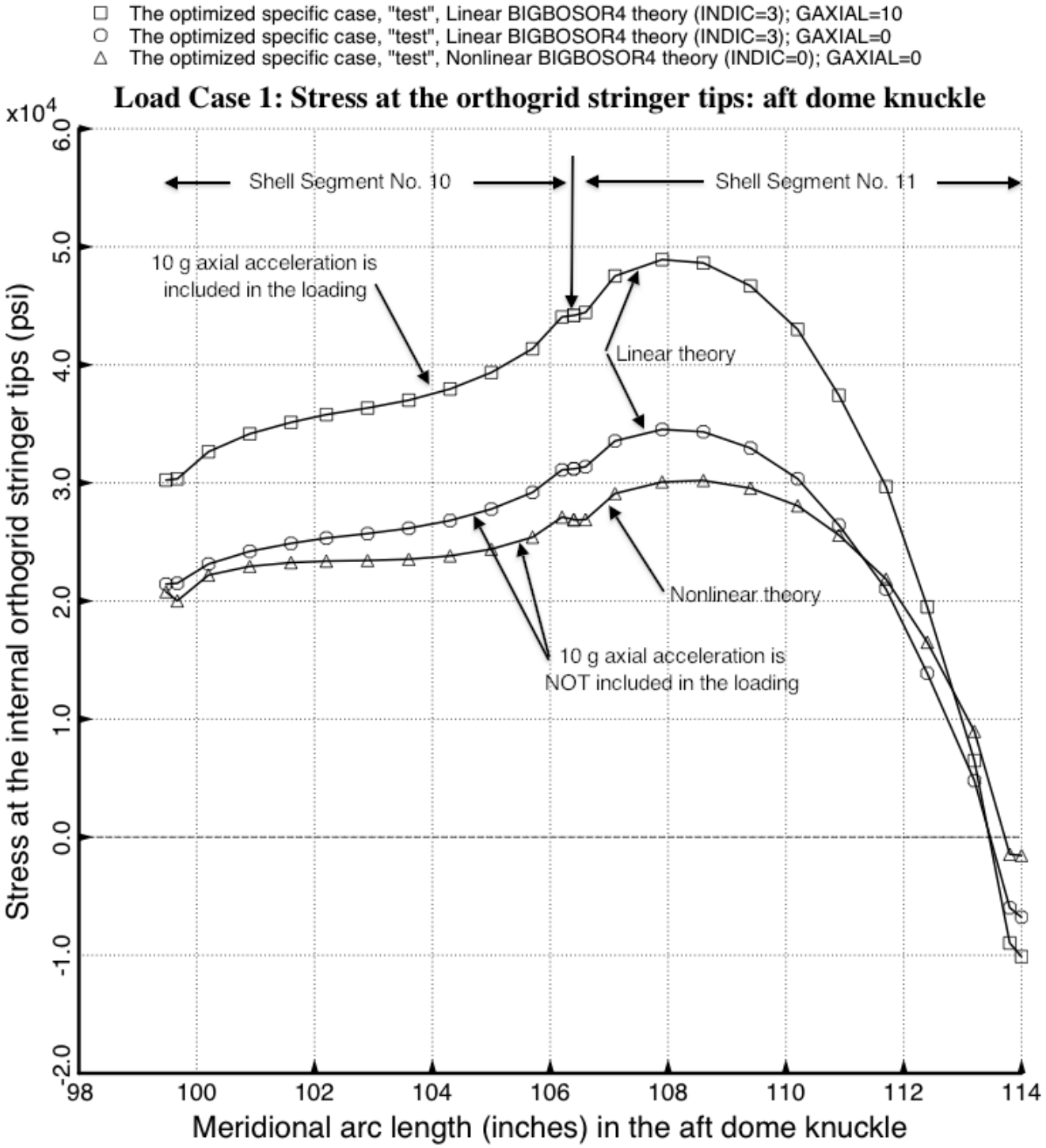

Fig. 21b **Stress from Load Case 1 at the tips of the internal orthogrid stringers in the knuckle region of the aft ellipsoidal dome of the optimized propellant tank from three different BIGBOSOR4 models**. The thermal loading (tank cool-down) and the concentrated loads applied by the struts to the propellant tank were not included in the BIGBOSOR4 models that generated the curves shown here. The locations of shell segments 10 and 11 are indicated in Fig. 1b.

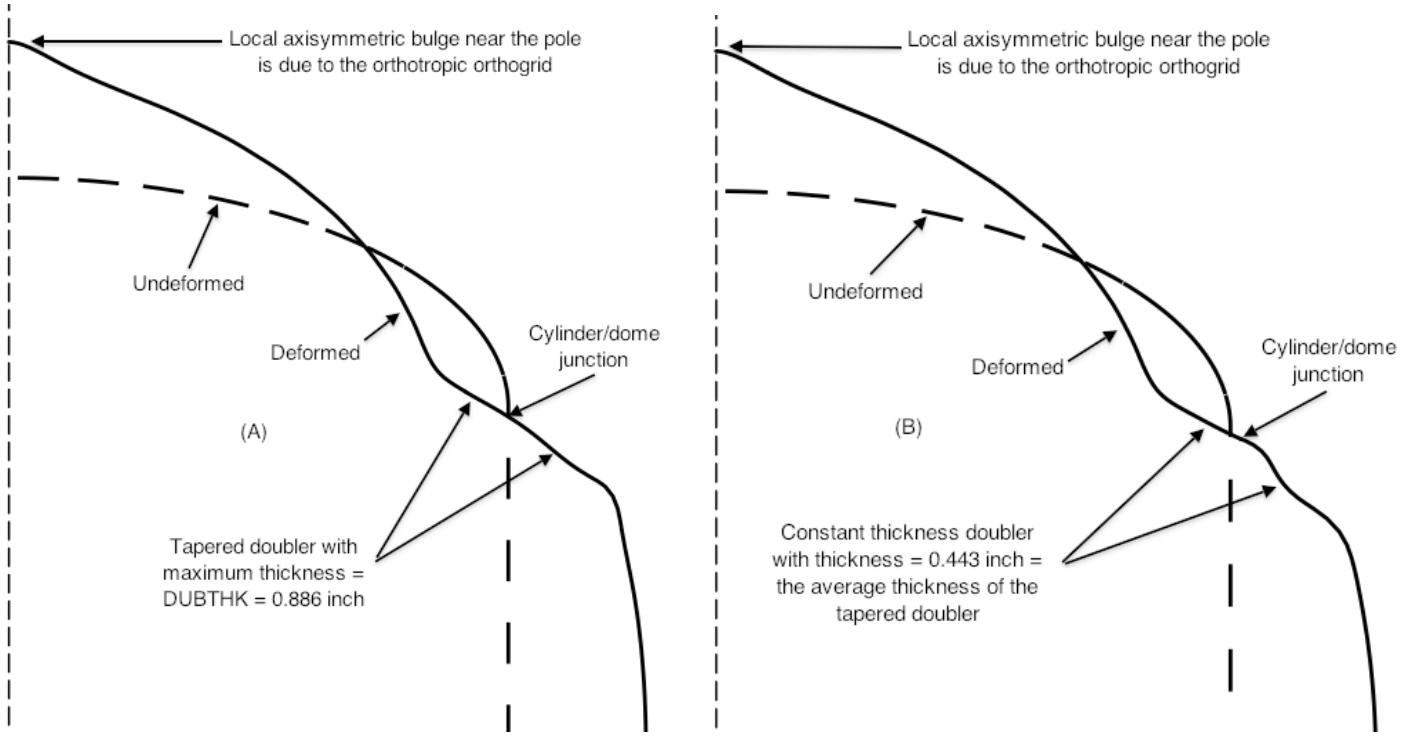

Fig. 21c **Enlarged views of the prebuckled states of the forward part of the optimized "test" propellant tank as deformed under Load Case 1 (10g axial acceleration + 25 psi internal pressure + 200-degree tank cool-down) along the meridian at the circumferential coordinate, theta = 6.0 degrees, as predicted by two GENOPT/BIGBOSOR4 models.** (A) The external doubler, approximately centered at the junction of the forward dome with the cylindrical part of the tank (Figs. 1b and 1c), is double-linearly tapered as shown in Fig. 1c, with its maximum thickness, DUBTHK = 0.886 inch, at the dome/cylinder junction, which is also where the forward ring of struts is attached to the centroid of the forward external propellant tank support ring. (B) The same overall geometry except that the external doubler has constant thickness over its entire 30-inch axial width equal to 0.443 inch, which is equal to the average thickness of the double-linearly tapered doubler. The deformation shown in (A) is the same as that shown in part (A) of Fig. 21a. The compressive stress at the forward dome/cylinder junction at the tips of the internal orthogrid stringers corresponding to (A) is about –23000 psi. **The maximum compressive stress at the same location corresponding to (B) is about –119000 psi, as shown in Fig. 21d.** This huge difference in the maximum compressive stress at the tips of the internal orthogrid stringers at the forward dome/cylinder junction is caused by the huge difference in the amount of local meridional bending of the wall of the propellant tank there (approximately midway between the two arrows), evident when the local deformation shown in (A) is compared with that in (B). **The STAGS models correspond to (B).** The maximum compressive stress at the tips of the orthogrid stringers predicted by the STAGS 360-degree model is close to –41240 psi, as shown in Fig. 26b and that predicted by the STAGS refined 45-degree model is close to –114000 psi, as shown in Fig. 26f. The STAGS 360-degree model shown in Fig. 24 is adequate for the prediction of vibration modal frequencies and buckling load factors, but not for the prediction of very localized stress concentrations that occur in the propellant tank where the struts apply concentrated loads. **The difference in predictions from the BIGBOSOR4 model with tapered doublers (A) and that with constant thickness doublers (B) highlights the need for a STAGS model with tapered doublers.**

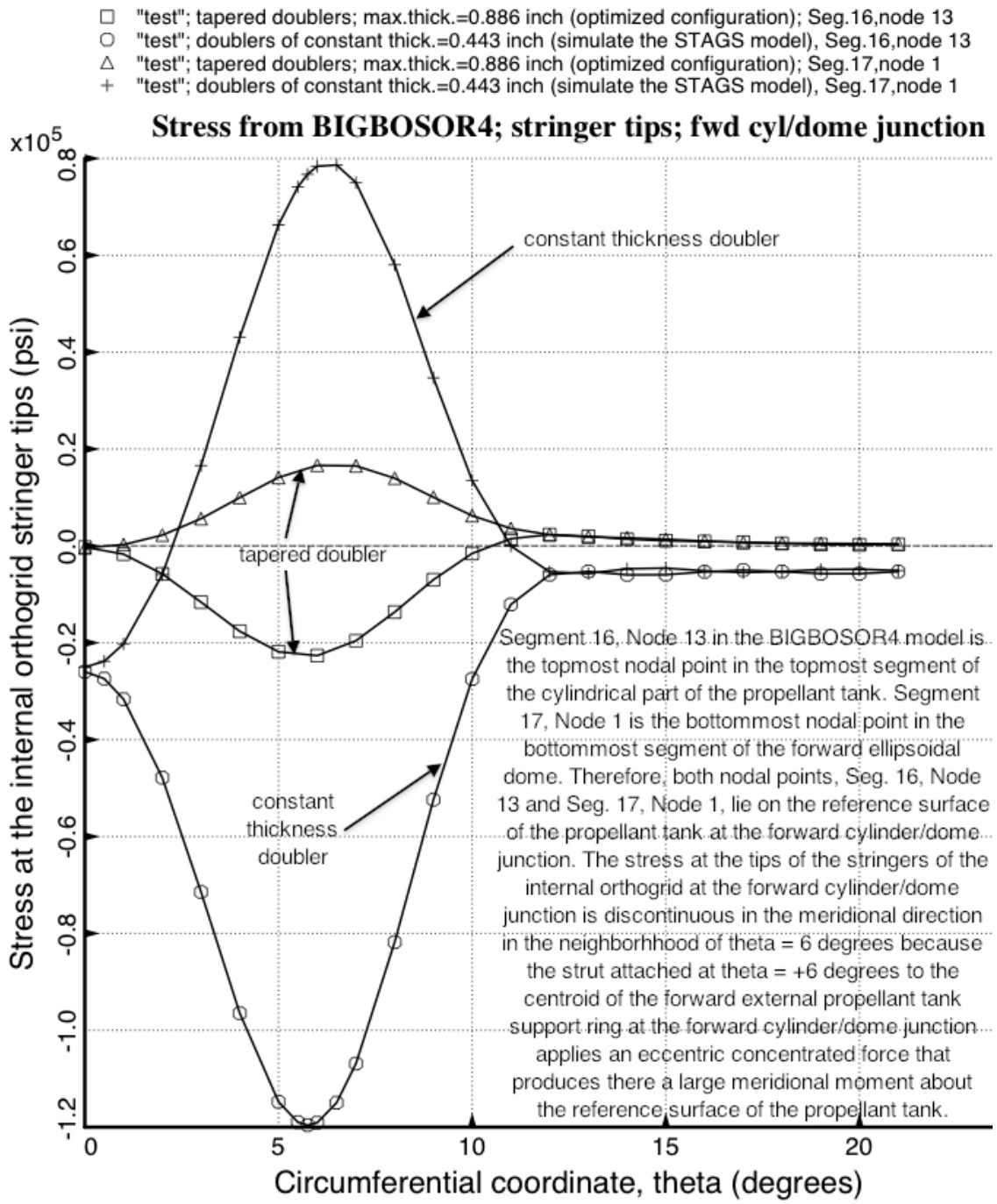

Fig. 21d The specific case, "test", propellant tank under **Load Case 1** (10 g axial acceleration, 25 psi internal pressure and 200 degree tank cool-down). **Plots of the stress at the tips of the internal orthogrid stringers from two BIGBOSOR4 models: Model 1 has tapered doublers with maximum thickness = 0.886 inch (the optimized configuration) and Model 2 has constant thickness doublers with thickness = 0.443 inch** (BIGBOSOR4 simulation of the STAGS model). The dramatic difference in the prediction of maximum stress from the two BIGBOSOR4 models, Model 1 and Model 2, arises mainly from the dramatic difference in the maximum meridional curvature changes at the forward cylinder/dome junction near the pinned struts (Fig.21c).

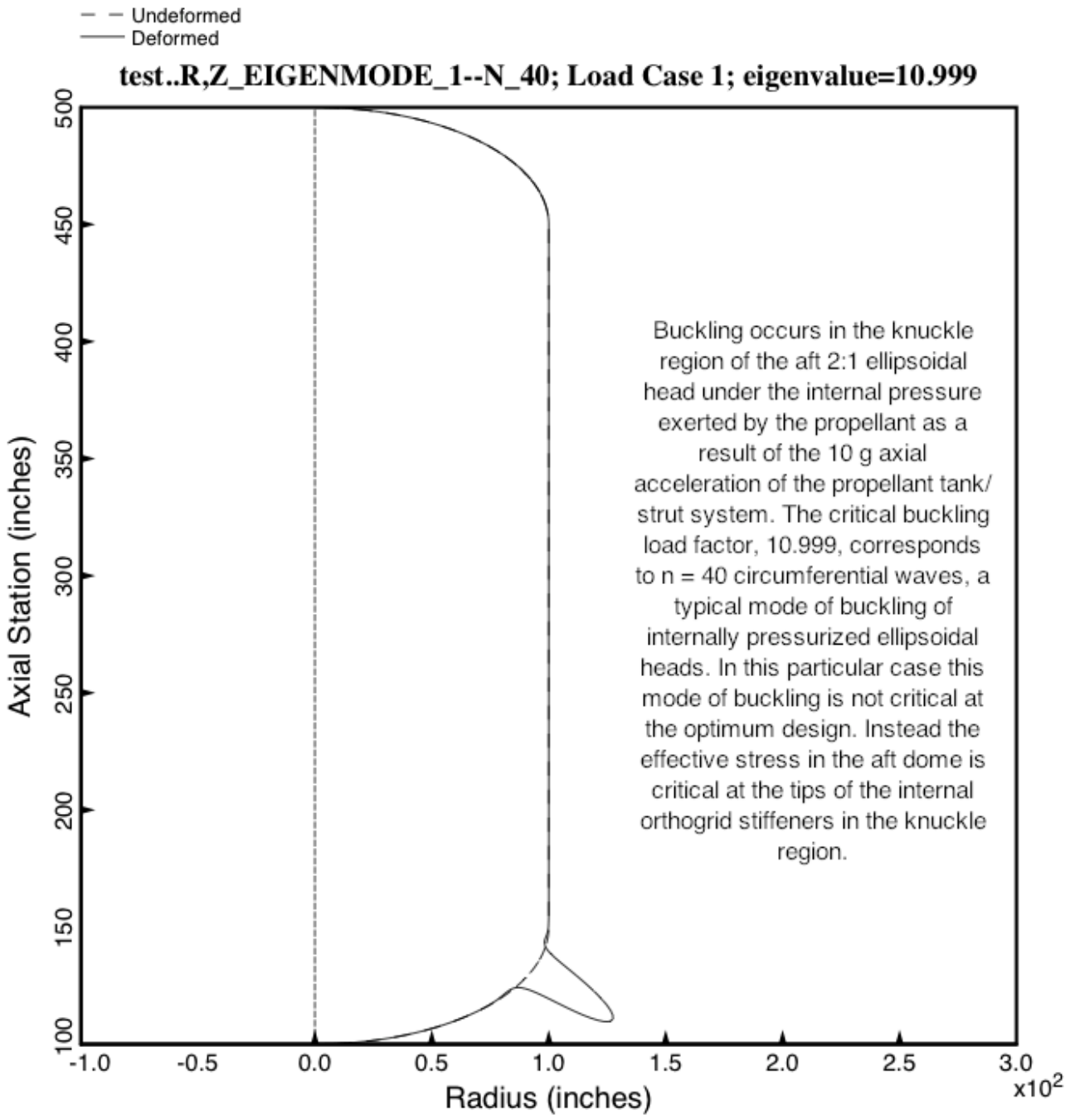

Fig. 22 Results from the specific case called "test": Optimized long propellant tank with two sets of struts (aft and forward), 4 pairs of struts in each set. **Shown here is the buckling mode of the propellant tank under Load Case 1**, 10g axial acceleration (upward acceleration). The aft dome buckles before the forward dome because the internal pressure exerted by the axially accelerating propellant is greatest at the bottom of the tank. NOTE: The buckling load factor would have been much less than 10.999 if the 25-psi internal ullage pressure had been included in Load Set A rather than in Load Set B (4.107 as listed in Fig. 31 versus 10.999 listed here).

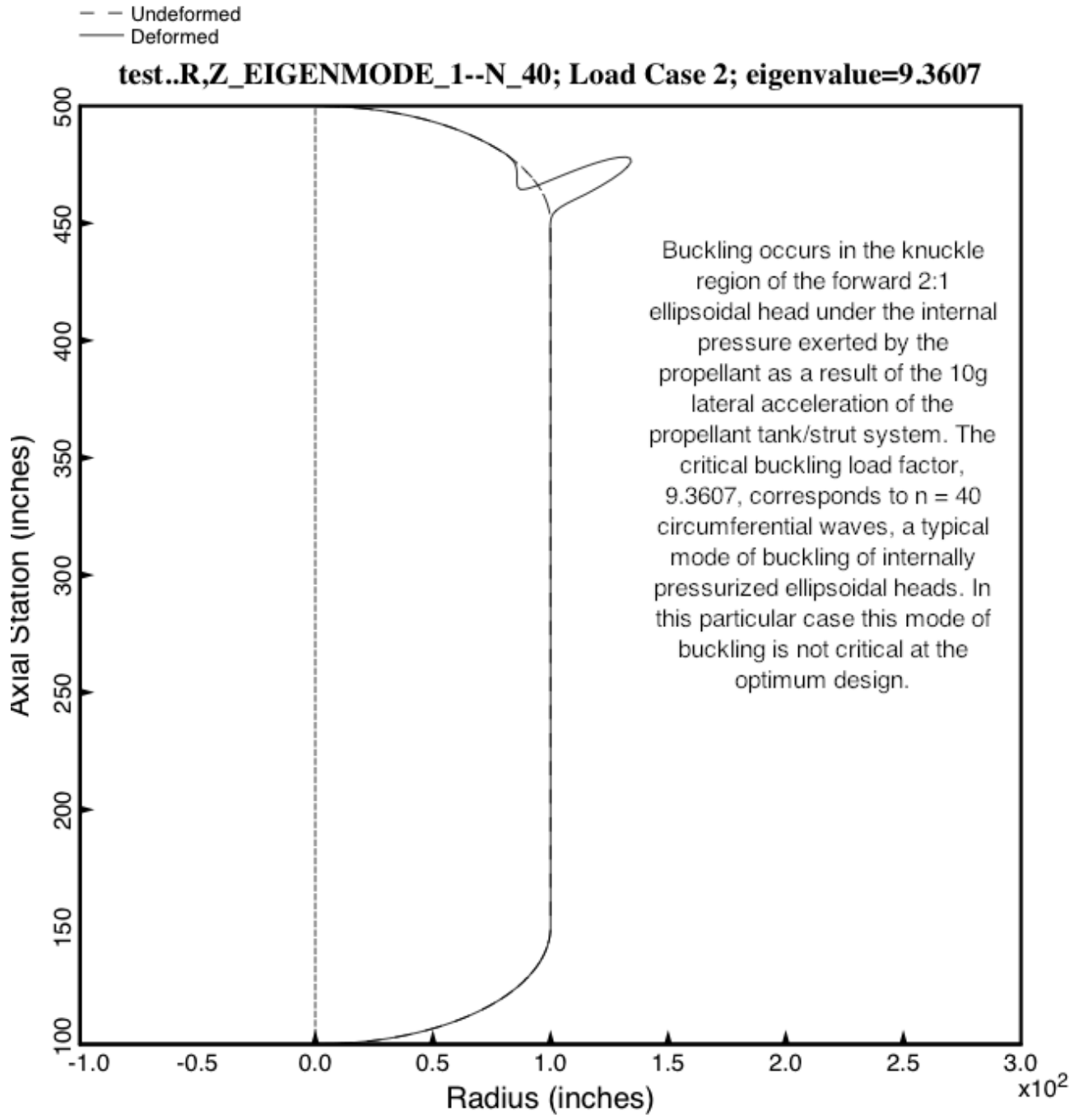

Fig. 23 Results from the specific case called "test": Optimized long propellant tank with two sets of struts (aft and forward), 4 pairs of struts in each set. **Shown here is the buckling mode of the propellant tank under Load Case 2, 10g lateral acceleration (leftward acceleration).** The forward dome buckles at a lower load factor than the aft dome because the skin thickness of the forward dome, THKFWD = 0.05775 inch, is significantly less than the skin thickness of the aft dome, THKAFT = 0.07150 inch.

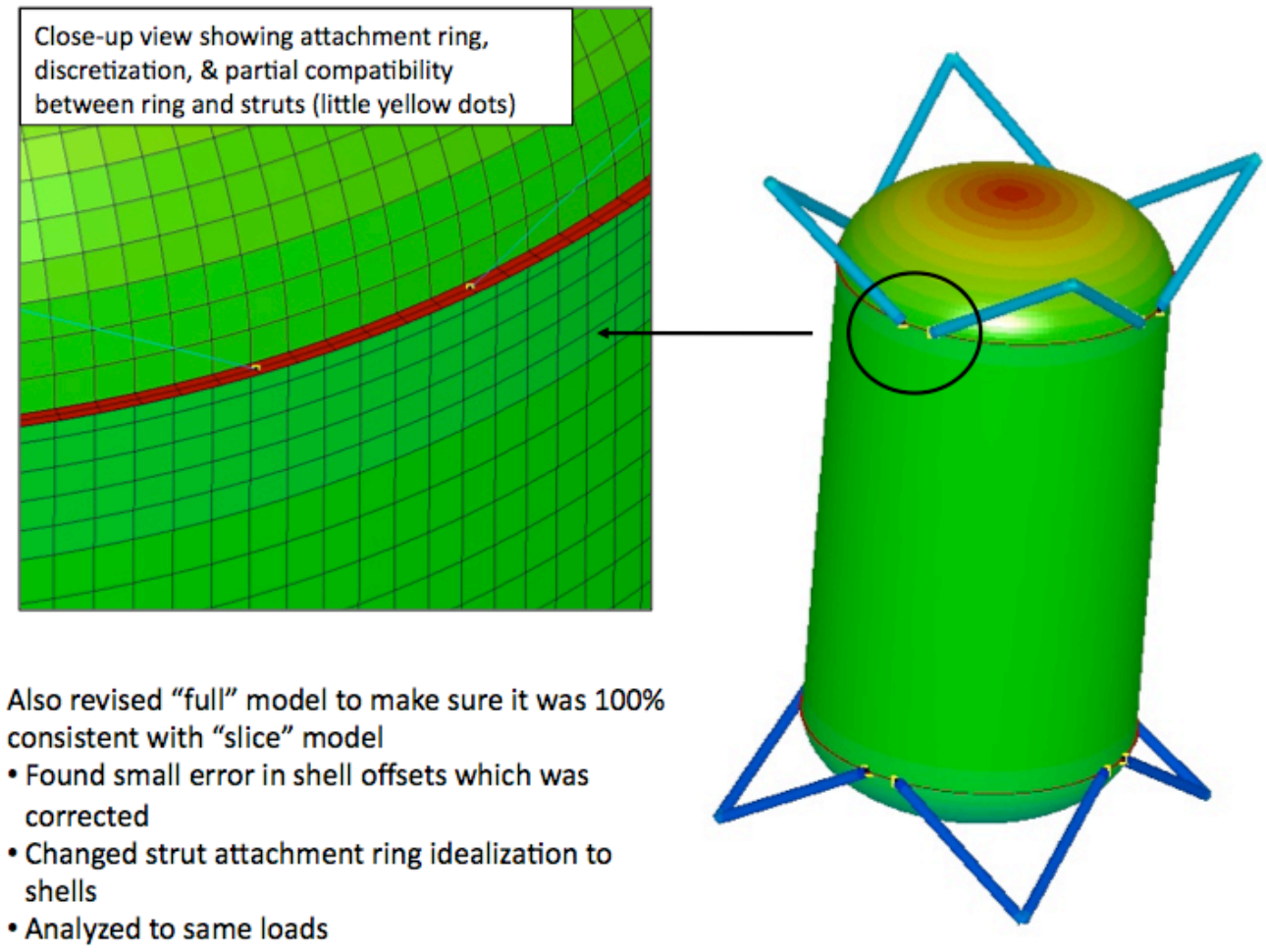

Fig. 24 **STAGS finite element model of the optimized long propellant tank with two sets of struts, aft (Lower) and forward (Upper), with 4 pairs of struts at each axial location.** The struts are pinned to the centroids of the aft and forward propellant tank external support rings and to rigid "ground". The STAGS "410" finite element is used in the model of the propellant tank shell wall.

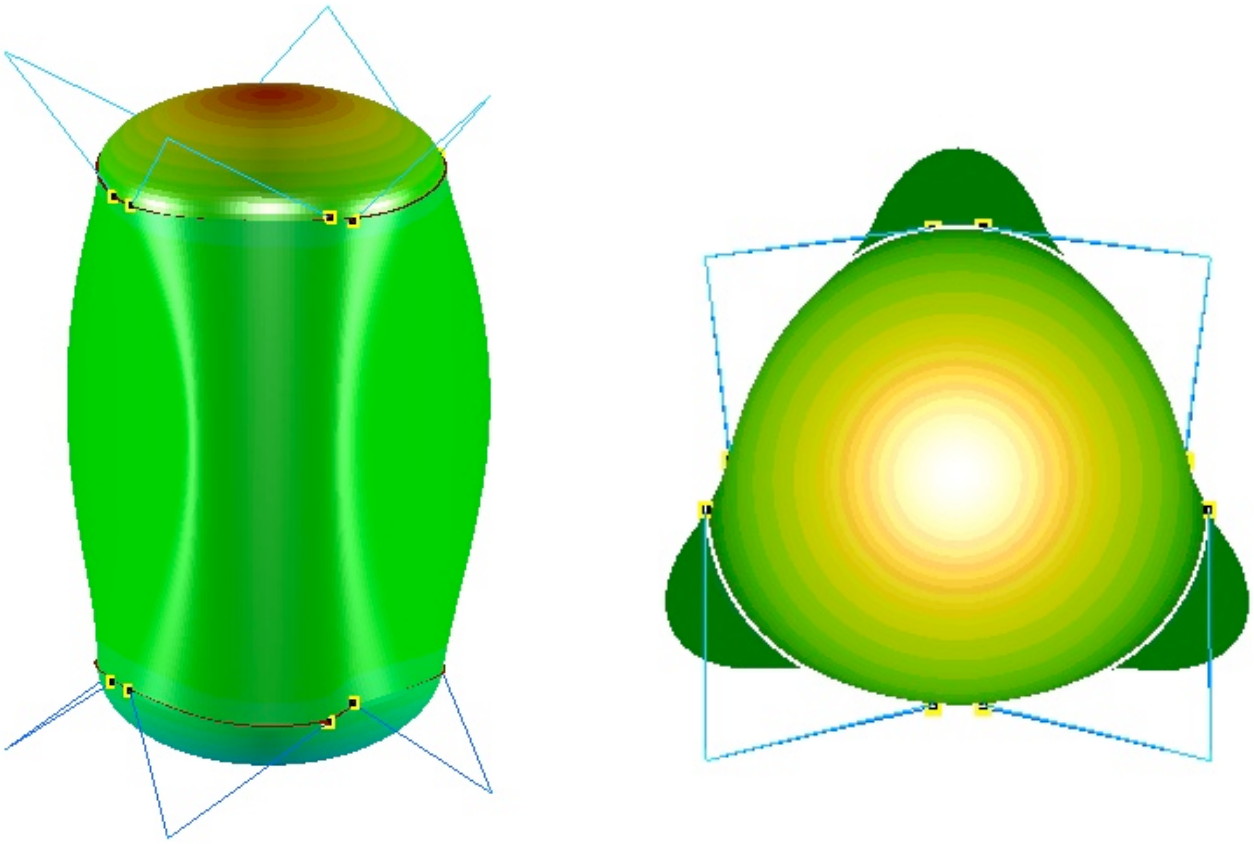

Fig. 25a **The lowest vibration mode from the STAGS model. The modal vibration frequency predicted by STAGS is 12.19 Hz.** This mode is a combination of shell deformation with n = 3 circumferential waves and uniform lateral motion of the propellant tank approximately as a rigid body with significant tension and compression in the supporting struts. The lateral tank motion with associated tension and compression in the struts can most easily be appreciated from the image on the right-hand side of this figure. In that image the uniform lateral component of the total motion of the tank is upward in the plane of the paper. The two components of vibration motion, lateral tank motion and n = 3 shell deformation motion, which are combined in a single mode in this STAGS model, are decoupled in the GENOPT/BIGBOSOR4 model displayed in Figs. 16a and 16b: the lateral/pitching motion depicted in Fig. 16a(C) with a frequency of 12.161 Hz and the n = 3 shell deformation motion depicted in Fig. 16b(F) with a frequency of 13.327 Hz.

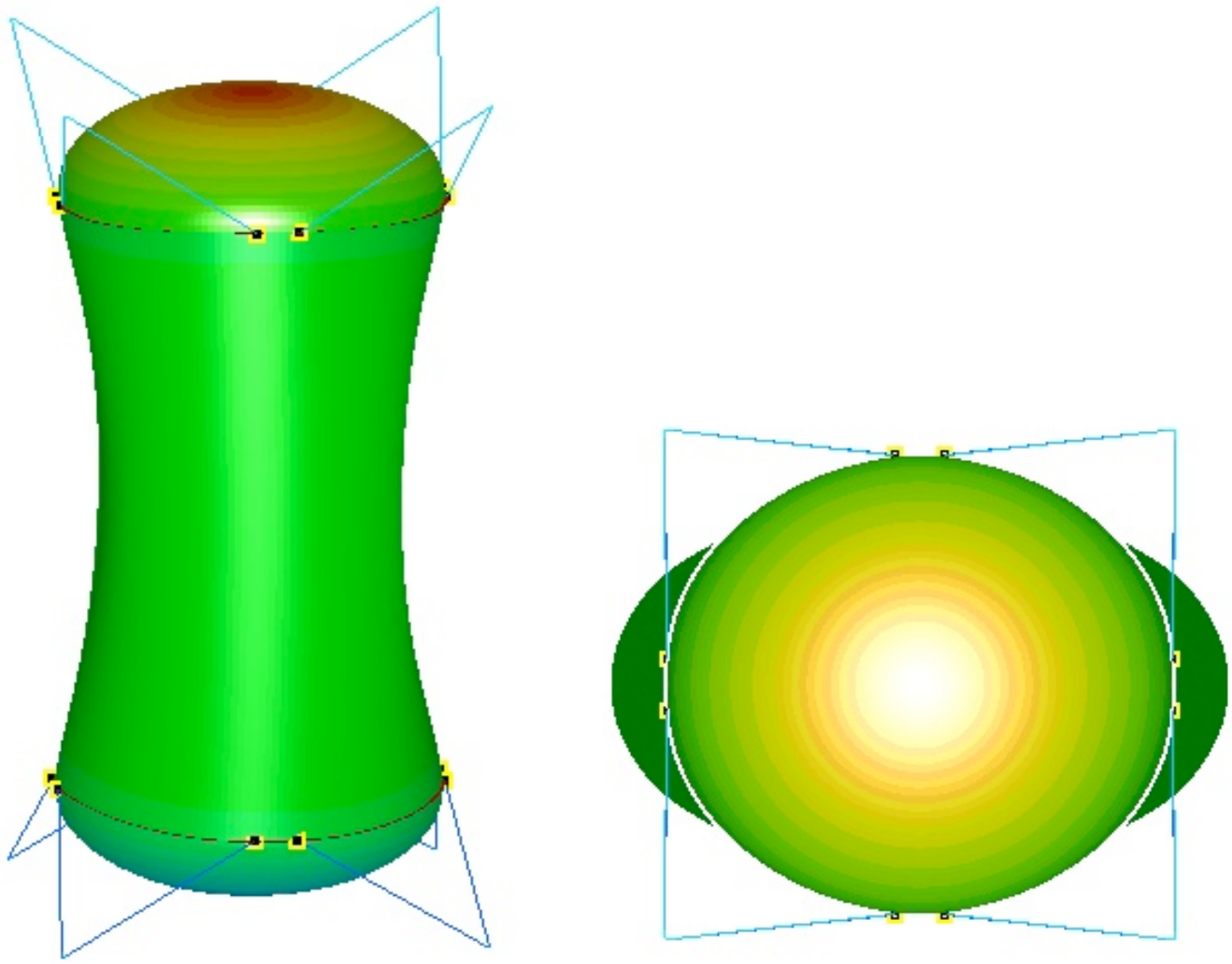

Fig. 25b **The second vibration mode from the STAGS model. The modal vibration frequency predicted by STAGS is 13.02 Hz**. This mode is essentially pure shell deformation with n = 2 circumferential waves. The analogous n = 2 shell deformation mode predicted by GENOPT/BIGBOSOR4 is displayed in Fig. 16b(E) with its associated modal vibration frequency equal to 13.237 Hz.

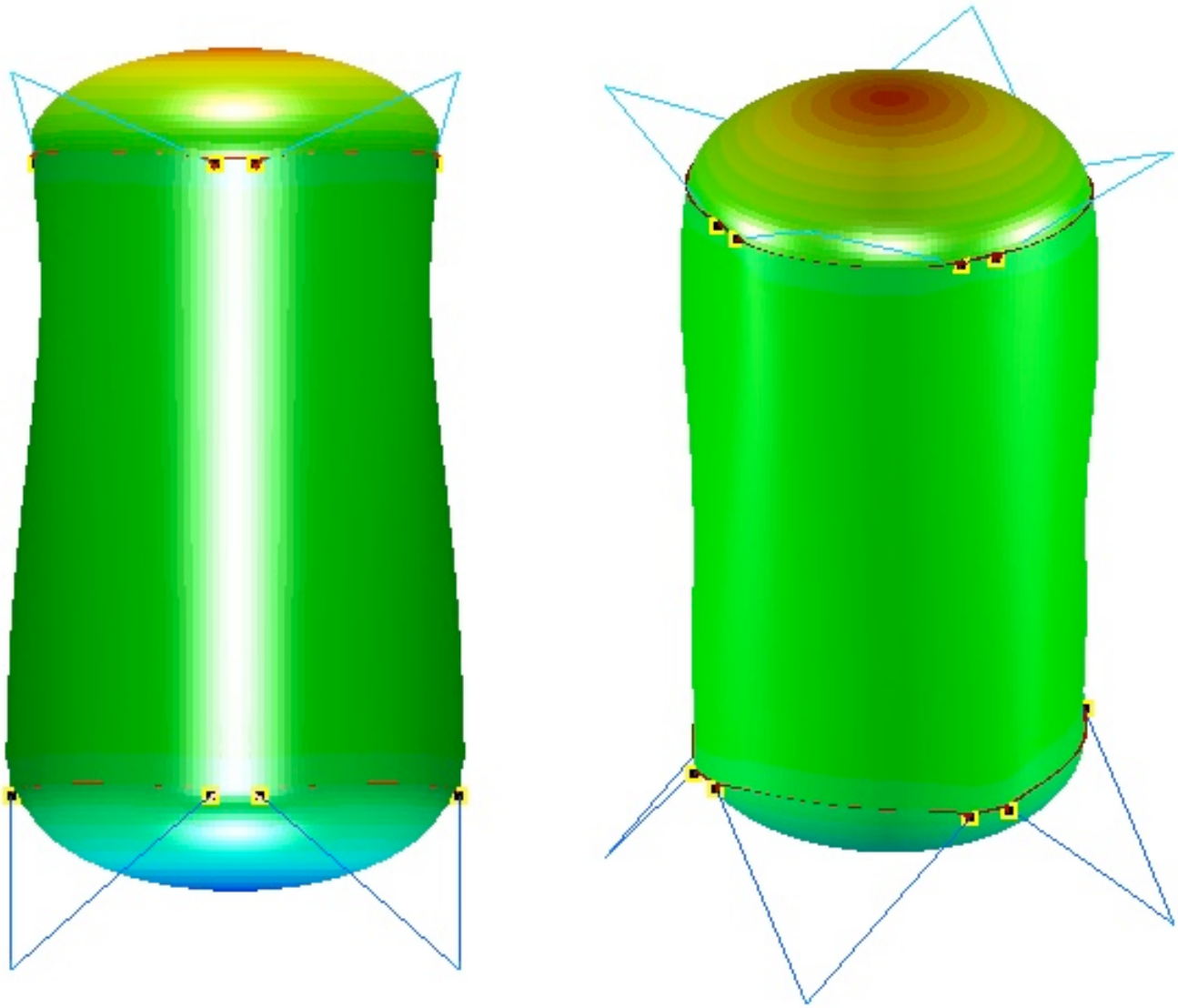

Fig. 25c **Two views of the third vibration mode from the STAGS model. The modal vibration frequency predicted by STAGS is 13.46 Hz.** This mode is a combination of shell "breathing" (n = 0 circumferential waves) and axial motion of the propellant tank approximately as a rigid body with significant tension and compression in the supporting struts. The axial tank motion with associated tension in the lower set of struts and compression in the upper set of struts can most easily be appreciated from the image on the left-hand side of the figure. In that image the axial component of the total motion of the tank is upward in the plane of the paper, as can be seen by the deformation of the aft struts (elongation) versus that of the forward struts (shortening). The axial motion of the propellant tank in the GENOPT/BIGBOSOR4 model is shown in Fig. 16a(A). It is associated with the modal vibration frequency 12.069 Hz, which is the lowest frequency determined by the GENOPT/BIGBOSOR4 model.

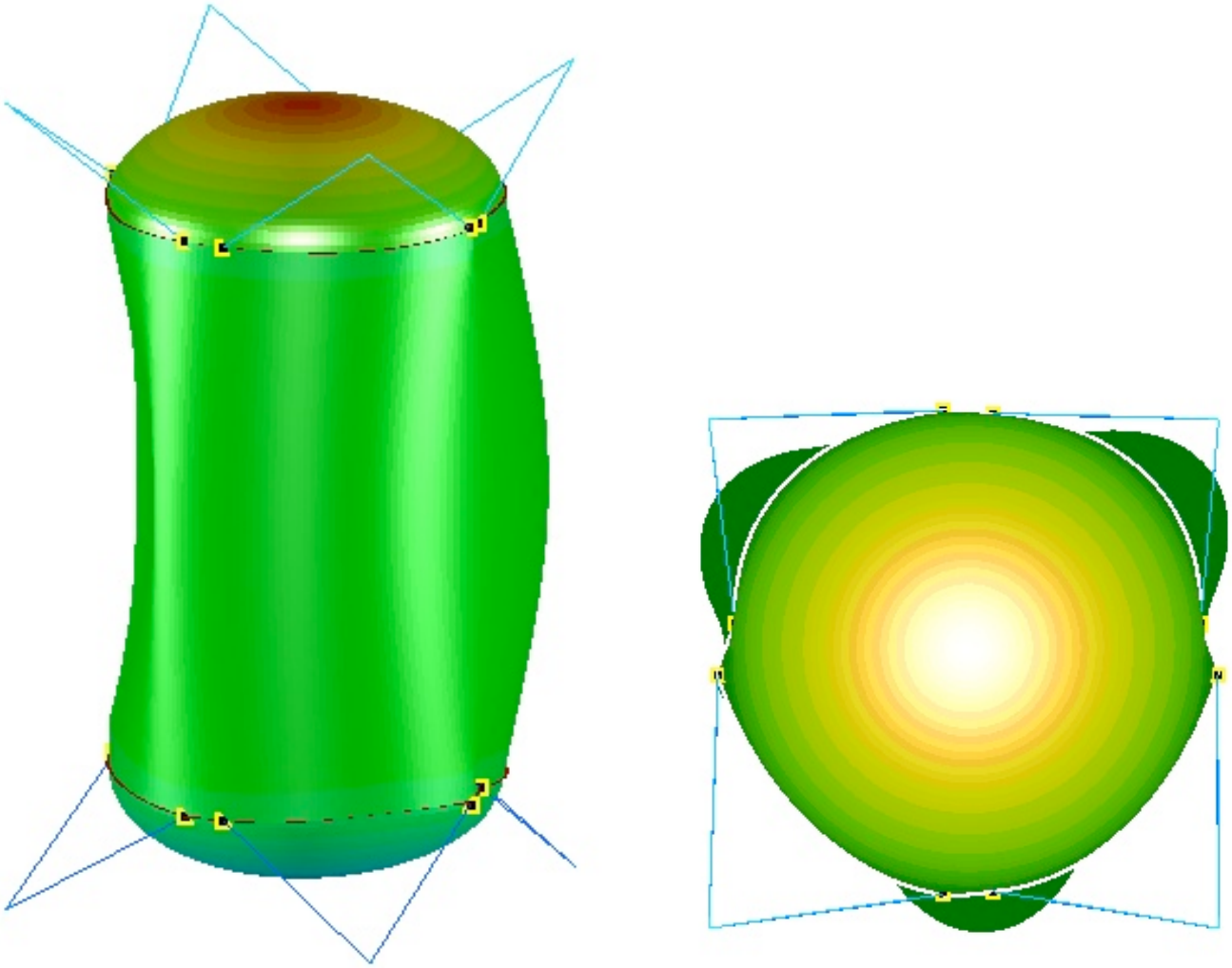

Fig. 25d **The fourth vibration mode from the STAGS model. The modal vibration frequency predicted by STAGS is 13.90 Hz.** This mode is analogous to that displayed by the STAGS model in Fig. 25a: a combination of shell deformation with n = 3 circumferential waves and uniform lateral motion of the propellant tank approximately as a rigid body with significant tension and compression in the supporting struts. While the two superficially similar STAGS vibration modes that are orthogonal to each other shown here and in Fig. 25a can exist, there is no analogous situation in which there exist multiple modes with primarily lateral tank motion in the decoupled GENOPT/BIGBOSOR4 model. As with Fig. 25a, the two components of total motion from STAGS shown here should be compared with the predictions from GENOPT/BIGBOSOR4 shown in Figs. 16a(C) and 16b(F).

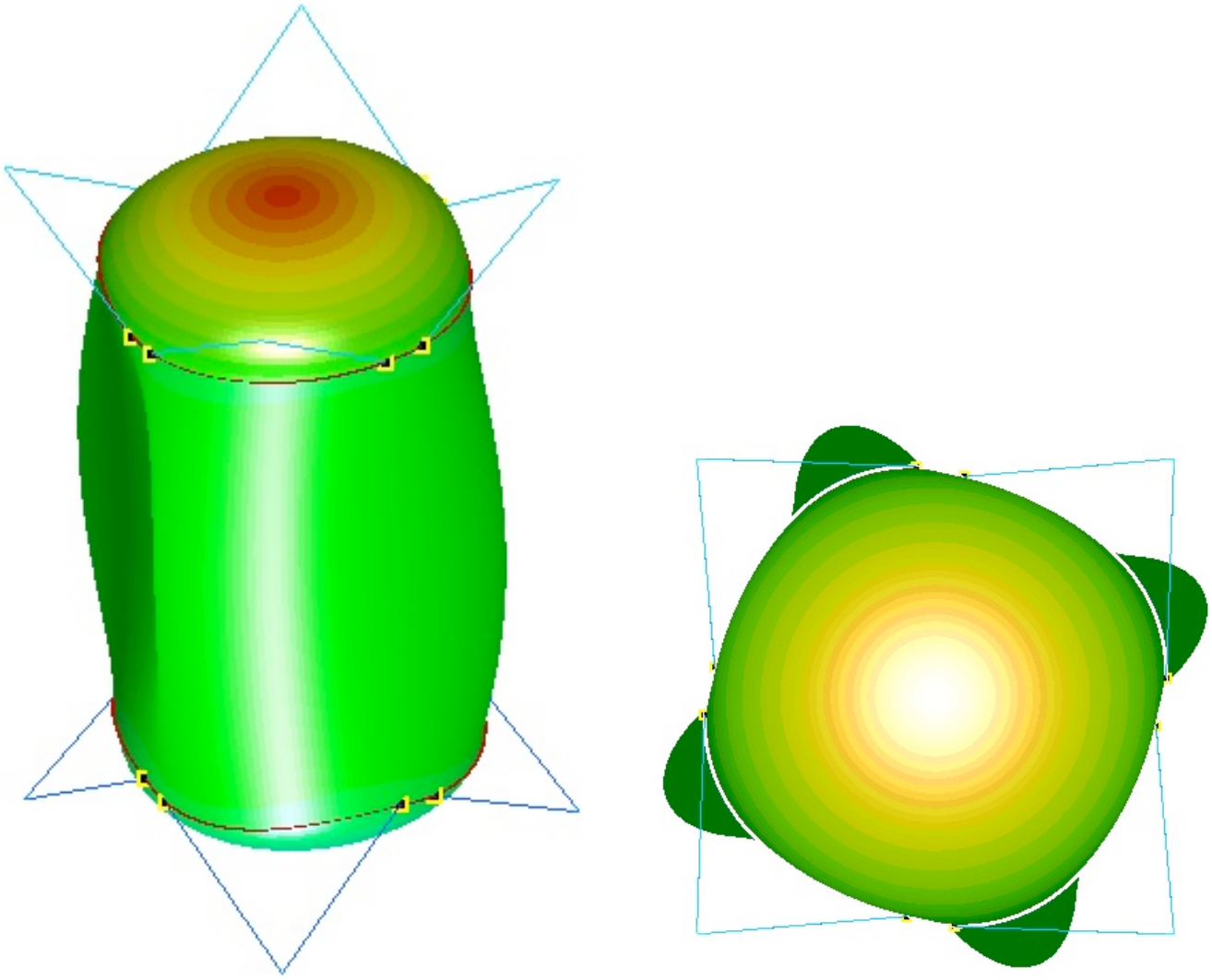

Fig. 25e **The fifth vibration mode from the STAGS model. The modal vibration frequency predicted by STAGS is 15.92 Hz.** This mode is a combination of shell deformation with n = 4 circumferential waves and uniform rolling of the propellant tank approximately as a rigid body with significant tension and compression in the supporting struts. The rolling motion with associated tension and compression in the struts can most easily be appreciated from the image on the right-hand side of the figure. In that image the approximately "uniform" rolling component of the total motion of the tank is counterclockwise. The two components of vibration motion, rolling tank motion and n = 4 shell deformation motion, which are combined in a single mode in this STAGS model, are decoupled in the GENOPT/BIGBOSOR4 model displayed in Figs. 16a and 16b: the tank rolling motion depicted in Fig. 16a(B) with a frequency of 17.787 Hz and the n = 4 shell deformation motion depicted in Fig. 16b(G) with a frequency of 16.676 Hz.

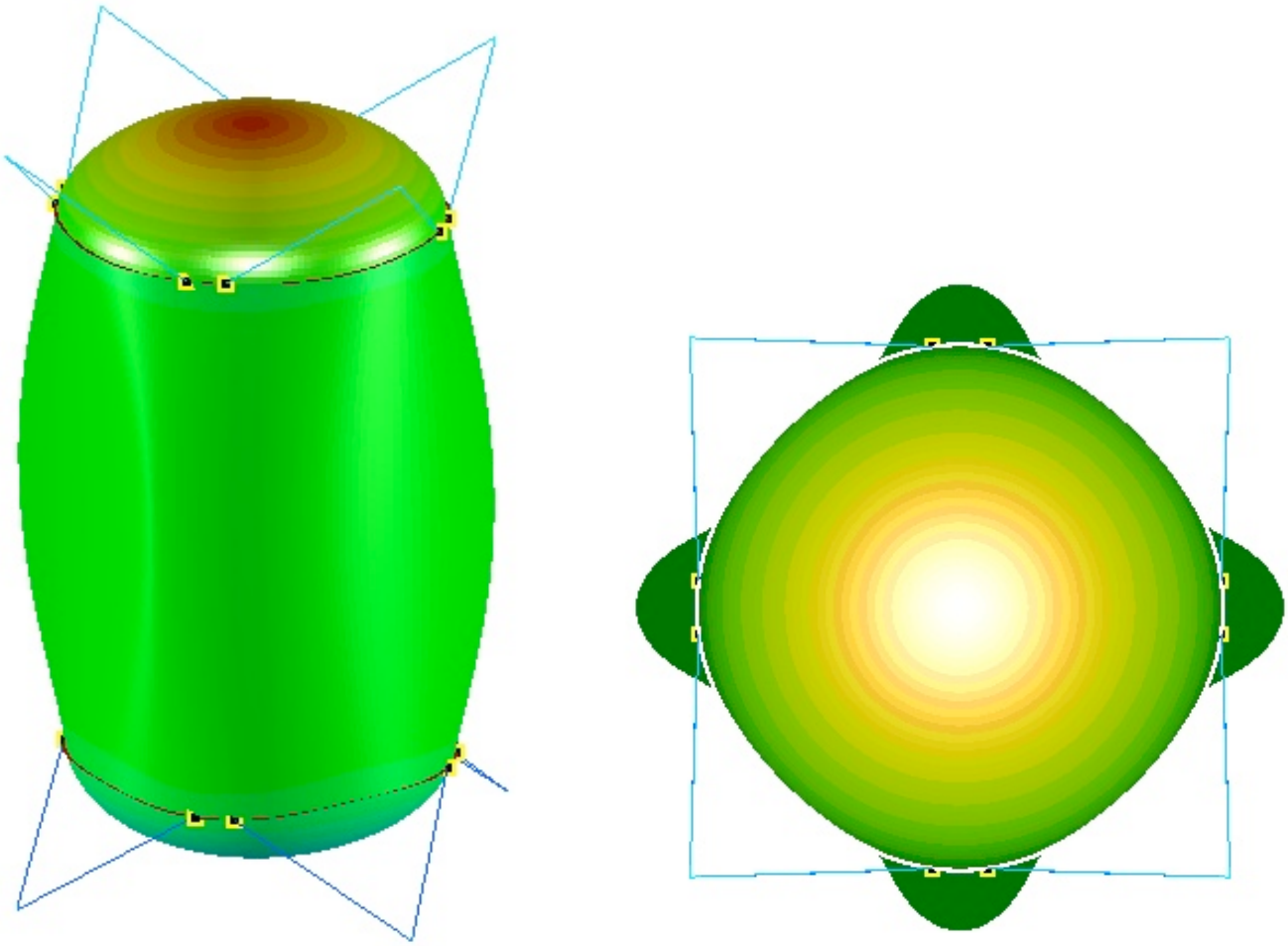

Fig. 25f **The sixth vibration mode from the STAGS model. The modal vibration frequency predicted by STAGS is 16.19 Hz**. This mode is essentially pure shell deformation with n = 4 circumferential waves. The analogous n = 4 shell deformation mode predicted by GENOPT/BIGBOSOR4 is displayed in Fig. 16b(G) with its associated modal vibration frequency equal to 16.676 Hz.

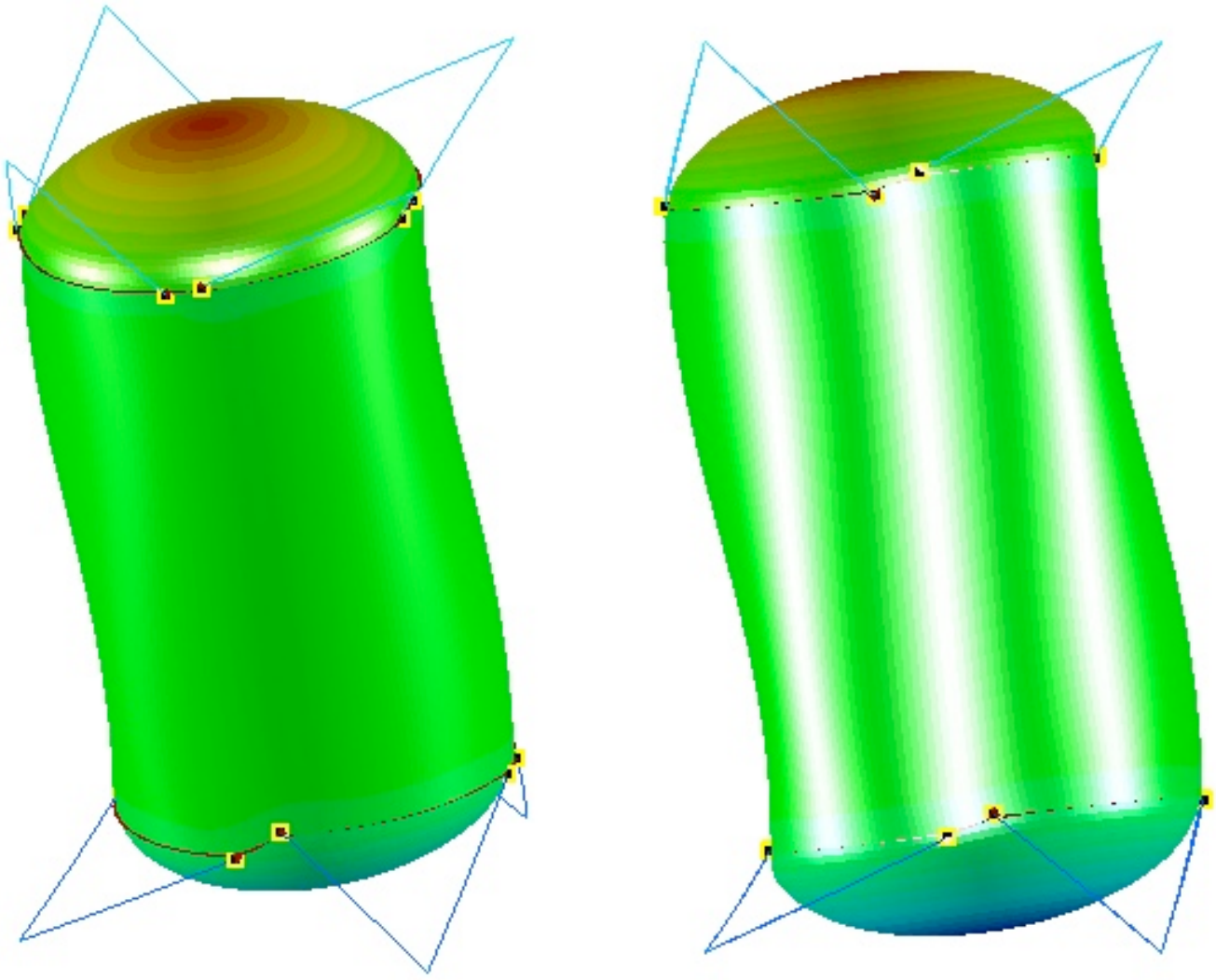

Fig. 25g **Two views of the seventh vibration mode from the STAGS model. The modal vibration frequency predicted by STAGS is 16.25 Hz.** This mode is a combination of shell deformation with m = 2 axial half-waves and mostly pitching motion of the propellant tank approximately as a rigid body with significant tension and compression in the supporting struts. The GENOPT/BIGBOSOR4 model predicts mostly pitching tank motion with a modal vibration frequency equal to 15.284 Hz, as displayed in Fig. 16a(D). Shell deformation modes with m greater than one-half axial wave were not computed for the GENOPT/BIGBOSOR4 model.

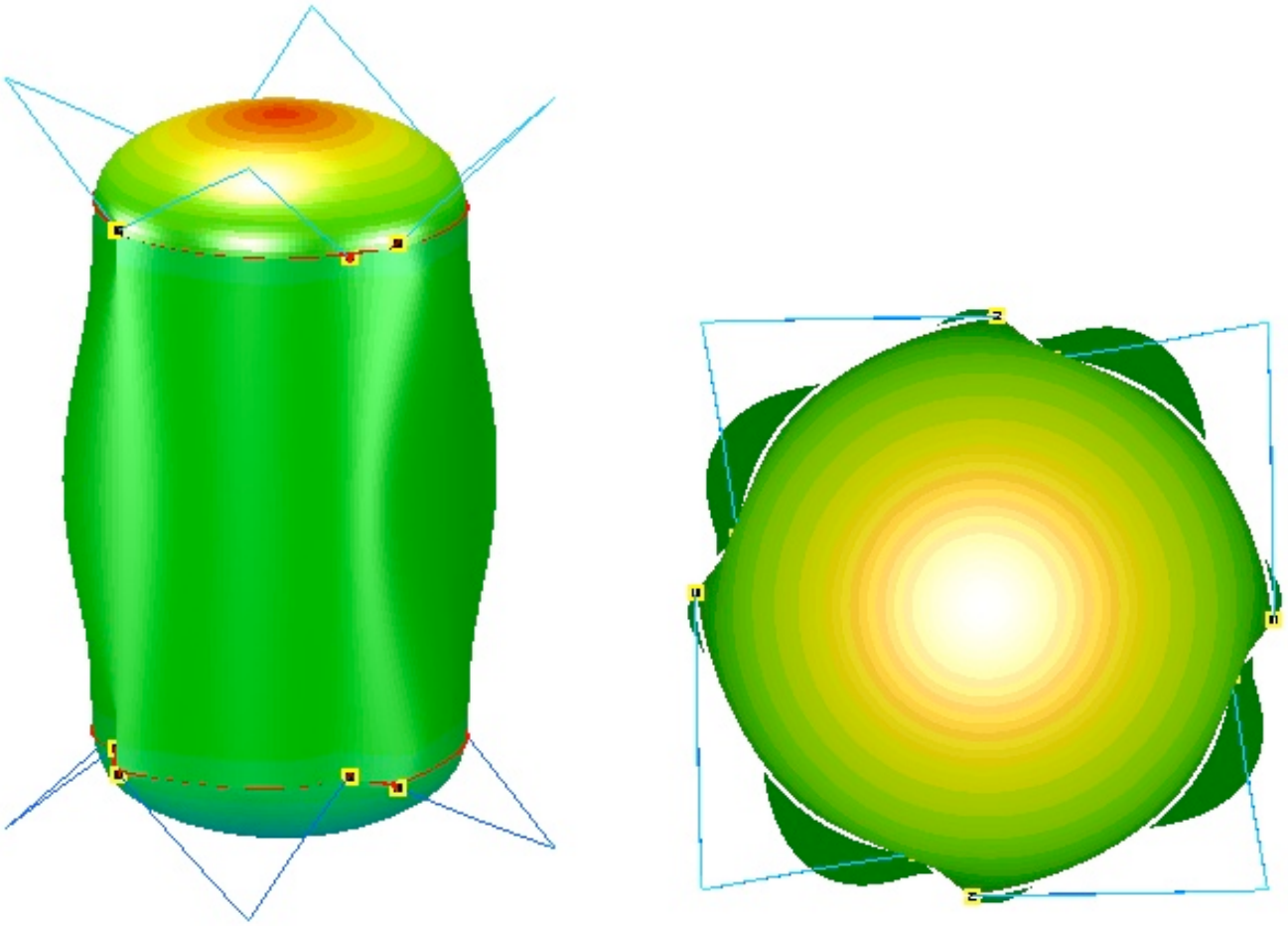

Fig. 25h **The eighth vibration mode from the STAGS model. The modal vibration frequency predicted by STAGS is 19.82 Hz.** The situation here is analogous to that depicted by the STAGS model in Fig. 25d (n = 3 circumferential waves + some tank lateral motion) and compared with Fig. 25a (n = 3 circumferential waves + some tank lateral motion). This mode is analogous to that displayed in Fig. 25e: a combination of shell deformation with n = 4 circumferential waves and rolling motion of the propellant tank approximately as a rigid body with significant tension and compression in the supporting struts. While the two superficially similar STAGS vibration modes that are orthogonal to each other shown here and in Fig. 25e can exist, there is no analogous situation in which there exist multiple modes with primarily tank rolling motion in the decoupled GENOPT/BIGBOSOR4 model. As with Fig. 25e the two components of total motion from STAGS shown here should be compared with the predictions from GENOPT/BIGBOSOR4 shown in Figs. 16a(B) and 16b(G).

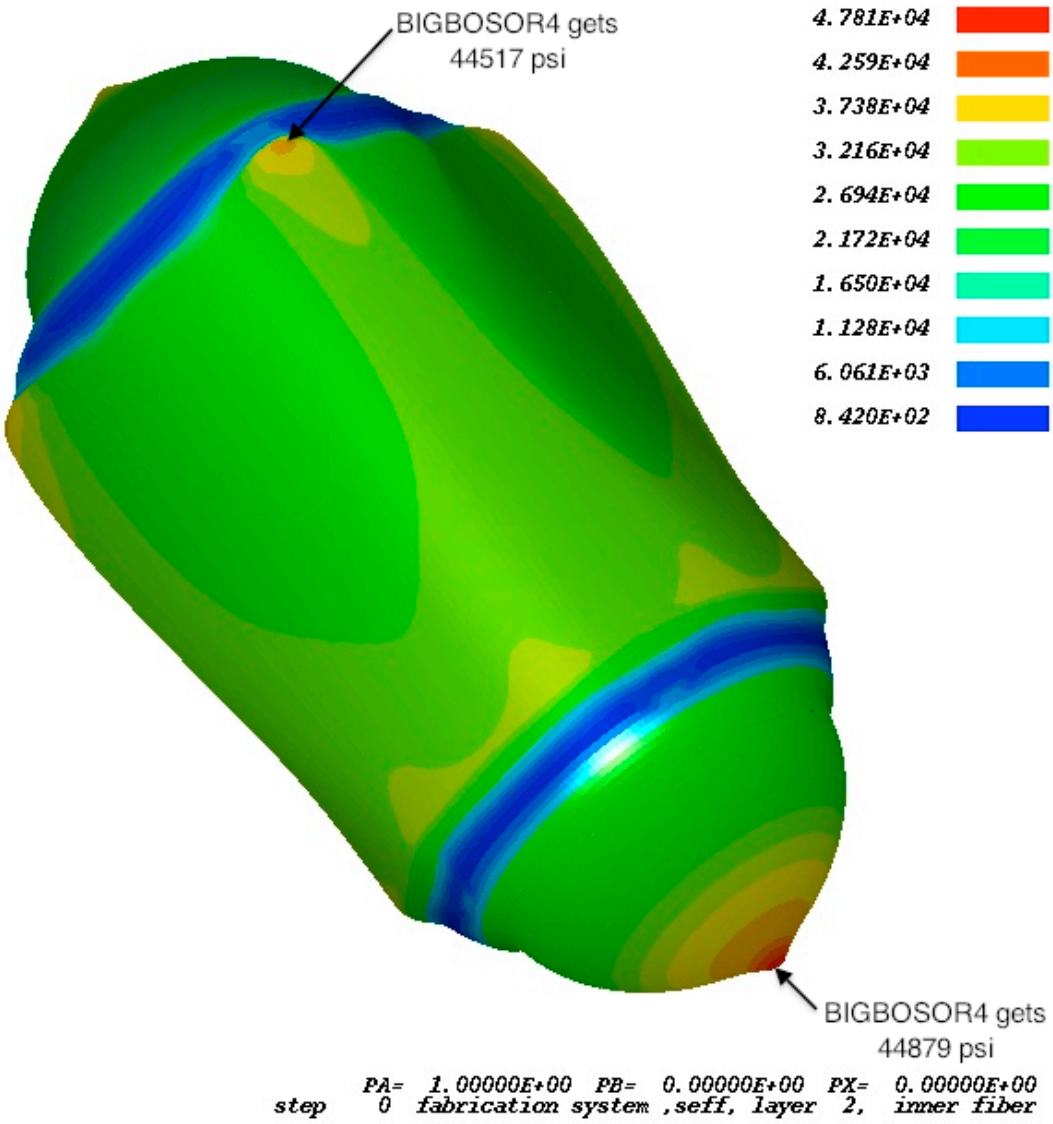

Fig. 26a Load Case 1 (10g axial acceleration + 25 psi internal pressure + 200-degree tank cool-down): **Outer fiber effective stress, "seff" (psi), in the skin of the optimized long propellant tank with aft and forward sets of struts, 4 pairs of struts at each axial location** (the specific case called "test"; struts not shown in this view). (NOTE: The caption above automatically produced by STAGS contains the string, "inner fiber". In this particular application of STAGS the normal vectors to the shell reference surface all point toward the interior of the tank. Therefore, what STAGS calls "inner fiber" corresponds to the external surface of the tank.) In the STAGS analysis that produced this figure all the loading is in Load Set A: 10g axial acceleration, 25 psi internal pressure, and 200 degrees tank cool-down. There is no Load Set B. In STAGS jargon the load factor for Load Set A is called "PA" and the load factor for Load Set B is called "PB". Compare with the GENOPT/BIGBOSOR4 prediction shown in Fig. 21a(A). What are external tapered doublers with maximum thickness = 0.886 inch in the GENOPT/BIGBOSOR4 model are replaced by external doublers of constant average thickness = 0.443 inch in this STAGS model. The predictions from BIGBOSOR4 are given in Fig. 21a(A), indicated there as Critical Point Nos. 1 and 3.

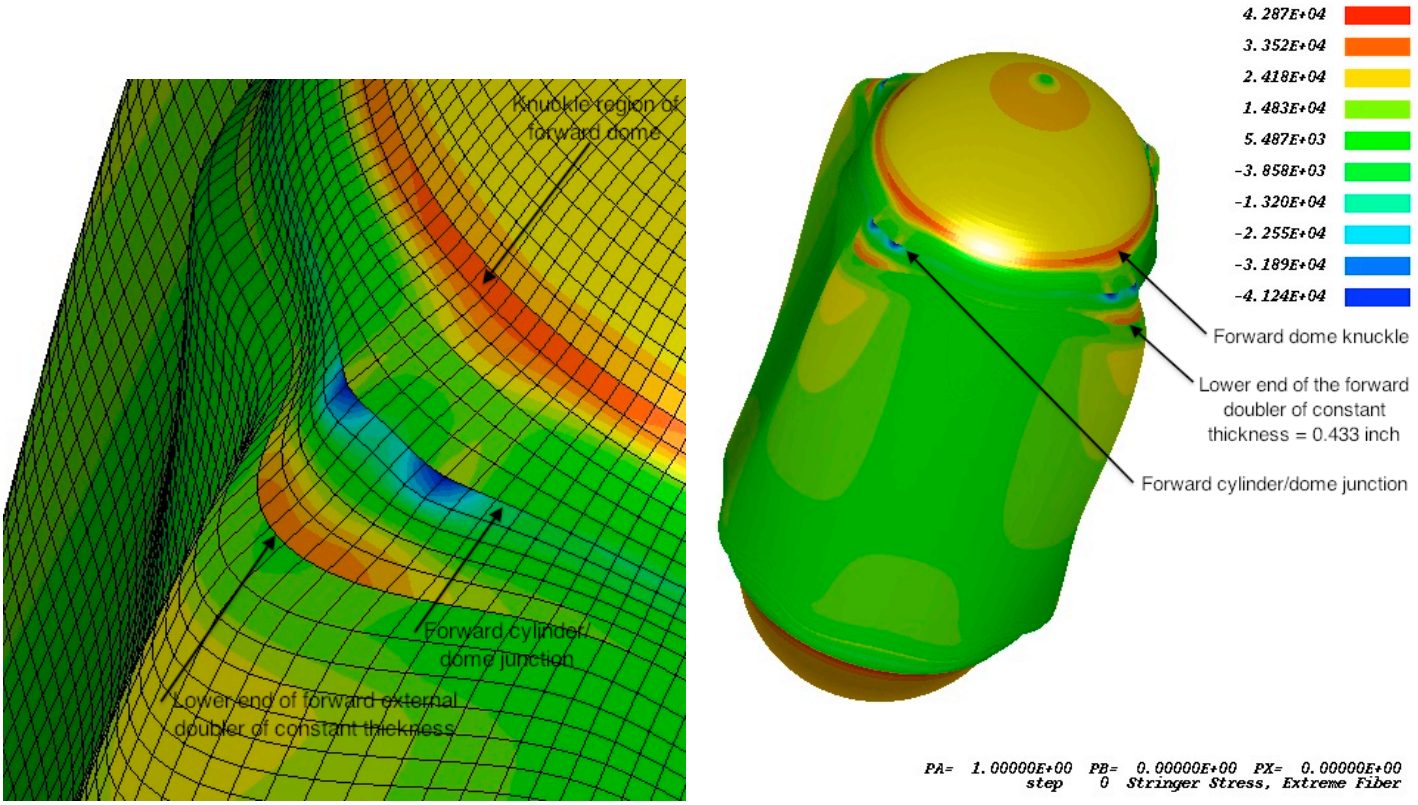

Fig. 26b **Load Case 1 (10g axial acceleration + 25 psi internal pressure + 200-degree tank cool-down): Stress (psi) at the tips of the internal orthogrid stringers** of the optimized long propellant tank with aft and forward sets of struts, 4 pairs of struts at each axial location. Compare with the GENOPT/BIGBOSOR4 prediction shown in Fig. 21a(A). In the STAGS model the internal orthogrid is modeled as an orthotropic layer of the propellant tank shell wall with "effective" meridional and circumferential stiffnesses equal to the actual material modulus reduced by the ratio of stringer thickness divided by stringer spacing and ring thickness divided by ring spacing, respectively. Note that the GENOPT/BIGBOSOR4 model with tapered external doublers [Fig.21a(A)] predicts significantly higher maximum **tensile** stress at the tips of the internal orthogrid stringers (Critical point no. 2 = 50000 psi) than does this STAGS model (maximum **tensile** stringer stress in the knuckle of the ellipsoidal dome = 42870 psi). In this STAGS model the external doublers have constant thickness = 0.443 inch. Figure 21c(B) shows predictions from a BIGBOSOR4 model with similar constant thickness doublers that yields dramatically higher maximum **compressive** stress at the tips of the internal orthogrid stringers (-119000 psi), indicating that the STAGS prediction of maximum compressive stress at the tips of the internal orthogrid stringers (-41240 psi) displayed here is not converged with respect to finite element mesh density. The **tensile** stress concentration at the tips of the orthogrid stringers that occurs at the lower edge of the forward external **constant thickness doubler** does not appear in the BIGBOSOR4 model with the external **tapered doubler**. Compare the maximum tensile and compressive stresses at the stringer tips shown here with those displayed in the much more refined STAGS 45-degree model displayed in Figs. 26c and 26e.

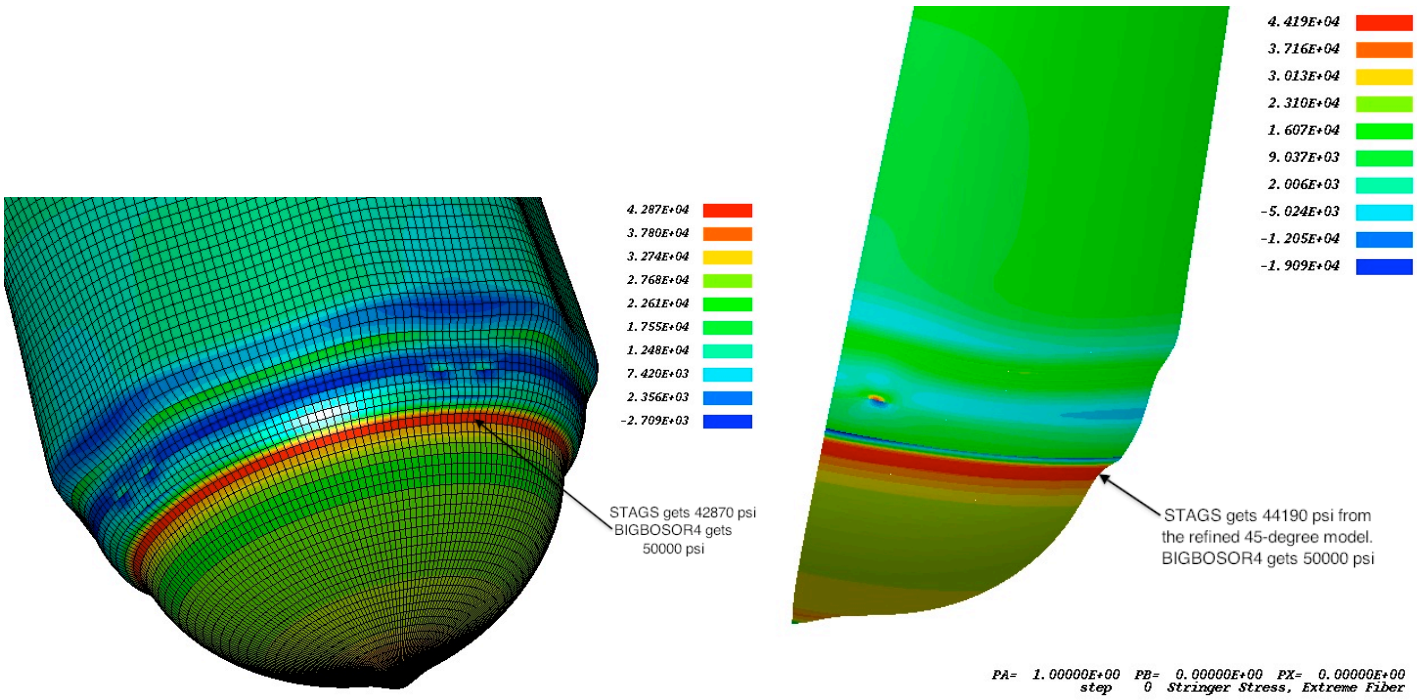

Fig. 26c **Load Case 1 (10g axial acceleration + 25 psi internal pressure + 200 degrees tank cool-down): Stress (psi) at the tips of the internal orthogrid stringers from the STAGS 360-degree model and from the refined STAGS 45-degree model** of the optimized long propellant tank with aft and forward sets of struts, 4 pairs of struts at each axial location. (The struts are not shown in this view.) This figure shows the aft end of the same STAGS model as that displayed in the previous figure. The maximum **tensile** stress at the tips of the orthogrid stringers (narrow red band) occurs in the knuckle region of the aft ellipsoidal dome and is essentially axisymmetric. It is generated almost entirely by the uniform internal pressure, 25 psi, plus the linearly varying normal pressure head applied by the propellant to the shell wall as a result of the 10 g axial acceleration. **Compare with the GENOPT/BIGBOSOR4 prediction of 50000 psi at Critical Point No. 2 as shown in Fig. 21a(A)**. Both the STAGS prediction shown here and the BIGBOSOR4 prediction shown in Fig. 21a(A) are generated from linear stress analyses.

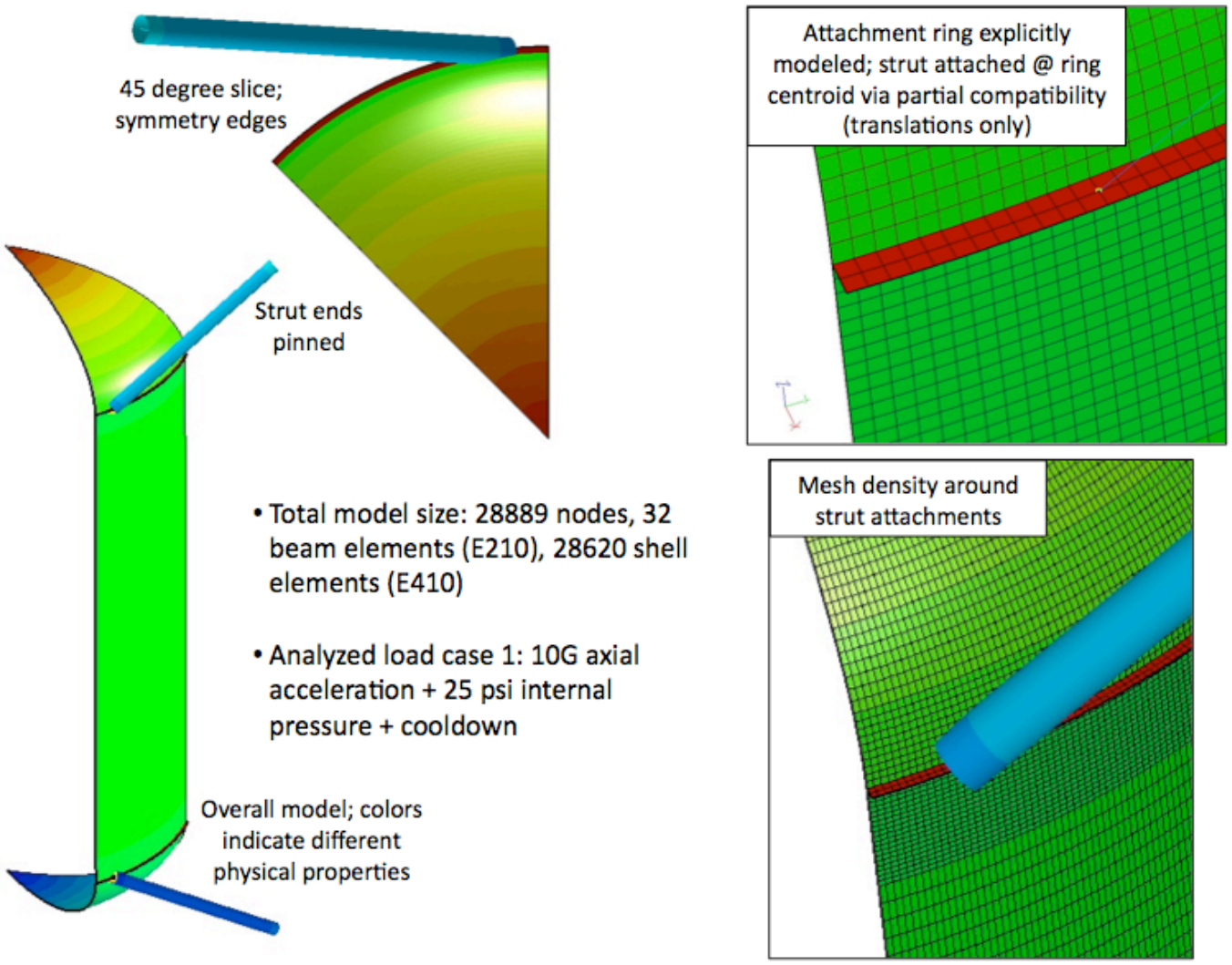

Fig. 26d **A very refined STAGS model of the tank/strut system for the prediction of stresses at the tips of the internal orthogrid stringers under Load Case 1 (10 g axial acceleration + 25 psi internal pressure + 200 degrees tank cool-down). Compare this model with the STAGS 360-degree model of the tank/strut system shown in Fig. 24.**

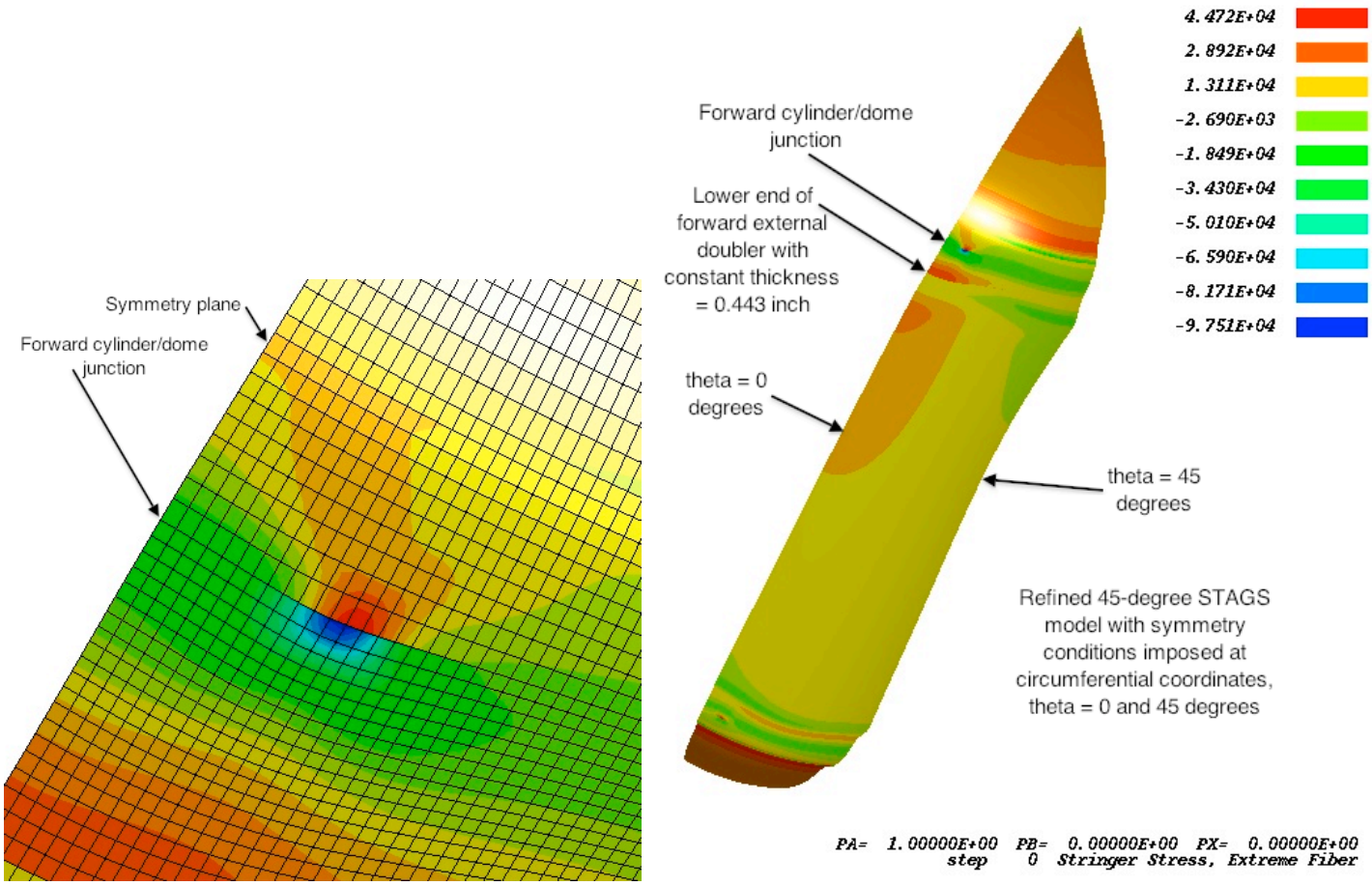

Fig. 26e **Load Case 1 (10g axial acceleration + 25 psi internal pressure + 200-degree tank cool-down): Stress (psi) at the tips of the internal orthogrid stringers predicted from the refined STAGS 45-degree model** shown in the previous figure. Compare with the orthogrid stringer tip stresses displayed in Fig. 26b. The maximum stresses at the tips of the stringers in the internal orthogrid "layer" of the shell wall at the forward cylinder/dome junction is much greater in this refined STAGS model than in the BIGBOSOR4 model with tapered external doublers, that is, the configuration that was optimized by GENOPT/TANK/BIGBOSOR4. However, it agrees fairly well with the predictions from the BIGBOSOR4 model with the constant thickness doublers, that is, the BIGBOSOR4 model that simulates the STAGS model. [See Fig. 21c(B).]

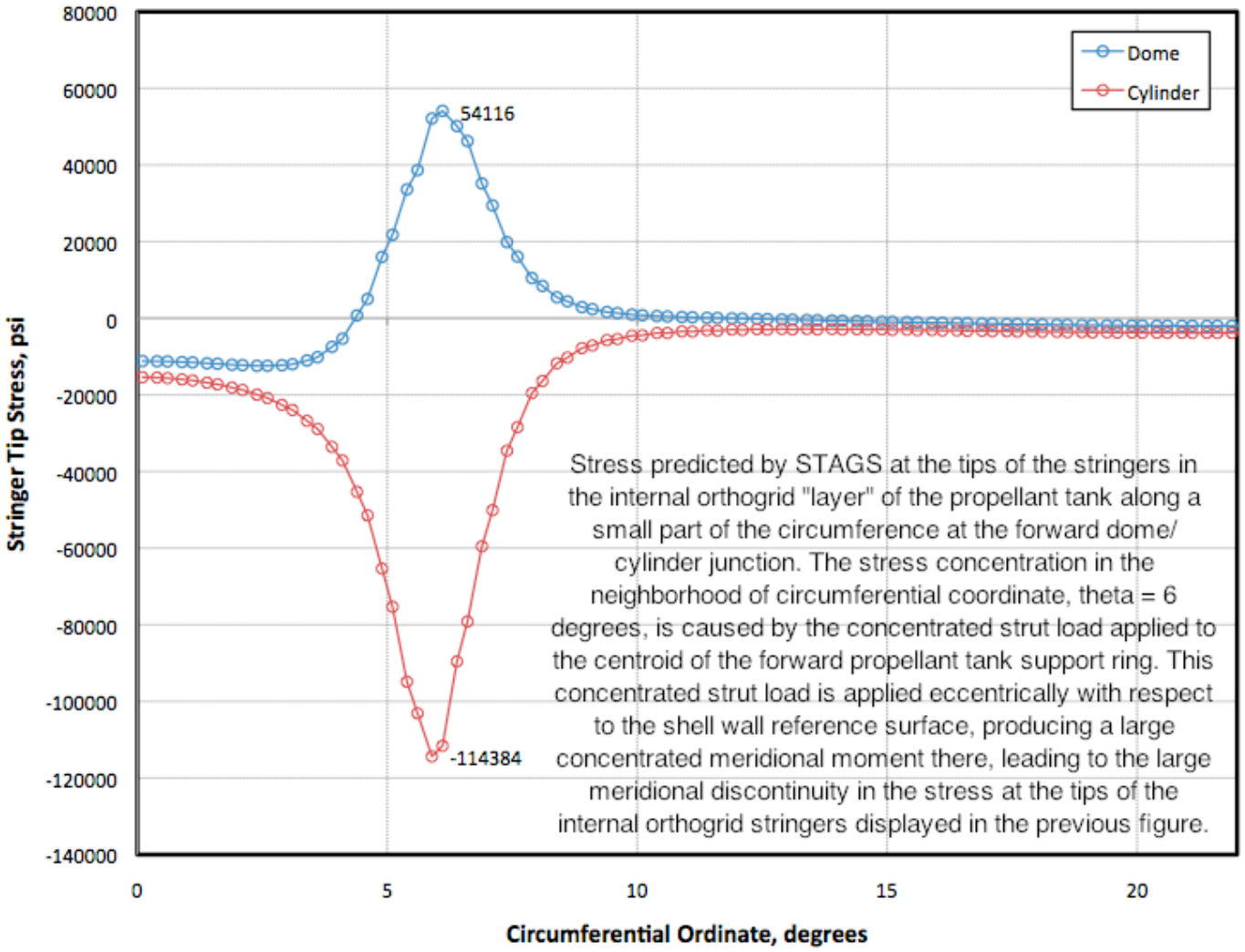

Fig. 26f The specific case, "test", propellant tank under **Load Case 1** (10 g axial acceleration, 25 psi internal pressure and 200 degree tank cool-down). **Plots of the stress at the tips of the internal orthogrid stringers from the refined STAGS 45-degree model** shown in Figs. 26d and 26e. **Compare with the stresses predicted by the BIGBOSOR4 model with constant thickness doublers (the BIGBOSOR4 model that simulates the STAGS model).** These "BIGBOSOR4" stresses are plotted at the same location and are shown in Fig. 21d.

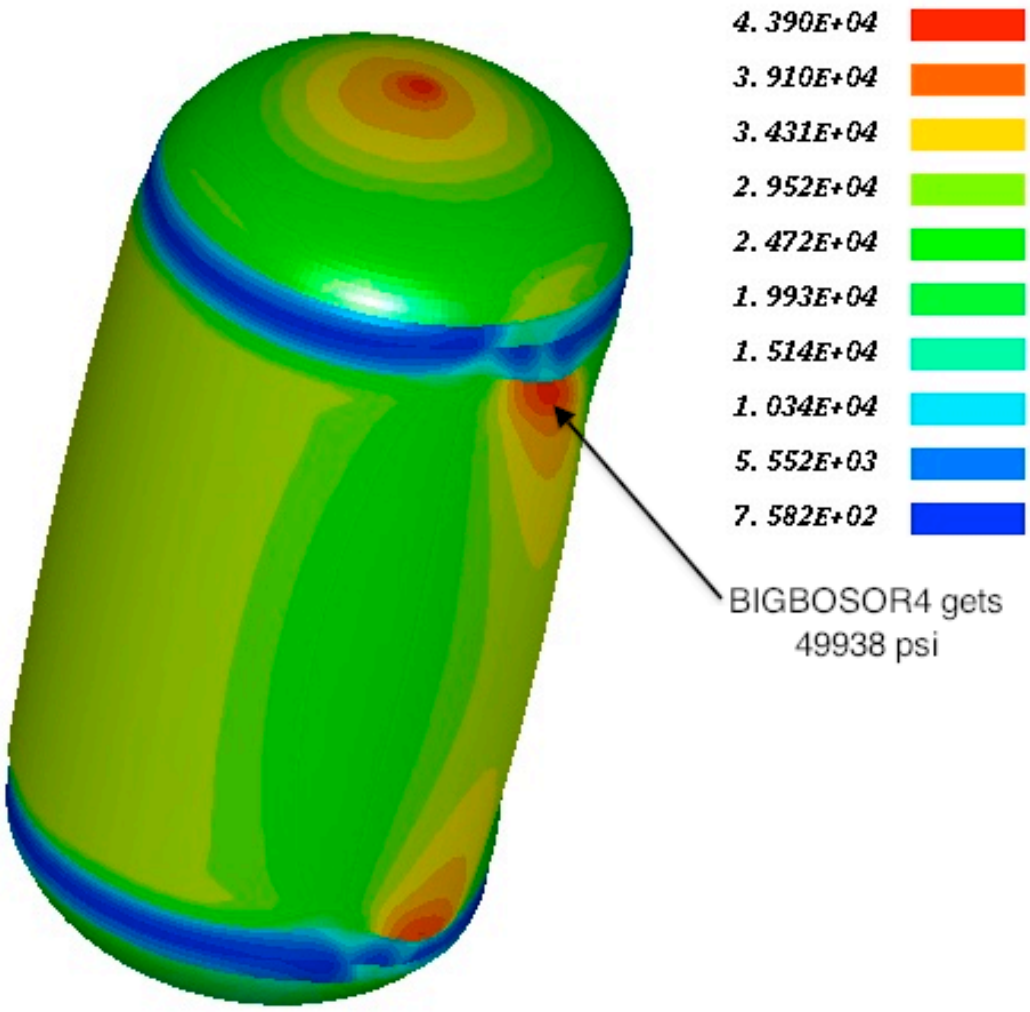

Fig. 27a **STAGS model under Load Case 2 (lateral acceleration + 25 psi internal pressure + 200-degree tank cool-down): Outer fiber effective stress, "seff" (psi), in the skin of the optimized long propellant tank** with aft and forward sets of struts, 4 pairs of struts at each axial location. (NOTE: The caption above automatically produced by STAGS contains the string, "inner fiber". In this particular application of STAGS the normal vectors to the shell reference surface all point toward the interior of the tank. Therefore, what STAGS calls "inner fiber" corresponds to the external surface of the tank.) In the STAGS analysis that produced this figure all the loading is in Load Set A: 10g lateral acceleration, 25 psi internal pressure, and 200 degrees tank cool-down. There is no Load Set B. In STAGS jargon the load factor for Load Set A is called "PA" and the load factor for Load Set B is called "PB". **Compare with the GENOPT/TANK/BIGBOSOR4 prediction shown in Fig. 21a(B).** The prediction of maximum effective stress in the skin from BIGBOSOR4 is indicated in Fig. 21a(B) as Critical Point No. 1: maximum effective stress = 49938 psi. In the BIGBOSOR4 model the external doublers are tapered with maximum thickness = 0.886 inch, whereas in this STAGS model the external doublers are of average constant thickness = 0.443 inch. No BIGBOSOR4 model with constant thickness doublers was constructed for analysis under Load Case 2.

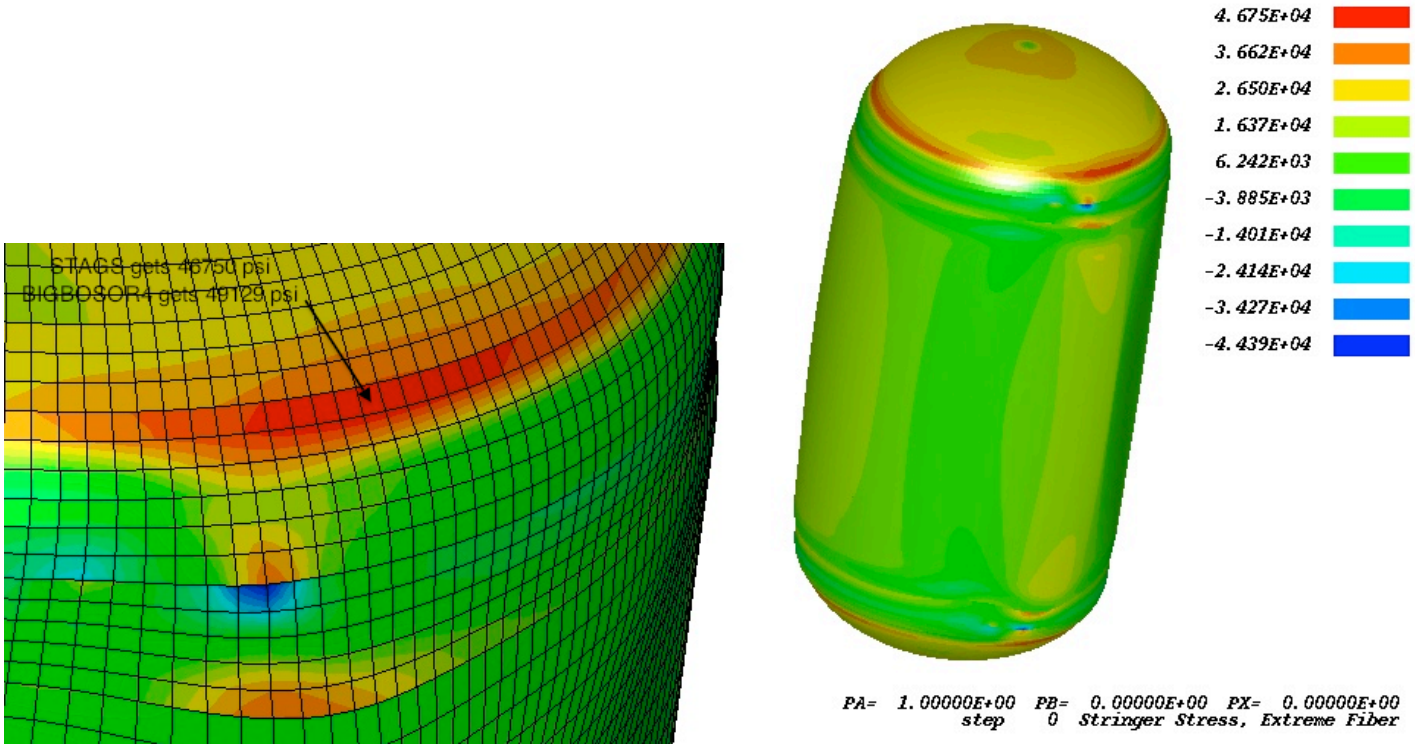

Fig. 27b **STAGS model under Load Case 2 (10g lateral acceleration + 25 psi internal pressure + 200-degree tank cool-down): Stress (psi) at the tips of the internal orthogrid stringers of the optimized long propellant tank** with aft and forward sets of struts, 4 pairs of struts at each axial location. Compare with the GENOPT/BIGBOSOR4 prediction shown in Fig. 21a(B), in particular Critical Point No. 2 indicated there, for which BIGBOSOR4 yields a prediction of 49129 psi. In the STAGS model the internal orthogrid is modeled as an orthotropic layer of the propellant tank shell wall with "effective" meridional and circumferential stiffnesses equal to the actual material modulus reduced by the ratio of stringer thickness divided by stringer spacing and ring thickness divided by ring spacing, respectively.

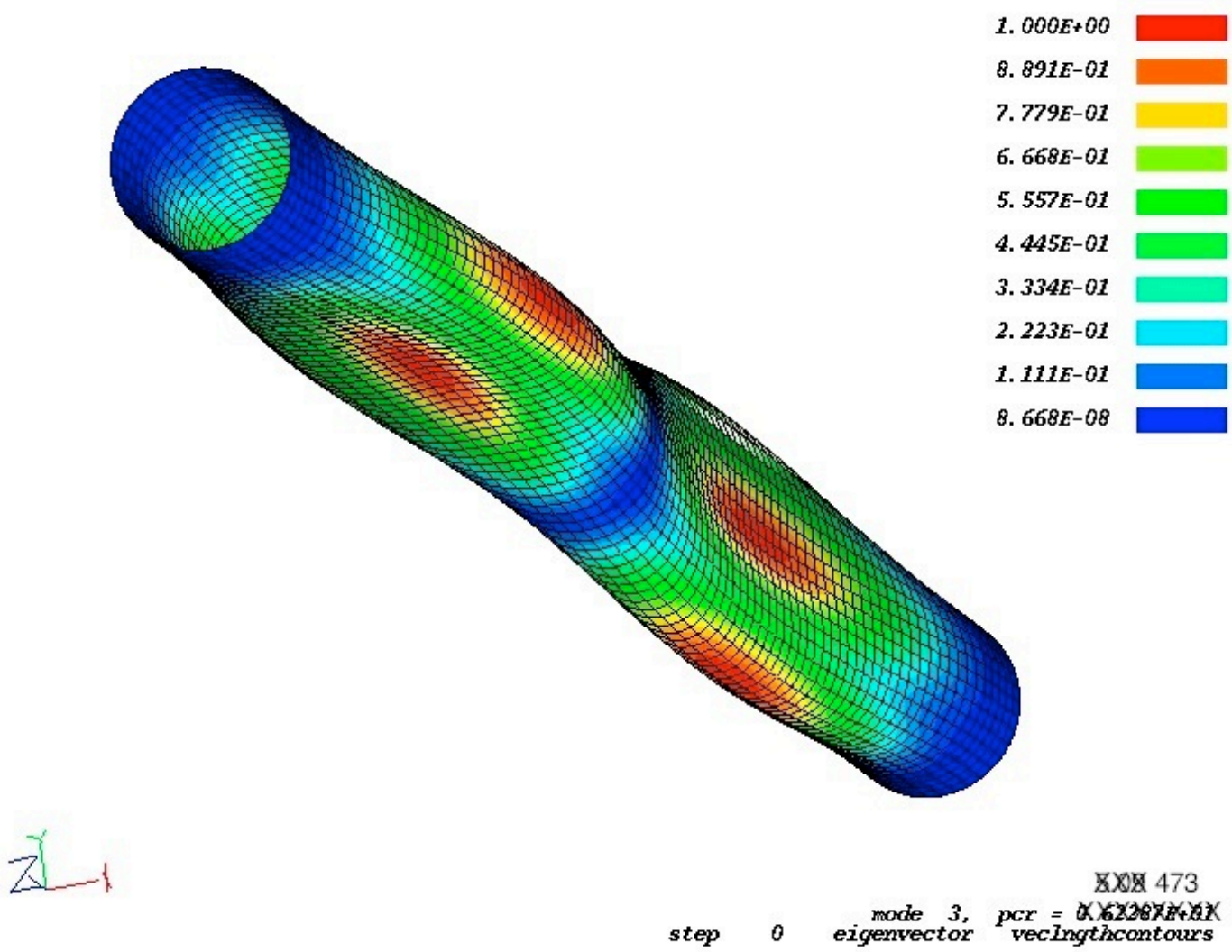

Fig. 28 **Load Case 1: STAGS prediction of the critical shell buckling mode and load factor, pcr = 4.73, for the entire length of an aft strut for the optimized long propellant tank/strut system** with two sets of struts, aft and forward, 4 pairs of struts in each set. The applied compressive load from the STAGS model is 24841 lbs. and the buckling load factor corresponding to this strut shell buckling mode is 4.73, which corresponds to the third eigenvalue (mode). The first two modes correspond to buckling of the strut as a column. **Compare with the strut shell buckling mode from BIGBOSOR4 shown in Fig. 20(A).** The difference in the BIGBOSOR4 and STAGS prediction for the buckling load factors here and in Fig. 20(A) is primarily due to the different prediction from GENOPT/TANK/BIGBOSOR4 and STAGS of maximum compressive load in an aft strut in Load Case 1 (axial acceleration): -22693 lbs according to GENOPT/TANK and -24841 lbs according to STAGS. [See Table 7(b, e).]

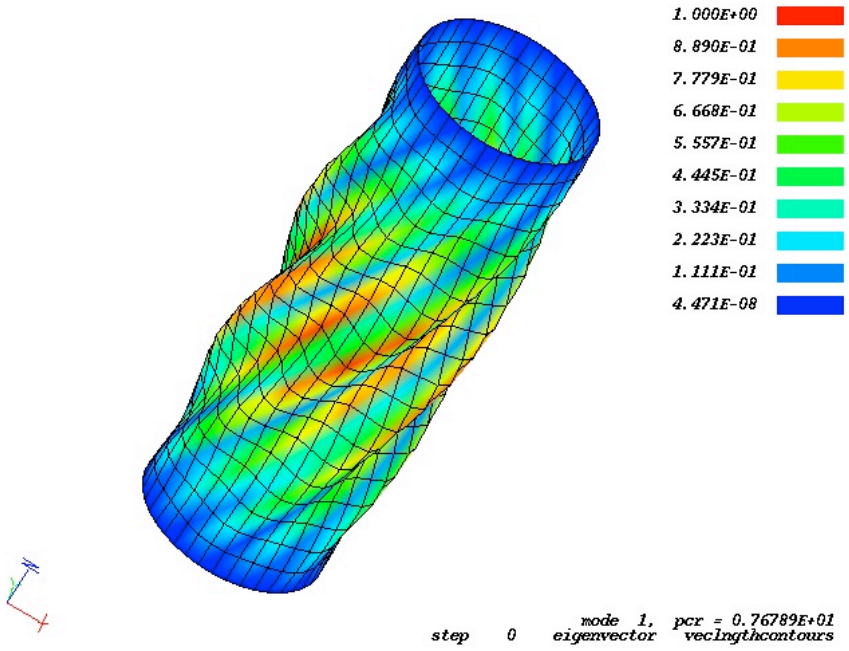

(A) Short segment of the aft strut, Load Case 1. Buckling load factor = 7.679 [See Fig. 20(C)]

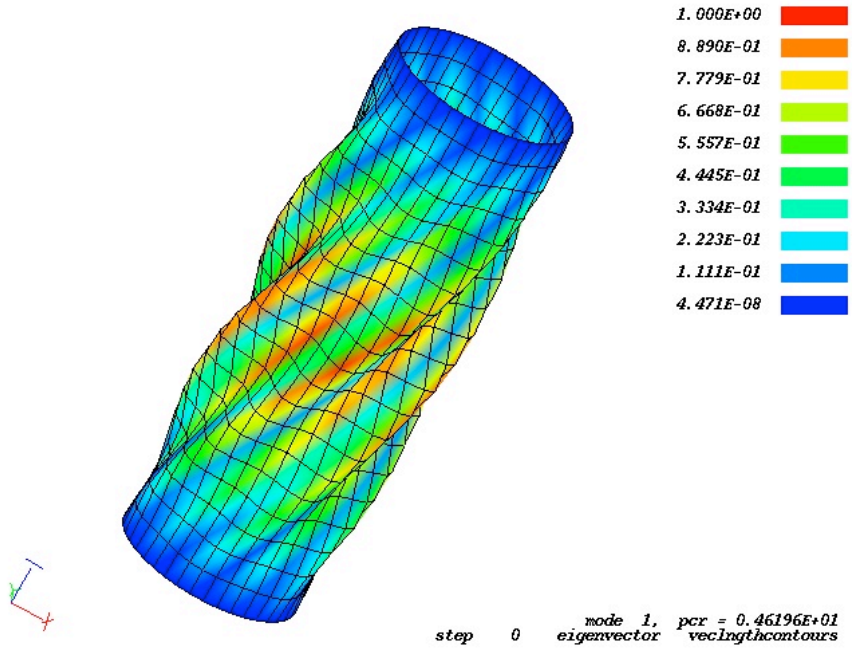

(B) Short segment of the aft strut, Load Case 2. Buckling load factor = 4.620 [See Fig. 20(D)]

Fig. 29 **STAGS predictions of shell buckling of a short segment of the aft strut in Load Cases 1 and 2**

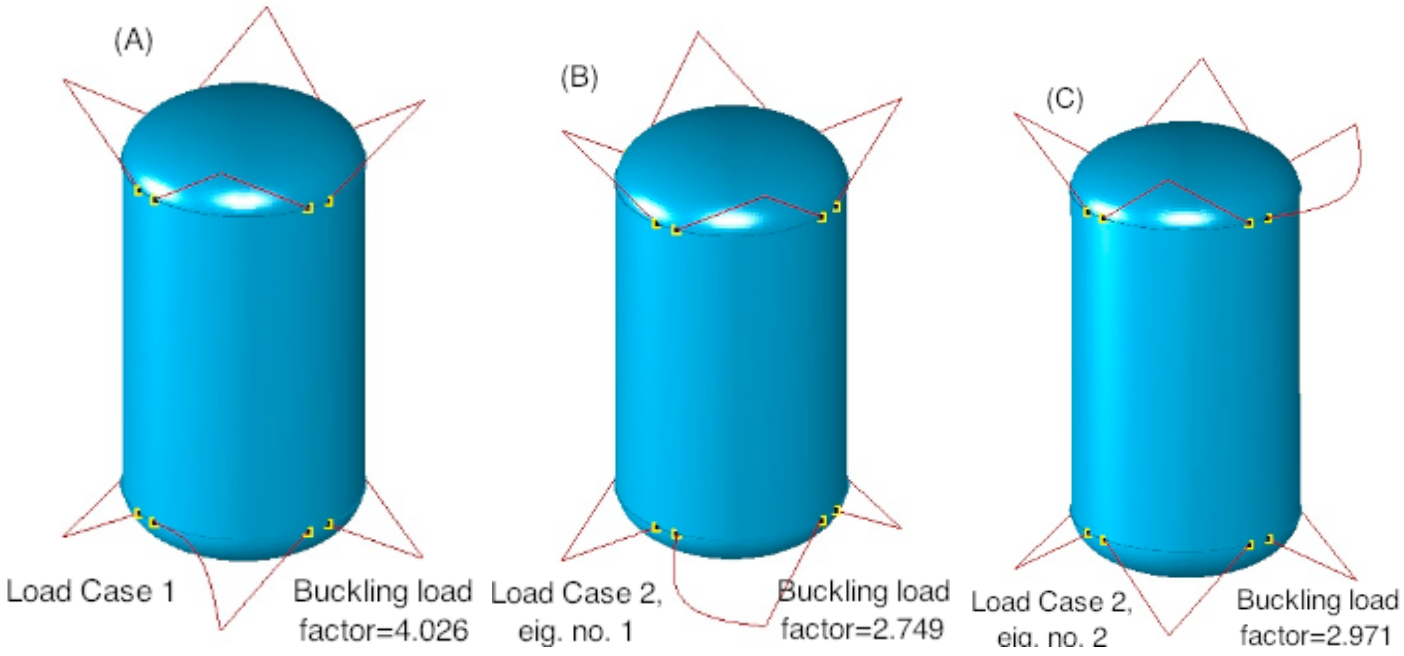

Fig. 30 **STAGS prediction of linear buckling of the tank/strut system. In each of the three frames the lowest buckling load factor corresponds to buckling of only one strut as a column.** All of the three loading components, 10g acceleration with associated spatially linearly varying normal pressure head, 25 psi uniform internal pressure, and 200-degree tank cool-down, are included in Load Set A ("eigenvalue" loads) in these particular buckling analyses. There is no Load Set B.
(A) Buckling of one of the aft struts under 10g upward **axial acceleration** plus 25 psi internal pressure plus 200-degree tank cool-down (eigenvalue no. 1 for Load Case 1).
(B) Buckling of one of the aft struts under 10g **lateral acceleration** plus 25 psi internal pressure plus 200-degree tank cool-down (eigenvalue no. 1 for Load Case 2).
(C) Buckling of one of the forward struts under 10g **lateral acceleration** plus 25 psi internal pressure plus 200-degree tank cool-down (eigenvalue no. 2 for Load Case 2).
Note that **Table 7(d) also includes STAGS predictions for buckling of the struts as columns.** The STAGS predictions listed in Table 7(d) are obtained from models in which only one pinned strut is included in each STAGS model; the propellant tank is absent. Therefore, any possible influence of the flexibility of the propellant tank on the STAGS buckling load factors listed in Table 7(d) is neglected. Notice that the strut buckling load factors computed from the STAGS model of the tank/strut system depicted here are almost exactly the same as those listed in Table 7(d): 4.026 here versus 3.99 in Table 7(d), 2.749 here versus 2.74 in Table 7(d), and 2.971 here versus 3.00 in Table 7(d). Therefore, according to predictions from STAGS, the flexibility of the propellant tank, included in the tank/strut system here, has virtually no influence on the buckling load factors predicted by STAGS.

The predictions from STAGS shown here are reasonably close to those predicted by GENOPT/TANK and listed in Table 7(d): 4.026 from STAGS versus 4.163 from GENOPT/TANK, 2.749 from STAGS versus 2.398 from GENOPT/TANK, 2.971 from STAGS versus 2.645 from GENOPT/TANK.

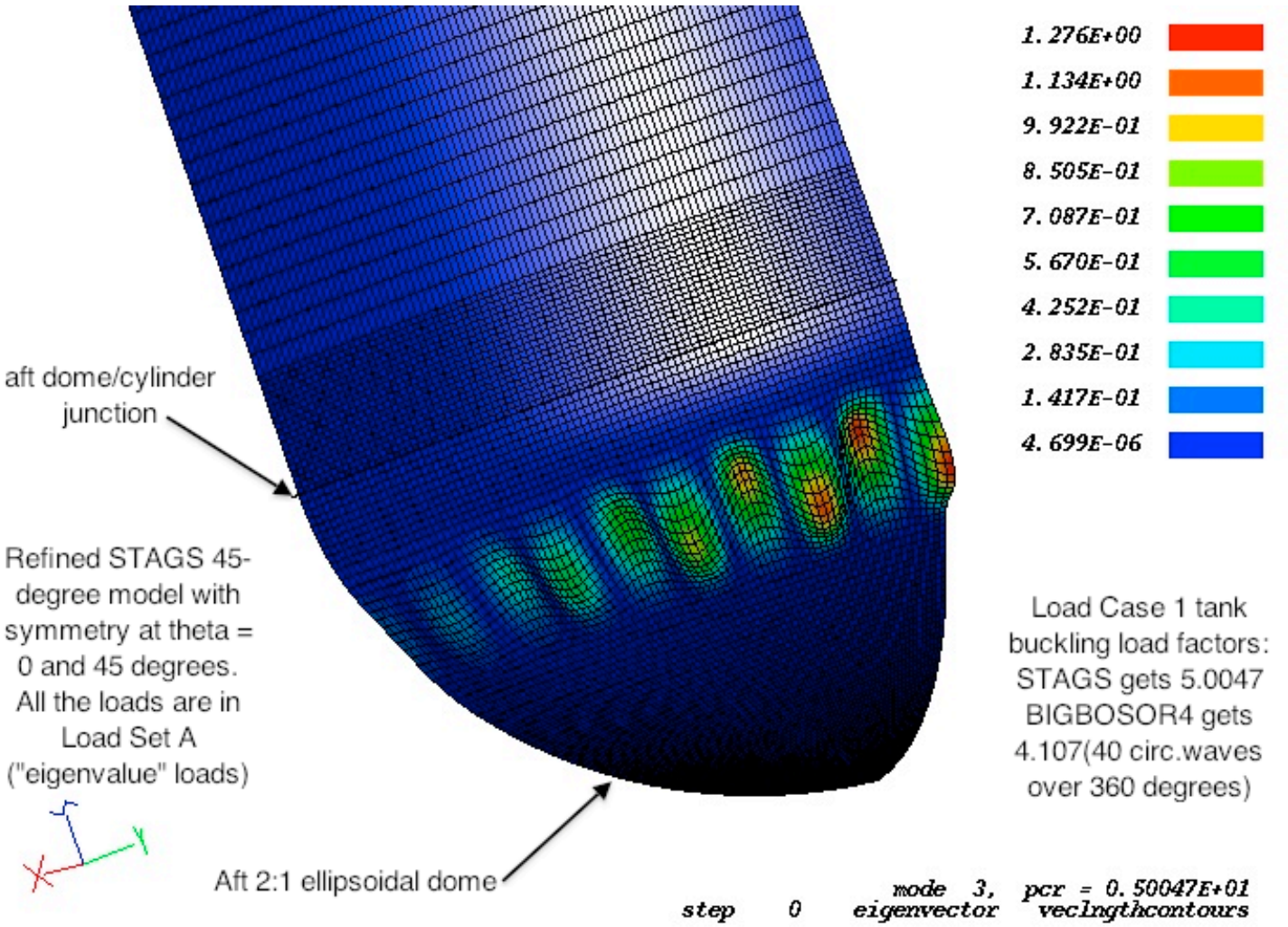

Fig. 31 **STAGS model of buckling of the propellant tank under Load Case 1** (10g axial acceleration plus 25 psi internal ullage pressure plus 200-degree tank cool-down). This is the same refined 45-degree STAGS model as that displayed in Fig. 26d except that this is a linear buckling model. In this STAGS model **all the load components are in Load Set A ("eigenvalue" loads). There is no Load Set B.** (For this problem it is very difficult to obtain with STAGS non-spurious buckling modes when there exist non-trivial loads in both Load Set A and Load Set B.) The struts shown in Fig. 26d are not shown in this view. In this STAGS model the fundamental (lowest) buckling load factor corresponding to buckling of the propellant tank is Buckling Mode No. 3. (The first two buckling modes involve buckling of the aft strut shown in Fig. 26d.) With all load components in Load Set A, BIGBOSOR4 obtains a buckling load factor of 4.107, which is somewhat lower than that predicted by this STAGS model (5.0047). The difference in predictions from BIGBOSOR4 and STAGS is caused primarily by the different widths of the external doublers in the two models. The critical buckling mode according to BIGBOSOR4 is the same as that shown in Fig. 22. Note that this STAGS model predicts 5 full circumferential waves over 45 degrees of circumference, which is the same as the 40 circumferential waves that BIGBOSOR4 predicts over 360 degrees of circumference. As shown in Fig. 22, with only the loads associated with the 10g axial acceleration in Load Set A and the 25 psi ullage pressure plus 200-degrees tank cool-down in Load Set B, BIGBOSOR4 predicts a much higher buckling load factor: 10.999.

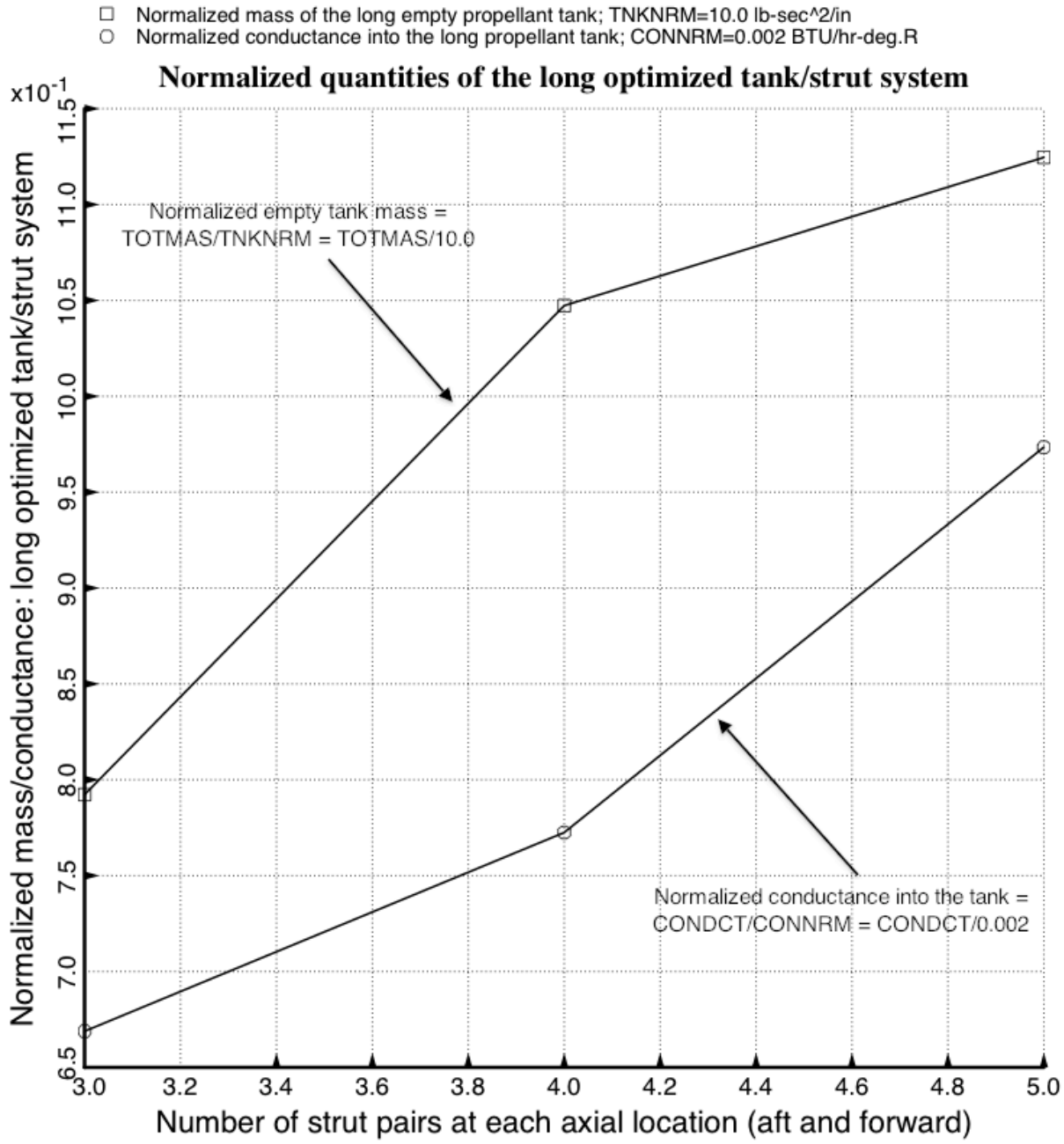

Fig.32 Results from the specific cases called "test", test3, etc: Optimized **long propellant tank with two sets of struts, aft and forward**. Shown here are the optimized empty tank mass and total conductance into the propellant tank as functions of the number of strut pairs at each axial location. Although the best design appears from this figure to have 3 pairs of struts at each axial location, note from Fig. 12 that in the "3-pair" optimized configuration the struts penetrate the wall of the propellant tank somewhat. Therefore, the configuration displayed in Figs. 5 and 6 (4 strut pairs at each axial location) is probably a better design even though the "4-pair" optimized objective, WGT x (TOTMAS/TNKNRM) + (1 – WGT) x (CONDCT/CONNRM), is somewhat higher than the optimized objective for the "3-pair" design.

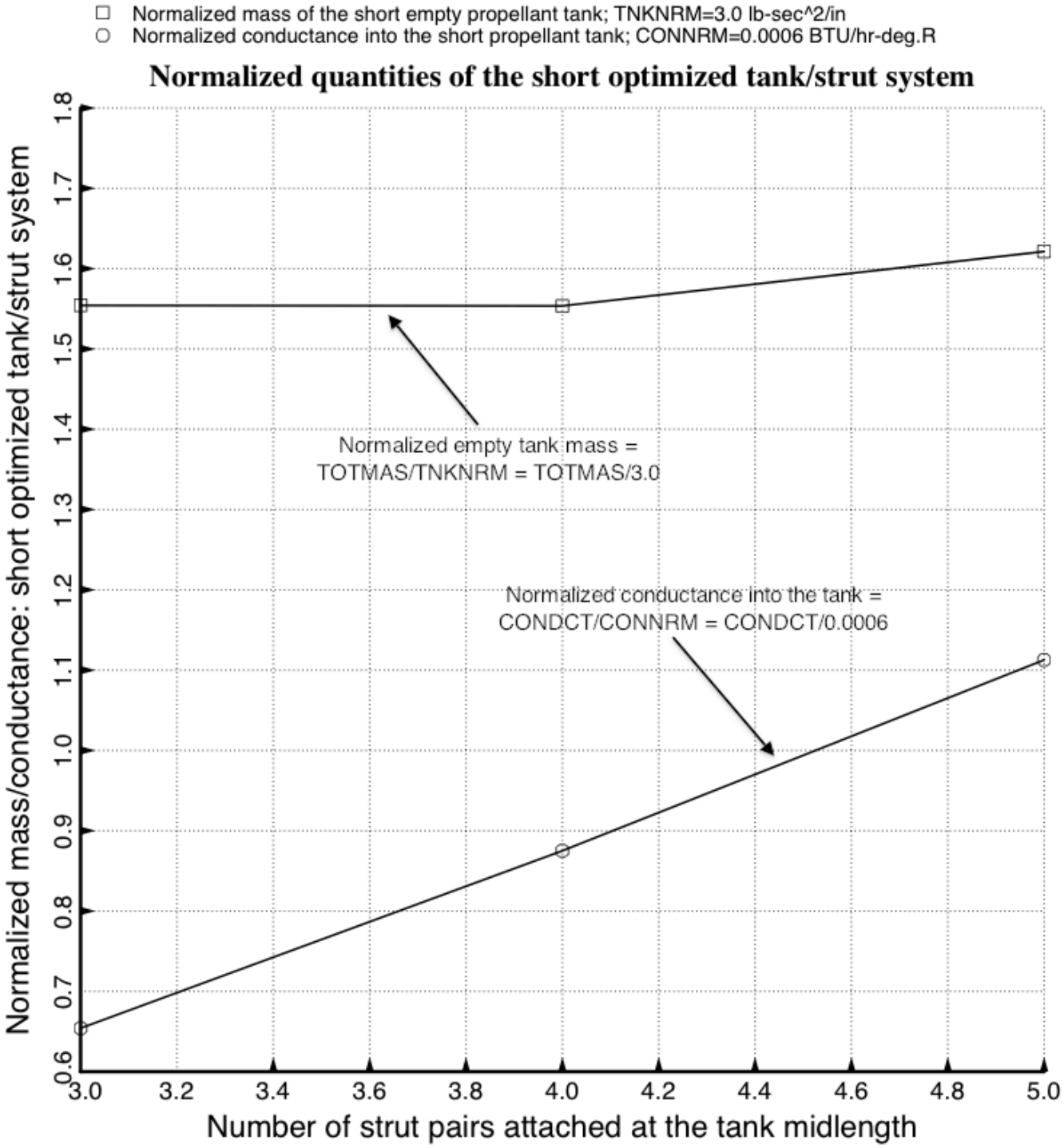

Fig.33 Results from the specific cases called "test2": Optimized **short propellant tank with one set of struts** attached at the midlength of the tank. Shown here are the optimized empty tank mass and total conductance into the short propellant tank as functions of the number of strut pairs.